Quantifying the effect of plume processes on aviation-induced aerosol: towards an improved estimate of the aviation-aerosol effect

Monica Sharma

Quantifying the effect of plume processes on aviation-induced aerosol: towards an improved estimate of the aviation-aerosol effect

QUANTIFYING THE EFFECT OF PLUME PROCESSES ON AVIATION-INDUCED AEROSOL: TOWARDS AN IMPROVED ESTIMATE OF THE AVIATION-AEROSOL EFFECT

Dissertation

for the purpose of obtaining the degree of doctor
at Delft University of Technology
by the authority of the Rector Magnificus,
Prof.dr.ir. H. Bijl,
chair of the Board for Doctorates
to be defended publicly on
Wednesday, 25 February 2026, 10:00

by

Monica SHARMA

Master of Science in Geoscience,
Technische Universität Bergakademie Freiberg, Freiberg, Germany
born in Ghaziabad, Uttar Pradesh, India.

This Dissertation has been approved by the promotors.

Composition of the Promotion Committee:

Rector Magnificus	Chairperson
Prof. dr. V. Grewe	Delft University of Technology, German Aerospace Center, Germany, *promotor*
Dr. I.C. Dedoussi	University of Cambridge, *promotor*

Independent members:

Prof. dr. ir. H.W.J. Russchenberg	Delft University of Technology
Prof. dr. A. Petzold	Bergische Universität Wuppertal, Germany
Prof. dr. P. Hoor	Johannes Gutenberg University Mainz, Germany
Dr. F. Yin	Delft University of Technology
Dr. M. Righi	German Aerospace Center, Germany
Prof. dr. ir. B.J.H. van de Wiel	Delft University of Technology, *reserve member*

This doctoral thesis was supported by the DLR aviation research programme (Eco2Fly project) and by the European Commission via their Horizon 2020 Research and Innovation Programme (ACACIA project, grant no. 875036).

Keywords: Aircraft exhaust plume model, double-box model, subsonic aircraft emission, plume dispersion, diffusion dynamics, aviation-induced aerosols, aerosol microphysics, sulfate, soot, particle mass and number concentrations, aerosol-indirect effect, aerosol-climate effect

Cover by: Jonas Hendricks, Aircraft landing at Corfu Airport

To my dearest grandfather, my mentor and inspiration, Sai Kaka— affectionately known as Aaba

CONTENTS

SUMMARY

Aircraft emissions at typical cruise altitude (approximately 9-13 km) comprise of a diverse array of chemical compounds, including aerosols and their precursor gases. Recent global modelling studies have suggested that these aviation-induced aerosol particles can be transported downward to the lower atmospheric layers, where they may influence and alter the microphysical properties of low clouds such as droplet size and distribution and hence modify their radiative characteristics. However, before these particles are transported downward, they undergo a series of chemical and microphysical transformations within the aircraft exhaust plume, collectively referred to as aging processes. Due to their coarser spatial resolution (~100 km), the global aerosol-climate models are limited in their ability to accurately represent the microphysical processes at the subgrid-scale level, consequently resulting in large uncertainties in estimating the aviation impact on aerosol particles generated by aircraft emissions. This especially concerns the aerosol number concentration and size, which are key quantities for estimating the aerosol indirect effect for low-level, liquid-phase clouds.

In this thesis, a double-box aircraft exhaust plume model is developed by extending the framework of the well-established MADE3 single-box model, incorporating additional parametrisation to capture the spatial and temporal evolution of aerosol dynamics within the aircraft exhaust plume. The plume model is designed to explicitly simulate the aerosol microphysics inside a gradually dispersing aircraft exhaust plume, together with a simplified representation of the vortex regime (starting ~10 s behind the aircraft) which simulates the interaction of aerosols with short-lived contrail ice particles. This thesis primarily focuses on sulfate (SO_4) and soot aerosols, together with the total number concentration of aerosols emitted in the exhaust plume of an aircraft. The model is specifically designed to provide a more accurate representation of the microphysical processes occurring within an aircraft exhaust plume which alters the aerosol dynamics at the plume scale. The plume model is initialised at the end of the jet phase, approximately 10 seconds after the emission, using measured initial size distribution parameters for standard aircraft operating conditions together with other aircraft operational and emission parameters such as fuel consumption, speed, and emission factors of emitted species. In order to ensure the validity of the double-box plume model, I performed different numerical and parametric tests. The numerical tests confirmed the correct implementation of the extension from single- to double-box plume model. The parametric study in combination with the tendency diagnostics showed that the model reliably captures the expected sensitivity of aerosol number and size to several physical parameters, in line with theory and with previous global applications of MADE3.

The plume model is used to quantify the aviation-induced particle number concentration at the end of the dispersion regime (~46 h) by comparing the results from the plume approach with the results obtained by the instantaneous dispersion approach commonly applied by the global models. The difference between the plume approach

and the instantaneous dispersion approach allows to define a plume correction: for typical cruise conditions over the North Atlantic and typical aviation emission parameters, the plume correction for aviation-induced particle number concentration ranges between –15% and –4% as quantified for the first time in this study, depending on the presence or absence of the short-lived contrail ice in the vortex regime, respectively. These negative corrections indicate that the plume approach simulates a lower aviation-induced particle number concentration than the instantaneous dispersion.

In order to understand the influence of the microphysical processes and diffusion dynamics on the aerosol evolution inside an aircraft plume, tendency diagnostics are implemented in the plume model to track the impact of the individual processes on the aerosol properties. This analysis shows that the negative value of the plume correction is due to the higher efficiency of the coagulation in the plume model, partly counteracted by nucleation, leading to a lower number concentration of aviation-induced particles in the plume approach. Sensitivity studies performed over different regions highlight a large variability in the plume correction between –12% for Europe and –43% for China, thus signifying the importance of background conditions for the plume microphysics. Parametric studies performed on various aviation emission parameters used to initialise the plume model further demonstrate the high relevance of short-lived contrail ice in the vortex regime, which accounts for the aerosol-ice interaction. These interactions lead to a considerable reduction in aviation-induced aerosol number concentrations, particularly in the early stages of plume evolution. Moreover, the parametric studies show a large sensitivity towards aviation fuel sulfur content (FSC), driving sulfur dioxide (SO_2) emissions and gas-phase sulfuric acid (H_2SO_4) formation, which in turn is a primary driver for the nucleation process.

The double-box aircraft exhaust plume model MADE3 (v4.0) presented in this thesis is ready for application in global model studies. The model configuration is highly flexible with low computational costs which means that it can be effectively implemented for both online and offline parametrisation. The results from the plume model can be used to better initialise the aviation emissions in global model simulations and can contribute to a refined quantification of the climate impact of aviation-induced aerosol particles on clouds.

SAMENVATTING

Vliegtuigemissies op typische kruishoogtes (ongeveer 9–13 km) bestaan uit een diverse reeks chemische verbindingen, waaronder aerosolen en hun precursor-gassen. Recente wereldwijde modelstudies hebben gesuggereerd dat deze door de luchtvaart geïnduceerde aerosoldeeltjes naar de lagere atmosferische lagen kunnen worden getransporteerd, waar ze de microfysische eigenschappen van lage wolken, zoals druppelgrootte en -verdeling, kunnen beïnvloeden en daardoor hun stralingskenmerken kunnen wijzigen. Voordat deze deeltjes echter naar lagere lagen worden getransporteerd, ondergaan ze een reeks chemische en microfysische transformaties binnen de uitlaatpluim van het vliegtuig, gezamenlijk aangeduid als verouderingsprocessen. Door hun grovere ruimtelijke resolutie (~100 km) zijn globale aerosol-klimaatmodellen beperkt in hun vermogen om de microfysische processen op subgrid-schaal nauwkeurig weer te geven, wat resulteert in grote onzekerheden bij het schatten van de impact van de luchtvaart op aerosoldeeltjes die door vliegtuigemissies worden gegenereerd. Dit geldt met name voor de aerosoldeeltjesaantallen en -grootte, die cruciale grootheden zijn voor het inschatten van het indirecte aerosol-effect op lage, vloeibare wolken.

In dit proefschrift is een double-box model van de vliegtuigaansluitende uitlaatpluim ontwikkeld door het bestaande MADE3 single-box model uit te breiden. Hierbij is extra parametrisatie opgenomen om de ruimtelijke en temporele evolutie van aerosoldynamica binnen de uitlaatpluim te simuleren. Het pluimmodel is ontworpen om expliciet de aerosol-microfysica in een geleidelijk verspreidende vliegtuigaansluitende uitlaatpluim te simuleren, samen met een vereenvoudigde representatie van het vortexregime (beginnende ~10 s achter het vliegtuig), dat de interactie van aerosolen met kortlevende contrail-ijskristallen simuleert. Dit proefschrift richt zich voornamelijk op sulfaat (SO_4) en roetaerosolen, samen met de totale aantalconcentratie van aerosolen die in de uitlaatpluim van een vliegtuig worden uitgestoten. Het model is specifiek ontworpen om een nauwkeurigere weergave te bieden van de microfysische processen die plaatsvinden in een vliegtuigaansluitende uitlaatpluim, wat de aerosoldynamica op pluimschaal beïnvloedt. Het pluimmodel wordt geïnitialiseerd aan het einde van de straalfase, ongeveer 10 seconden na emissie, met gemeten initiële grootteverdelingsparameters voor standaard vliegoperaties, samen met andere operationele en emissieparameters van het vliegtuig, zoals brandstofverbruik, snelheid en emissiefactoren van uitgestoten stoffen.

Om de validiteit van het double-box pluimmodel te waarborgen, zijn verschillende numerieke en parametrische tests uitgevoerd. De numerieke tests bevestigden de correcte implementatie van de uitbreiding van het single-box naar het double-box model. De parametrische studie, in combinatie met tendensdiagnostiek, toonde aan dat het model betrouwbaar de verwachte gevoeligheid van aerosol aantal en grootte voor verschillende fysieke parameters vastlegt, in overeenstemming met theorie en eerdere globale toepassingen van MADE3.

Het pluimmodel wordt gebruikt om de door de luchtvaart geïnduceerde aerosol-

aantallen aan het einde van het verspreidingsregime (~46 h) te kwantificeren door de resultaten van de pluim-aanpak te vergelijken met de resultaten van de instantane verspreidingsaanpak die vaak door globale modellen wordt toegepast. Het verschil tussen de pluim- en instantane verspreidingsaanpak maakt het mogelijk een pluimcorrectie te definiëren: onder typische kruiscondities boven de Noord-Atlantische Oceaan en met typische luchtvaarteigenschappen varieert de pluimcorrectie voor de door de luchtvaart geïnduceerde aerosol-aantallen tussen –15% en –4%, afhankelijk van de aanwezigheid van kortlevende contrail-ijskristallen in het vortexregime. Deze negatieve correcties geven aan dat de pluim-aanpak lagere door de luchtvaart geïnduceerde aerosol-aantallen simuleert dan de instantane verspreidingsaanpak.

Om het effect van microfysische processen en diffusiedynamica op de evolutie van aerosolen in een vliegtuigaansluitende pluim te begrijpen, zijn tendensdiagnostieken in het pluimmodel geïmplementeerd om de impact van individuele processen op de aerosol-eigenschappen te volgen. Deze analyse toont aan dat de negatieve waarde van de pluimcorrectie te wijten is aan de hogere efficiëntie van coagulatie in het pluimmodel, gedeeltelijk tegengewerkt door nucleatie, wat leidt tot een lagere aantalconcentratie van door de luchtvaart geïnduceerde aerosolen in de pluim-aanpak. Gevoeligheidsstudies in verschillende regio's laten een grote variabiliteit zien in de pluimcorrectie, variërend van –12% voor Europa tot –43% voor China, wat het belang van achtergrondcondities voor de pluimmicrofysica benadrukt. Parametrische studies van verschillende emissieparameters die gebruikt worden om het pluimmodel te initialiseren, tonen verder het grote belang van kortlevende contrail-ijskristallen in het vortexregime, die verantwoordelijk zijn voor de aerosol-ijsinteractie. Deze interacties leiden tot een aanzienlijke reductie van de door de luchtvaart geïnduceerde aerosol-aantallen, met name in de vroege stadia van de pluimevolutie. Daarnaast tonen de parametrische studies een grote gevoeligheid voor het zwavelgehalte van vliegtuigbrandstof, dat zwaveldioxide (SO_2) emissies en gasfase zwavelzuur (H_2SO_4) vormt, wat op zijn beurt een primaire drijver is voor het nucleatieproces.

Het double-box vliegtuigaansluitende uitlaatpluimmodel MADE3 (v4.0) dat in dit proefschrift wordt gepresenteerd, is klaar voor toepassing in globale modelstudies. De modelconfiguratie is zeer flexibel met lage rekencapaciteit, waardoor het effectief kan worden toegepast voor zowel online als offline parametrisatie. De resultaten van het pluimmodel kunnen worden gebruikt om de initialisatie van vliegtuigemissies in globale modelsimulaties te verbeteren en kunnen bijdragen aan een verfijnde kwantificering van de klimaateffecten van door de luchtvaart geïnduceerde aerosolen op wolken.

1

INTRODUCTION AND MOTIVATION

1.1. ATMOSPHERIC AEROSOLS AND THEIR IMPORTANCE IN THE CLIMATE SYSTEM

Aerosols are defined as dispersed systems of particulate matter in either solid or liquid phases, suspended in the atmosphere [1, 2]. Aerosol particles, including e.g. sulfate (SO_4), nitrate (NO_3), black and organic carbon (BC and OC, respectively), sea salt and pollen, can originate from both natural sources (e.g., volcanic eruptions, deserts, sea spray, wildfires) and anthropogenic activities (e.g., fossil fuel combustion, biomass burning, mining, cement production). Fossil fuel combustion, for instance, accounts for approximately 72% of global sulfur dioxide (SO_2) emissions, which are the primary precursors of SO_4 aerosols in the troposphere [3, 4]. Between 1990 and 2015, global sulfur emissions decreased by 32% [5–7] primarily due to a combination of regulatory policies, technological advancements, and changes in fuel use. Model-based studies estimate the global annual SO_2 reduction at 5.2% per year with regional variations [8, 9]. The most significant reduction occurred in Europe, where emissions dropped by 54%, while North America saw a modest decline of 7%. The reduction in Europe corresponds to an average decrease of 3.3% per year between 2000 and 2015 [8]. In contrast, sulfur emissions in regions such as Eastern Asia and India increased by 50% during the same period [8, 9].

Based on their source of origin, aerosol particles are classified as either primary or secondary aerosols. Primary aerosols are directly emitted from natural sources and anthropogenic sources, while secondary aerosols form in the atmosphere from precursor gases. Atmospheric aerosols can be further classified based on their chemical composition and physical properties. However, characterizing aerosol particles according to their specific chemical composition is inherently complex due to the large variety of involved chemical species. To simplify this classification, aerosols are grouped into types or species that correspond to the chemical characteristics of their sources. Examples include inorganic species (e.g., SO_4, ammonium NH_4, NO_3), organic species (e.g., organic carbon or particulate organic matter (POM)), soot (carbonaceous species resulting from incomplete combustion of biomass and fossil fuels), and biogenic aerosol species [10].

1

Furthermore, aerosol particles exhibit a range of sizes and mixing states. Their sizes vary from a few nanometers (nm) to several tens of micrometers (μm), with typical atmospheric concentrations ranging from 1 to 10^8 cm^{-3}. The aerosol mixing state is defined as the distribution of chemical species across a population of particles. This can be internally mixed, when the particles consist of the same mixture of chemical species, or externally mixed when they consist of pure chemical species and have distinct compositions [2]. The mixing state typically changes over time as a result of microphysical properties changing the properties of the particles.

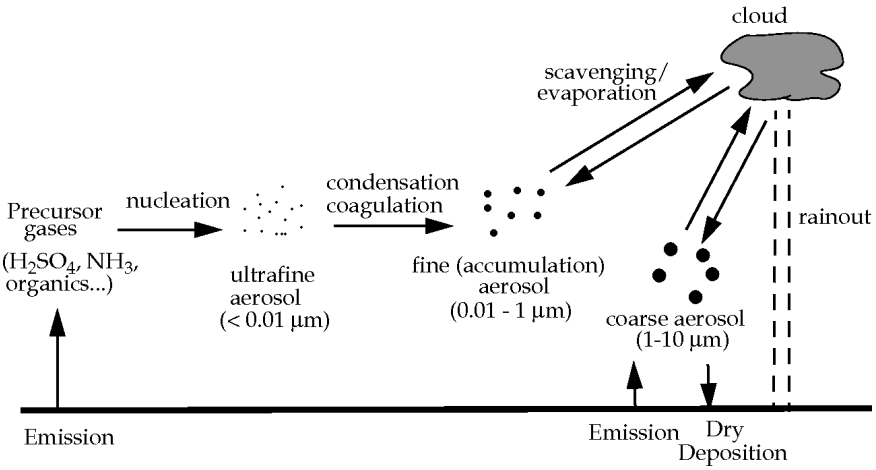

Figure 1.1: Illustration of the key microphysical processes driving the transformation of aerosol particles in terms of their mass, number and size in the atmosphere, often termed as aging process. This figure is taken from https://www.global-climate-change.org.uk/6-6-1.php, last access: 03.07.2025.

Aerosols are highly complex particles, therefore to fully characterize an aerosol population, a detailed comprehensive data is required to understand their dynamics. This includes information on the aerosol species mass, number concentration, size distribution, in different size ranges and mixing state. Each of these factors plays a crucial role in understanding the particles behaviour and impact on both climate and air quality. Aerosols are highly dynamic, and their interactions with other atmospheric components such as gases and cloud droplets further influence their properties and affects the environment.

The typical life-cycle of atmospheric aerosols includes the emission of primary particles and the formation of secondary particles from precursor gases. These particles are transported through the atmosphere via advection and vertical motions. Their properties evolve through chemical and microphysical aging process, and they are eventually removed from the atmosphere by sedimentation and scavenging to the Earth's surface. During the process of aging, aerosol particles are subject to several chemical and microphysical changes in the atmosphere (see Fig. 1.1) which can affect their size, composition and mixing state [2]. These processes include, for instance, gas-to-particle conversion, condensation of low-volatile gases onto the existing particles, and coagulation of particles while colliding with each other. Aerosol particles have different atmospheric

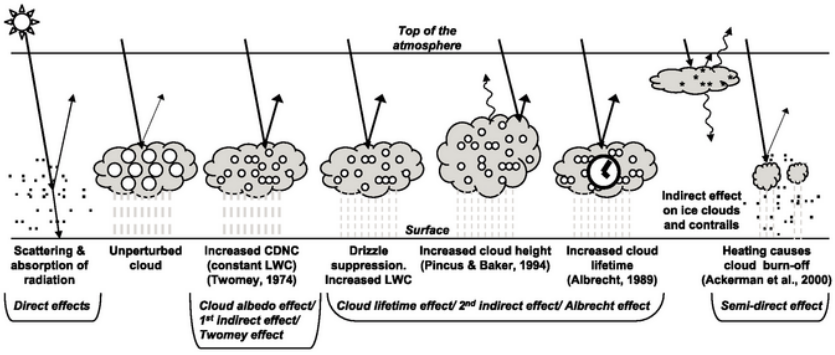

Figure 1.2: Schematic representation of aerosol effects, highlighting two key mechanisms relevant to this study: the direct effect and the indirect effect, specifically aerosol-cloud interactions. The small black dots denote aerosol particles, while the larger open circles represent cloud droplets. This figure is taken from IPCC 4th Assessment Report (chapter-2) [4].

lifetimes, from a few minutes to hours or days, depending on their chemical and microphysical properties [10].

Once airborne, aerosol particles significantly affect the global radiation budget by interacting with both incoming solar radiation and outgoing terrestrial radiation through various mechanisms [4]. These interactions can be categorized as direct effects or aerosol-radiation interaction (ARI), and indirect effects or aerosol-cloud interactions (ACI), see Fig. 1.2. ARI is the absorption and scattering of the incoming solar radiation by aerosols, resulting in a warming and a cooling effect, respectively. ACI is the impact of aerosols on the microphysical properties of the clouds, such as droplet or ice crystal number concentration as well as liquid and ice water content, affecting cloud reflectivity and lifetime [4, 11]. For example, aqueous-phase aerosol particles favour the formation of cloud droplets in liquid clouds, while solid and/or crystalline particles contribute to the formation of ice crystals in ice and mixed-phase clouds.

Among the aerosol types, SO_4 particles are particularly significant for both ARI and ACI due to their optical properties, to their ability to mix with other components (e.g., coating of insoluble particles via condensation), and to their efficiency as cloud condensation nuclei (CCNs) in liquid clouds. Clouds play a key role in regulating the Earth's global temperature by either cooling the atmosphere through reflection of incoming solar radiation or warming it by absorbing and trapping terrestrial radiation [12]. The combined effect strongly depends on the cloud type, its microphysical properties and altitude. Ice clouds, for instance, have a net warming effect as they trap the outgoing infrared radiation, while low clouds promote cooling by reflecting incoming solar radiation, thereby enhancing Earth's albedo [13]. Cloud droplets form after the condensation of supersaturated water vapour on the surface of the soluble or hydrophilic aerosol particles such as sulphate, while the homogeneous droplet formation is highly unlikely in the atmosphere as the pure water droplets require very high supersaturation to form

without any seed [11]. Through their impact on cloud formation, albedo, and lifetime, aerosols contribute to the radiative effects of clouds, making them pivotal in influencing the global climate. Studies also reveal that only a selected fraction of atmospheric aerosols (generally those with diameters of approximately 0.1 μm or larger) can act as CCNs [14, 15]. However, in addition to particle size, this also depends on additional factors such as the chemical composition, mixing state and the environmental conditions [16].

The aim of this thesis is to understand the transformation of aviation-induced aerosols due to the subgrid-scale microphysical processes inside an aircraft plume, to help understanding their role in altering the microphysical properties of the low clouds and thereby contribute to the understanding of aviation climate effects.

1.2. THE ROLE OF AVIATION-INDUCED AEROSOLS

The emitted aircraft exhaust at typical cruise altitude (9-13 km) [3] consists of a blend of both CO_2 and non-CO_2 compounds. As for other anthropogenic sectors, CO_2 is one of the prominently emitted components from aviation which persists in the atmosphere for decades to centuries [17] and contribute significantly to the global radiation budget. However, only one third of the aviation-induced climate effect is attributable to the CO_2 emissions, whereas the non-CO_2 emissions are responsible for the remaining two thirds [18, 19]. The latter are released in the form of gases, such as nitrogen oxides (NO_x=NO+NO_2), water vapour (H_2O), sulfur dioxide (SO_2), volatile organic compounds (VOC), and aerosols, mainly sulfate (SO_4) and soot (see Fig. 1.3). Water vapour and soot particles are also associated to the formation of contrails [20]. Unlike CO_2, the atmospheric lifetime of these emitted gases and aerosol particles is relatively short, usually hours to days depending on the location and altitude of release, during which they contribute to aviation climate effect.

The climate effect is usually expressed using a metric called effective radiative forcing (ERF). This is defined as "the energy gained or lost by the Earth system following an imposed perturbation (for instance in greenhouse gases, aerosols or solar irradiance) and is determined by the change in the net downward radiative flux at the top-of-the-atmosphere after the system has adjusted to the perturbation but excluding the radiative response to changes in surface temperature" [21]. According to this definition, a positive (negative) ERF represents a warming (cooling) effect. Based on a previous study [18], the net ERF as contributed by the global aviation (CO_2 + non-CO_2, including contrail cirrus, but excluding the effect of AIR) is about +0.1 W m^{-2}, representing about 3.7% of the total anthropogenic ERF reported by the IPCC AR6 [21]. With an increasing demand of commercial air transportation, the fuel consumption is expected to increase which will eventually increase the global aviation emissions compared to the previous years [22] and may further increase to the aviation ERF.

Considering the well-known radiative properties of CO_2, Fig. 1.3 shows a significantly positive forcing (+34.3 mW m^{-2}) exerted by the aircraft CO_2 emissions with a high level of confidence. Among the non-CO_2 emissions, contrail cirrus also exhibits a substantially large positive forcing (+57.4 mW m^{-2}), accompanied by a large uncertainty as a result of the complex processes involving the formation and evolution of contrails. Aviation-induced NO_x emissions have multiple climate effect, contributing both positive and neg-

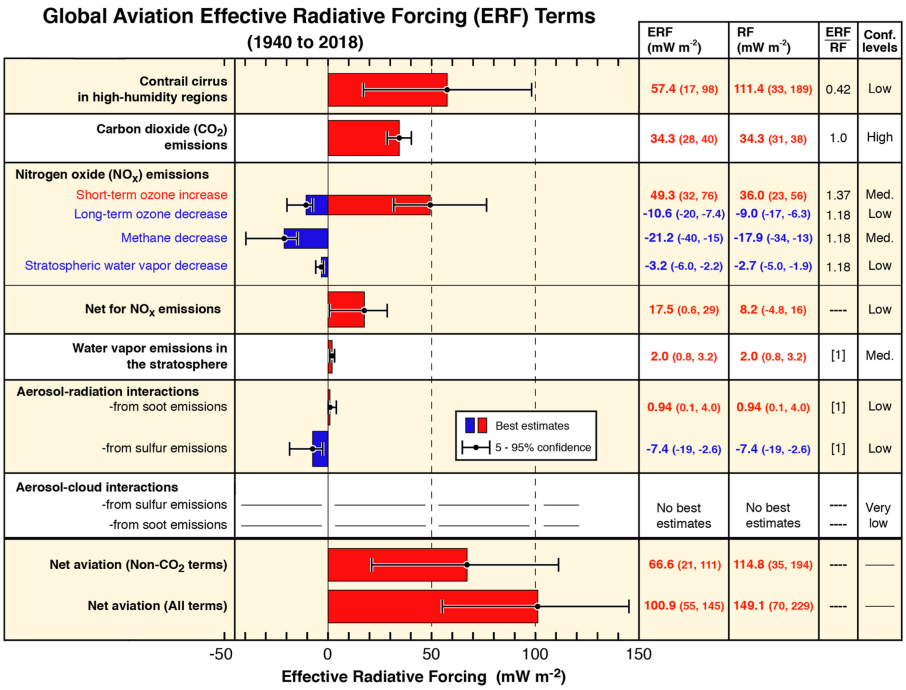

Figure 1.3: Schematic overview of the effective radiative forcing (ERF) components attributed to the global aviation emissions from 1940 to 2018, categorizing the aviation-induced climate effects as warming (red bars) and cooling (blue bars). Here, the bars represent the best estimates, while the whiskers represent the confidence interval of 5-95%. This figure is taken from Lee et al. [18].

ative forcings. NO_x induces a reduction in methane lifetime and since methane is a greenhouse gas this results in a net cooling effect (–21.2 mW m^{-2}). This partly offsets the warming effect due to NO_x-induced ozone (O_3) formation (+49.3 mW m^{-2}). Furthermore, the aviation-induced NO_x also contributes to an indirect reduction in the stratospheric water vapor y altering the CH_4 concentration, which eventually leads to a cooling effect of about –2.8 mW m^{-2}. The net effect of NO_x emissions, however, is positive, although its exact magnitude is uncertain. Water vapour emissions in the stratopshere contributes a warming of +2.0 mW m^{-2}.

In terms of aviation emitted aerosols, the aviation soot and SO_4 are considered as the predominant sources of primary and secondary aerosol particles. Soot particles are emitted by an aircraft engine as a result of incomplete combustion. These particles are composed of a mixture of black carbon (BC) and organic carbon (OC) [23]. The ARI of aviation soot imposes a positive ERF or warming effect on the global climate (+2.86 mW m^{-2} as suggested by Lee et al. [18]), by absorbing the incoming short-wave radiations and confining the terrestrial long-wave radiations [24]. The water vapour emissions could lead to contrail formation on emitted soot particles [18, 25–27]. These soot particles can also influence the properties of natural cirrus clouds, which could lead to either a warming or a cooling effect depending on the atmospheric conditions and par-

ticle properties [28–33]. However, the related processes are still highly uncertain and no best estimate of the resulting ERF is currently available.

The aviation-induced SO_4, however, have a negative ERF or the cooling effect of about –20 mW m^{-2} (ARI) as suggested by Lee et al. [18]. These aviation-induced SO_4 particles also have the potential to alter the microphysical properties of the low-level liquid clouds by increasing their cloud droplet number concentration (CDNC), thus increasing the cloud reflectivity and inducing a short-wave cooling [27]. Although Fig. 1.3 does not include a best estimate for the aerosol-indirect effect, a previous study by Gettelman et al. [27] reports a cumulative effect (both direct and indirect) of –46 mW m^{-2}, particularly for the SO_4 aerosol particles in the atmosphere. While the aviation-induced ARI shows a net cooling effect, the aerosol-cloud interaction or the ACI remains highly uncertain due to the uncertainties in both cloud microphysics as well as model parametrisations which makes it difficult to assess the total climate effect of aviation-induced aerosols. Due to these inherent complexities of ACI, some of the previous studies have reported a wide range of uncertainties which are discussed in details in Sect. 1.3 and are the main motivation of this thesis.

1.3. EXISTING UNCERTAINTIES AND SCIENTIFIC CHALLENGES

As discussed in the previous section, several studies [18, 29, 32, 34] demonstrate a large range of uncertainties associated with the aviation-induced ACI resulting from several complex factors, including limitations in observational data, complex cloud microphysics, variability in aerosol properties and modelling parametrisations. Global climate models are the main tools to quantify the climate effects (including the aviation-related ERFs). Climate models are complex numerical systems representing the involved physical, chemical and dynamic processes, and their impact on the Earth radiation budget. Given the complexity of these processes and the different temporal and spatial scales on which they act, these models need to make several assumptions and simplifications in order to represent the aforementioned processes in a feasible way. One such simplification concerns the way emissions (and specifically aircraft emissions) are treated in the models. Existing global climate models typically consider a homogeneous and instantaneous mixing of air masses in a large-scale grid box, neglecting essential processes at the plume-scale [35–39]. This is an intrinsic limitation of global models due to their coarse spatial resolution (~100 km), making it impossible to resolve the subgrid-scale non-linear plume processes and transformation of emitted aerosol particles in the expanding and dispersing aircraft plume [40]. This may in turn affect the simulated properties of aviation-induced particles, resulting in large uncertainties and a possible overestimation of their climate effect [18]. This may also explain the large diversity in the currently available model-based estimate of the radiative forcing from the interactions of aviation-aerosol with low-level clouds. Fig. 1.4 shows the climate effects derived from the aviation-induced aerosols effect as calculated by the existing studies. Here, Righi et al. [34] quantified an ERF of –15.4 mW m^{-2} and –69.5 mW m^{-2}, depending on the assumed size of emitted SO_4 particles, with smaller sizes (and hence higher particle numbers) resulting in a the stronger climate effect. A similar sensitivity was found by Gettelman and Chen [41], who reported an ERF of –164 mW m^{-2}, –46 mW m^{-2} and −23 mW m^{-2} for an initial SO_4 particle size of 8 nm, 14 nm and 21 nm, respectively. Ad-

ditionally, Kapadia et al. [42] estimated an ERF of –23.6 mW m^{-2}, also showing that the ERF of aviation-aerosol is sensitive to the sulfur content of the jet fuel. The most recent assessment by Righi et al. [43] quantified an ERF of –64 mW m^{-2}.

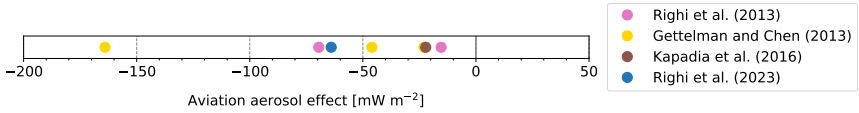

Figure 1.4: The bar-plot represent the values of aerosol-indirect effect in mW m^{-2} for aviation-induced SO_4 as taken from existing literature [27, 34, 42, 43].

To account for these limitations and to contribute to a reduction in these uncertainties, in this thesis I develop and apply a double-box plume model to examine the microphysical transformation of aircraft-induced aerosol particles within an aircraft exhaust plume and to quantify the impact of these processes on the resulting particle properties at the end of the plume dispersion. The plume model explicitly accounts for the aerosol transformation processes inside a growing and dispersing aircraft plume. I consider two approaches and compare the properties of aviation-induced aerosols at the end of the plume dispersion in both approaches. In the plume approach, the plume dispersion is explicitly simulated using two model boxes representing the plume and the background. In the instantaneous dispersion approach, the plume is instantaneously dispersed into the background within a single box, an approach adopted by coarse-resolution global models. I define the difference between these two approaches as the plume correction for the aviation-induced particles properties, i.e. mass and number concentration and size. The results of the plume model can later be applied to develop conversion factors (see Ch. 7) for particle mass and number emissions by aviation, and used as an input to global model simulations, thus correcting for the unresolved plume processes in these models.

1.4. RESEARCH QUESTIONS

In order to accurately quantify the climate effect of aviation emissions, it is essential to obtain a full understanding of the aviation-induced aerosol effect, particularly in the context of aerosol-cloud interactions. To achieve progress in this area, a comprehensive analysis of the non-linear microphysical processes of aerosols at plume scales is required. Accordingly, this thesis addresses the following research questions:

1. **How are aviation-induced aerosols dispersed and transformed in the vortex and dispersion regime of an aircraft exhaust plume?** The objective is to explore a new method to attain an improved representation of aerosol microphysical processes inside a gradually dispersing aircraft plume.

2. **What are the typical concentrations and size distributions of aviation-induced aerosol particles at the end of the plume dispersion?** The objective is to acquire a thorough understanding of the microphysical processes involved in the particle transformation and their effects on species mass concentration, particle number

concentration and particle size distribution inside a dispersing aircraft plume, especially towards the end of the dispersion regime. In addition to this, I compare the plume-scale processes with an approach representative of the global models, to quantify the impact of the plume processes and calculate a corresponding plume correction.

3. **On which parameters and initial conditions do these typical concentrations depend?** The objective is to examine different aircraft operational parameters together with the background conditions along the flight path which may affect the plume-scale processes and the resulting aviation aerosols and their properties.

4. **How can the existing uncertainties surrounding the aerosol indirect effect, particularly with regard to aviation-induced sulfate aerosols and aerosol number concentrations, be reduced?** The objective is to introduce an application concept to later integrate the outcome of this thesis into global climate models, thus allowing for a refined assessments of the impact of aviation aerosol on low-level clouds.

1.5. WHAT THIS RESEARCH DELIVERS

To answer the research questions outlined above, a double-box plume model is developed in this thesis based on the aerosol microphysics of the MADE3 (third-generation Modal Aerosol Dynamics model for Europe, adapted for global simulations) submodel [Sect. 2.2; 44]. Here, I extend MADE3 into a two-box configuration, to represent an aircraft plume and the surrounding background, respectively, as well as their interaction, following the approach by Petry et al. [45], originally developed for gas-phase chemistry. The plume model allows to explicitly simulate the particle transformation processes within the dispersing aircraft plume, while accounting for the diffusion dynamics and the entrainment of background air into the dispersing plume. The aerosol processes are represented using the MADE3 microphysical routines and account for particle coagulation, condensation of low-volatility gases on existing particles, nucleation of sulfuric acid (H_2SO_4) into aerosol SO_4 (new particle formation), and gas-to-particle partitioning. In addition to the standard MADE3 aerosol microphysics, the plume approach in the double-box plume model also features a simple, physically-based representation of the aerosol coagulation with contrail ice crystals during the short vortex regime (~2 min) at the beginning of the plume evolution. As the focus of this study is on aviation aerosol, I focus in particular on SO_4 aerosols, commonly found in the young aircraft plume or formed via oxidation of precursor SO_2 into H_2SO_4 and subsequent condensation or nucleation, as well as soot particles. The double-box plume model is initialised with typical aircraft operational parameters from available literature (engine and fuel type, fuel sulfur content, emission indices) along with the aerosol size parameters representative of a young aircraft plume, shortly after the emission [46]. The model is also driven by the background concentration of particles and precursor gases at typical cruise altitude and by the basic meteorological parameters (temperature, pressure and relative humidity). In order to explore the impact of the initialisation parameters on the particle transformation inside a dispersing aircraft plume, I perform a series of sensitivity studies, providing an insight on the range of variability in terms of aviation-induced aerosol effects. This also allows to identify the most sensitive parameters of the double-box plume model and

the related uncertainty in the resulting plume correction, thus providing insights for future measurement campaigns targeting aviation effects on aerosol and climate [see e.g., 47].

Several existing models are capable of simulating regional and gaseous chemistry of fine aerosol particles [48], including the chemistry of particles in the aircraft plumes and their transformation via dispersion and microphysical transformation [38, 40, 45, 49–51]. The double-box plume model presented here specifically addresses the limitations of global models to simulate the impact of aviation aerosols, by comparing the instantaneous approach typical of those models with a more sophisticated representation of the aerosol processes at the plume-scale. Note that in this thesis, I do not aim to develop a plume dynamic model to simulate the eddies in the wake vortices as done, for example, in Unterstrasser et al. [52]. My main goal is to develop a model that can improve the representation of microphysical processes responsible for aerosol transformation inside a dispersing aircraft plume, which are relevant for the indirect effect of aviation emitted aerosols and the resulting climate effect.

The double-box plume model is implemented in the framework of the Modular Earth Submodel System [MESSy; 53] and can be flexibly applied by varying a large number of input parameters. Thanks to its extremely low computational demand (few seconds on a single CPU), it can be used to explore a wide variety of scenarios and conditions and, in principle, it can also be implemented as an online parametrisation within a global model, to account for the unresolved aerosol processes in a dispersing plume.

1.6. DISSERTATION STRUCTURE

The structure of this thesis is organized into nine chapters, each addressing distinct aspects of the development and application of the double-box aircraft exhaust plume model MADE3 (v4.0). The present chapter established the foundational context and introduced the research topic, delineating the objectives and significance of the study together with the framed research questions for this study. Chapter 2 provides a brief overview of the existing global aerosol modelling approach with MADE3 within the global chemistry-climate model EMAC, along with a detailed description of the aerosol submodel MADE3, which is widely used to study the climate impacts of atmospheric aerosols. In addition, the chapter also introduces the classification of aircraft plume regimes based on the time after emission, which serves as the basis for the functionality of the plume model later introduced in this thesis. Chapter 3 provides a comprehensive description of the double-box plume model, detailing its theoretical and technical underpinnings and key components such as the online sulfate chemistry and the plume diffusion dynamics required to run the plume model, also emphasizing on the technical aspects of model initialisation, the implementation of the tendency diagnostics to quantify the impact of individual microphysical processes on the aerosol properties, alongside the presentation of numerical tests designed to validate the accuracy and performance of model. Chapter 4 presents the offline methodology used to calculate the aviation effects and plume corrections based on the plume model output. This methodology is subsequently employed in all analyses throughout the thesis. Furthermore, the chapter introduces the first application of the plume model using a reference setup representative of typical conditions over the North Atlantic, illustrating its practical relevance and functionality

in real-world scenarios together with a sensitivity experiment on the nucleation process. Chapter 5 focuses on the model application in different regions to understand the impact of different background conditions on the model results. Chapter 6 encompasses a series of parametric studies performed on several plume model parameters, which assess the sensitivity of the plume model on initial parameters and their robustness across varying conditions. Finally, Chapter 7 proposes a concept to introduce conversion factors to estimate aviation number emission in global model implicitly account for the plume processes analysed in this work. This chapter also summarises the technical and methodological limitations of the model.

The thesis concludes in Chapter 8 by providing comprehensive technical explanations that answer the research questions. Finally Chapter 9 provides the insight into the outlook discussing potential future applications of the plume model along with potential extensions of the model and its implications for advancing research in the field. This structured approach ensures a comprehensive understanding of the plume model development, initialisation parameters and methods involved along with the prospective applications, thereby contributing significantly to the scientific discourse surrounding the topic.

2

AEROSOL MODELLING AND AVIATION

The preceding chapter introduced the background of this thesis, including the emission sources of aerosols (both natural and anthropogenic) and the atmospheric processes that govern the particles size and composition during their lifecylce in the atmosphere. It also highlights the significance of aerosols in the atmosphere, particularly their role in global radiation budget and finally discussing the existing uncertainties and challenges in modelling the climate effect of aviation-induced aerosols which has motivated this study. To elaborate further, the current chapter focuses on the existing numerical model capable of simulating aerosol dynamics and assess their climate effects and briefly discusses the large-scale atmospheric chemistry model EMAC with the aerosol submodel MADE3 (Sect. 2.1), which has been applied by several studies to quantify the climate effects of aviation-induced aerosols [27, 34, 42]. Particular attention is given to the modal aerosol submodel (MADE3; Sect. 2.2) and the different microphysical processes of MADE3 box model, responsible for the transformation of the aviation-aerosol particles. MADE3 is capable of simulating the evolution of atmospheric aerosols in terms of both size and composition and is designed for global and regional applications, making it well-suited to be extended into a double-box plume model for studying the microphysical evolution of aviation-induced aerosol particles within the aircraft exhaust plume. Prior to exploring the technical aspects of the plume model (Chapter 3), it is essential to establish a foundational understanding of an aircraft plume, as outlined in Sect. 2.3. This section discusses the dynamics of an aircraft plume along with its distinct phases or regimes, categorized based on the time of emission and their chemical microphysical characteristics. It also highlights the regimes that are most relevant to the scope of this thesis.

2.1. GLOBAL CLIMATE MODELS

The EMAC (ECHAM/MESSy Atmospheric Chemistry) model coupled with the aerosol submodel MADE3 (third-generation Modal Aerosol Dynamics model for Europe, adapted for global simulations) provides a robust framework for investigating the climate effects of aviation-induced aerosols. EMAC is a numerical chemistry and climate simulation system [32] combining the general circulation model (GCM) ECHAM5, with the Modular Earth Submodel System (MESSy) framework that includes submodels describing tropospheric and middle atmospheric processes and their interaction with oceans, land, and human influences. The EMAC model can be run at various horizontal and vertical resolutions depending on the scientific objective and computational resources. Typically, the horizontal resolution in EMAC ranges from T42 (~2.8° x 2.8°) to T106 (~1.1° x 1.1°), where "T" stands for triangular truncation in spectral space. In vertical scale, EMAC employs 31 to 91 vertical hybrid levels extending from the surface up to around 0.1 hPa (approximately 80 km altitude) [54, 55]. This resolution flexibility enables the model to simulate wide range of processes from the surface to the atmosphere, covering troposphere, stratosphere and mesosphere, allowing the model to perform both global-scale and regional-scale studies.

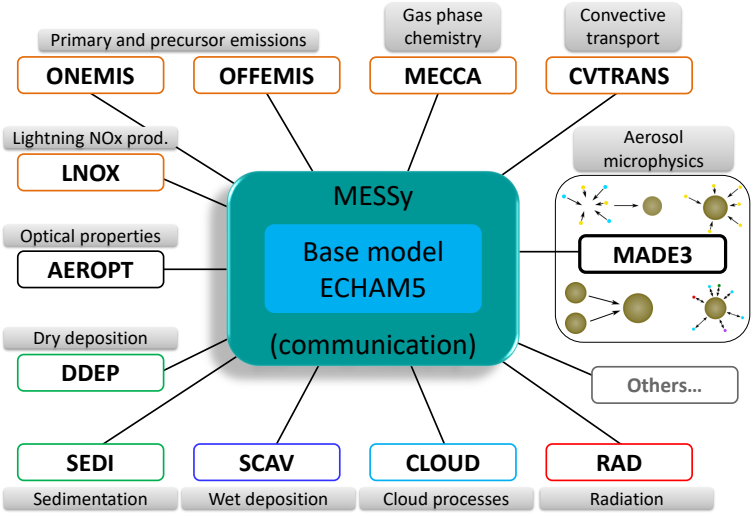

Figure 2.1: Schematic illustration of the MESSy infrastructure highlighting the base model ECHAM5 along with some of the submodels including the aerosol submodel MADE3 connected to the MESSy interface layer.

The Modular Earth Submodel Sytem [MESSy; 56] is a framework developed to modularize complex Earth System Models (ESMs) from process based modules known as submodels, thereby enhancing flexibility, transparency, and reproducibility in the atmospheric chemistry and climate modelling. These submodels represent different atmospheric processes, such as, emissions, aerosol microphysics and chemistry, heterogenous reaction rates, transportation, deposition etc. which are coupled using a standard-

ized user interface based on Fortran95 standard (ISO/IEC-1539-1) [53] within the MESSy framework (Fig. 2.1). MESSy is designed to allow users to activate or deactivate submodels according to the requirements of specific simulations. This modular architecture not only supports code reusability and easier model development but also facilitates the comparison of different process representations within a common modelling environment. As per Joeckel et al. [53], the MESSy framework is further updated to support parallel computing and the expansion of the submodel libraries. This evolution has significantly contributed to advancing atmospheric chemistry modelling by enabling comprehensive, traceable simulations of chemical and physical processes in the atmosphere under various temporal and spatial scales.

EMAC together with the aerosol submodel MADE3 is a comprehensive global-aerosol climate modelling system [57] that integrates detailed aerosol microphysics (Sect. 2.2) with atmospheric chemistry and climate dynamics [58]. The integration of MADE3 into EMAC enables the simulation of various aerosol processes, including gas–aerosol partitioning, new particle formation, coagulation, particle and precursor emissions, transport by advection, convection, and turbulent diffusion, aerosol precursor chemistry in the gas and liquid phases, cloud and precipitation scavenging of aerosols, as well as their dry deposition and sedimentation [57].

2.2. MADE3 AEROSOL MODEL

MADE3 is an aerosol microphysics scheme which is a part of MESSy. MADE3 represents nine aerosol species in nine lognormal modes (see Fig. 2.2) resulting from the combination of three mixing states i.e. fully soluble, insoluble, and mixed particles, with three size ranges, namely the Aitken, accumulation, and coarse mode [44, 57]. In this thesis I refer to the MADE3 species black carbon (BC) as soot for consistency with the terminology of aviation-related literature, although black carbon and soot are not exactly the same [23, 33]. Soot is a general term for the carbon-rich combustion particles and consists of a mixture of BC, organic carbon (OC), ash and other materials. In contrast, BC is the light-absorbing fraction of soot, composed of pure elemental carbon and is a well-defined term often used in climate research. Aerosol dynamics in MADE3 is calculated through various microphysical processes such as coagulation, condensation of low-volatility gases onto existing particles, nucleation (new particle formation) and gas-particle partitioning. The simulation of these processes in the model relies on the characteristics of the aerosol population. For instance, condensation requires a sufficient particle surface area, while a high density of small particles can trigger the coagulation process with larger particles, thereby altering particle number density [59]. Beyond these processes, MADE3 accounts for the internal redistribution of particles within and between different modes while maintaining the same mixing state. This adjustment is governed by assigned thresholds, enabling the model to manage the intra- and intermodal distribution of aerosol particles. These processes ensure that particles of the same type, whether remaining in the same mode or transitioning to another, are appropriately represented based on the prioritized microphysical properties of individual compounds [44].

Coagulation of aerosol particles. To simulate the particle coagulation process, MADE3 uses the Brownian coagulation kernel $\beta(D_1, D_2)$ as a function of the median diameters of

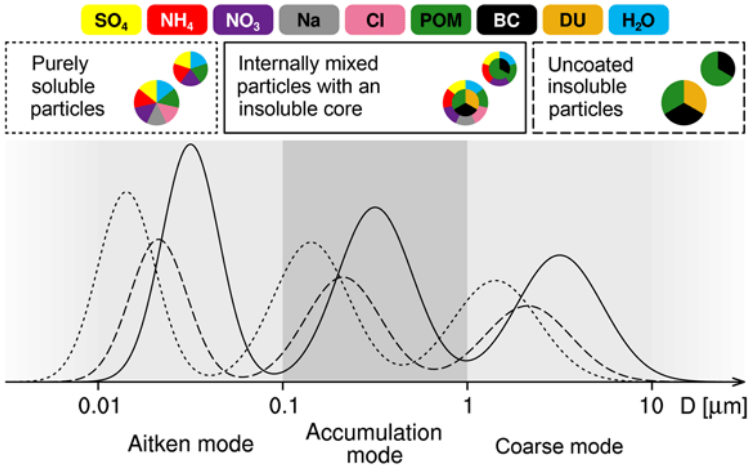

Figure 2.2: Schematic illustration of the aerosol submodel MADE3 [57]. It represents the aerosol species (shown by different colours) in three modes (Aitken, accumulation and coarse) in their corresponding mixing states (soluble, mixed and insoluble). The figure is taken from [44].

the coagulating modes D_1, D_2 [60] . The Brownian coagulation kernel defines the rate at which two particles collide due to their random motion. The coagulation process results in a reduction of smaller size particles with a corresponding growth of large size particles. It should be noted that coagulation is only responsible for changes in particle number concentration while conserving the mass. In MADE3, the coagulation routine is responsible for modelling the collision and merging of the particles which influence the size distribution and overall composition of the aerosol particles. This particle interaction results in a transfer of mass within and between the modes, ensuring that particle size distributions and mixing states are accurately represented. Coagulation in the model can be categorized based on Aquila et al. [61]:

1. Intermodal coagulation resulting in particle transfer to the larger mode.

2. Intramodal coagulation between particles of the same mode.

3. Assignment of the particles to different mixing states depending on the mass fraction x of the soluble material and water in final particles:

   (a) $x = 1$: soluble mode,

   (b) $0.1 \leq x < 1$: mixed mode,

   (c) $x < 0.1$: insoluble mode.

After determining the target mode of the coagulation process based on the above criteria, number concentrations are updated by solving the differential equation for the respective target modes at each timestep.

$$\left(\frac{dN_k}{dt}\right)_{\text{coag}} = \sum_{l=1}^{9}\sum_{m=1}^{9}\left(a_k^{lm}\int_0^\infty\int_0^\infty \beta(D_1D_2)\,n_l(D_1)\,n_m(D_2)\,dD_1D_2\right) \tag{2.1}$$

Here, $\frac{dN_k}{dt}$ refers to the rate of change of number concentration of aerosol particles in mode k. The matrix elements lm in the coagulation coefficient (Eq. 2.1) are used for the assignment of number concentration of the coagulated particles to the target mode. Similar to the number, mass concentration equations are also integrated for the growth and loss due to inter- and intramodal transfer rate [44].

The growth of aerosol particles in MADE3 is calculated using Brownian coagulation kernel $\beta(D_1, D_2)$ using two different expressions, depending on the size of particles. Since a single formula cannot accurately model all size ranges, blending of continuum and free molecular kernels allows physically realistic modelling across all atmospheric conditions [44, 60]. After calculating the coagulation kernels for both continuum and free molecular regimes, respectively, the model combines them using the halved harmonic mean to obtain an effective coagulation rate. This is further used to update and redistribute the particle number and mass concentrations across the aerosol modes, ensuring a realistic representation of coagulation in the model [44, 60].

Condensation of vapours onto existing particle surface. This process represents the condensation of low-volatility gases on existing particles by calculating the transfer rate of molecules from the gas phase to the aerosol phase at each timestep. Here, I focus explicitly on the condensation of H_2SO_4 (gas), which is a precursor gas contributing to the formation of sulfate aerosols in the model. Since H_2SO_4 has low vapour pressure, re-evaporation is denied and gas phase molecules are irreversibly transferred to aerosols. The H_2SO_4 condensation rate (Eq. 2.2) is calculated depending on the availability of aerosol particles to condense on. The total condensation flux of H_2SO_4 is the sum of rate of change of H_2SO_4 mass concentration ($c_{H_2SO_4,k}$) in mode (k):

$$\left(\frac{dc_{H_2SO_4,k}}{dt}\right)_{\text{cond}} = \int_0^\infty \frac{dm_p(D)}{dt}\,n_k(D)\,dD \tag{2.2}$$

where, $\frac{dm_p(D)}{dt}$ denotes the rate of mass change for an individual particle of diameter D. $n_k(D)$ is the particle number size distribution function for mode k. It is important to note here that the rate of mass change of particle, $\frac{dm_p(D)}{dt}$, depends on particle diameter D relative to the mean free path $\lambda_{H_2SO_4}$ of the H_2SO_4 molecules in the gas phase. Given the large size range of atmospheric aerosols, two limiting cases are considered i.e., continuum regime ($D \gg \lambda_{H_2SO_4}$) and kinetic or free molecular regime ($D \ll \lambda_{H_2SO_4}$).

The remaining H_2SO_4 after the condensation process is available for SO_4 formation via nucleation. The condensation rate in the model thus determines the possibility of transfer from the gas to the aerosol phase through the means of either condensation or nucleation, resulting in a competition between the two processes. In addition to H_2SO_4 (gas), secondary organic aerosols (SOAs) are also formed via condensation process similar to that of H_2SO_4 [44, 61], although this compound is not relevant for this thesis.

Formation of new particles via nucleation. The nucleation process in the model is parametrised based on empirical or semi-empirical formulations by Kulmala et al.

(1998) or Vehkamäki et al. (2002) [62, 63], which simulates the formation of SO_4 particles via homogeneous nucleation of H_2SO_4 and H_2O. The parametrisation calculates the mass formation rate of new particles, which are assigned to the Aitken soluble mode. The corresponding particle number is calculated assuming a typical diameter of 3.5 nm for newly nucleated particles [44, 57]. It is important to mention that the nucleation process is highly sensitive towards the ambient meteorological conditions (temperature and relative humidity) and becomes dominant for low-temperature and high-humidity conditions, especially in combination with low availability of aerosol particles for condensation to take place. Due to the high concentrations of aircraft-induced SO_2 in the plume and considering the importance of H_2SO_4 precursor gas in the formation of SO_4 aerosol particles, I have incorporated an online calculation of the H_2SO_4 production rate as a new implementation in the model configuration (details are discussed in **Sect. 3.4**).

Gas-to-particle partitioning. Gas-to-particle partitioning refers to the process by which volatile or semi-volatile chemical species, such as ammonia (NH_3/NH_4), nitric acid (HNO_3/NO_3), hydrochloric acid (HCl/Cl) are transferred between the gas and the aerosol phase, depending on environmental conditions like temperature, humidity, and the availability of other reacting species. This partitioning process is essential in accurately modelling secondary aerosol formation, which occurs through condensation and evaporation. MADE3 assumes that gas-to-particle partitioning reaches a thermodynamic equilibrium between the gas phase and the particle phase. Gas-to-particle partitioning influences the mass and chemical composition in each mode. MADE3 uses EQSAM (Equilibrium Simplified Aerosol Model) which is a thermodynamic equilibrium model [64, 65] simulating the gas-to-particle partitioning of aerosol water, low-volatile and semi-volatile species.

Particle renaming is applied in MADE3 to avoid the merging of different modes in case of the particle growth from one mode to another (such as Aitken to accumulation) through either condensation or coagulation [66]. In the MADE3 framework, renaming is triggered during a time step if one of two criteria is met: (1) the volume growth rate of the Aitken mode surpasses that of the corresponding accumulation mode, or (2) the median diameter of the Aitken mode exceeds 30 nm while its particle number concentration is greater than that of the accumulation mode. Along with this transfer of particle number concentration, the corresponding mass concentration is also reassigned. Importantly, renaming occurs only between modes of the same particle mixing state – either within the soluble, insoluble, or mixed modes [44].

Particle aging in MADE3 is represented as a transformation process of aerosol particles from insoluble to mixed mode via condensation of soluble aerosols on insoluble surfaces, which may result in a change of solubility [44]. This process affects both mass and number concentrations and unlike the renaming process, here the transfer may occur between different mixing states (insoluble, soluble and mixed), but within the same size range (Aitken, accumulation and coarse). The particle aging routine of MADE3 considers a soluble mass fraction threshold of ≥10% for transferring the particles from the insoluble to the mixed mode (details are discussed in [61] [44]).

2.2.1. AEROSOL LOGNORMAL SIZE DISTRIBUTION

Our atmosphere contains a substantial number of aerosol particles, both natural and anthropogenic, with the size range from just a few nanometers (nm) to around 100 micrometers (μm) (Sect. 1.1). Given this wide range, the aerosol particles are commonly described using the lognormal size distribution of particle number (or mass) concentrations. The number size distribution describes the amount of particles exist in a given size range.

The lognormal size distribution is characterized by the aerosol number concentrations n_N for a given D_p diameter, considering the 9 lognormal modes of MADE3 using the standard equation based on Seinfeld and Pandis. [1]:

$$n_N(D_p) = \frac{dN_j}{dD_p} \frac{N_t}{\sqrt{2\pi} D_p \ln \sigma_j} \exp\left[-\frac{(\ln D_p - \ln \widetilde{D}_{pj})^2}{2(\ln \sigma_j)^2} \right]. \tag{2.3}$$

where N_t and $\widetilde{D}_{pj}$ are the lognormal parameters for total particle number concentration and median diameter as simulated by the model. The geometric standard deviation σ_j is assigned as constant in MADE3. Here, j stands for the respective modes in the MADE3. The term $\frac{dN_j}{dD_p}$ indicates the number of particles per unit diameter interval at a given D_p. The lognormal representation is particularly useful in atmospheric research as it provides an accurate representation of observed aerosol population in the atmosphere and simplifies the analysis of particle evolution in terms of their size distributions, due to processes like coagulation and condensation.

2.2.2. VALIDATION OF MADE3

In its box-model configuration, MADE3 has been evaluated and validated [44] through comparisons with observational data, sensitivity studies, and inter-model comparisons-with its predecessor MADE for fine particles (size ≤ 2 μm) [67] with good agreement between the two versions and then against the particle-resolving aerosol model PartMC-MOSAIC with a good agreement for coarse mode particle size (above about 2 μm) and some differences in the fine particle size (below about 2 μm), which could be relevant for simulating climate effects on global scale. MADE3 has also been evaluated against ground-level and aircraft-based in situ measurements in its 3D configuration as part of the global model EMAC (ECHAM/MESSy Atmospheric Chemistry Model) [57], showing that it can reasonably reproduce the global distributions of aerosol mass and number concentrations, with a performance comparable to the one of other global aerosol models. EMAC with MADE3 has also been used in several studies focusing on aerosol and aerosol-cloud interactions, with a specific focus on the impacts of the transport sectors, including aviation [32, 33, 43, 68]. Hence MADE3 is a well-established aerosol scheme and its microphysical core is a suitable basis for the development of the double-box plume model presented in this thesis.

2.3. AIRCRAFT PLUMES

At the typical cruise altitude for a commercial aircraft or a subsonic jet (9–13 km), the evolution of an aircraft exhaust plume in a stably stratified atmosphere is categorized in

three main regimes based on their time of emission and other chemical and microphysical characteristics (see Fig. 2.3). These regimes include- the jet regime, the vortex regime and the dispersion regime [38, 39, 52, 69, 70].

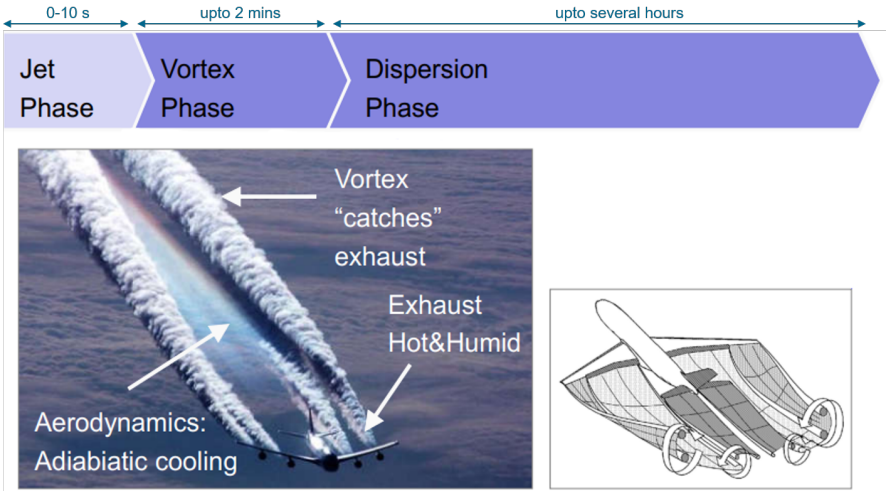

Figure 2.3: Schematic illustration of aircraft exhaust plume as emitted at the cruise altitude. The horizontal bar represents the three main phases (also referred to as regimes) of an aircraft plume, based on their time of emission: the jet regime, vortex regime and dispersion regime. Adapted from *Lecture Slides on Climate impact of air traffic – Part 1*, by Professor Volker Grewe, 2020.

The first and shortest regime of an aircraft plume is jet regime and it lasts for about 10 seconds. In this regime the hot and humid exhaust with extremely high emission concentrations at engine temperature [~400-600° C; 71, 72] mixes with the ambient air upon emission, which leads to rapid cooling and thereby often leads to supersaturation with respect to liquid water. Under such conditions water droplets can form and immediately freeze due to low ambient temperatures (typically below ∽233 K) resulting in the formation of ice particles that contribute to the contrail formation [20, 25, 73]. Subsequently, in the vortex regime, the emitted exhaust is trapped inside the wake vortices formed behind the aircraft. This regime lasts about 1 to 2 minutes before the vorticity dissipates [74] releasing exhaust and ice crystals into the dispersion regime where the crystals mostly sublimate. Studies suggest that in only 15% of the cases contrail ice particles are formed amongst which ∽87% are short-lived contrails which sublimates within the first few minutes [75–77]. The plume is assumed to be kinetically stable at the end of the vortex regime as it eventually enters the dispersion regime which begins with the breaking of trailing vortex pairs into the turbulent motion [69]. During this regime, the plume is further diluted via atmospheric processes (such as turbulence) and can be transported over long distances, influencing the atmospheric composition on larger scales [37, 78]. This is the longest regime of an aircraft exhaust plume and it can last from several hours to days [37, 38]. In this regime, the aviation-induced aerosol particles undergo several chemical and microphysical changes, due for instance to coagulation, as well as sedimentation. If the emitted ultrafine particles (<5 nm; primarily consists

of sulfate aerosols) survive in sufficient numbers by the end of the dispersion regime, they can be transported towards lower atmospheric layers where they may act as CCNs in liquid clouds, hence contributing to the aerosol indirect effect [34, 41]. During the dispersion regime, the plume undergoes spatio-temporal expansion both laterally and vertically behind the aircraft following turbulent mixing with the ambient background concentrations [69]. The plume model described in this thesis (Chapter 3) simulates the two regimes of an aircraft plume i.e., vortex regime and dispersion regime, to examine the non-linear microphysics responsible for the transformation of aviation-induced aerosol particles inside an aircraft plume.

2.4. SUMMARY

This chapter provided a brief overview of the global climate model EMAC, which comprises the ECHAM/MESSy atmospheric chemistry model and, specifically for this work, the aerosol submodel MADE3, which is used to study the effect of aviation-emitted aerosols. MADE3 is a well-established two-moment aerosol scheme that calculates changes in aerosol number and mass concentrations, as well as the particle composition. It represents nine aerosol species distributed across nine lognormal modes. Aerosol dynamics in MADE3 is simulated through processes such as nucleation, condensation, coagulation, and gas-to-particle partitioning, all within a single-box configuration. In order to study the aerosol microphysics at the plume scale, I extended the single-box MADE3 configuration [57] to the double-box plume model configuration sharing the same core mechanism for aerosol microphysics. The plume model developed in this thesis aims to explicitly simulate the aerosol dynamics in the dispersion regime of an aircraft plume, together with a simplified representation of the vortex regime which accounts for the interaction between the aviation-induced aerosols and the contrail ice crystals.

3

PLUME MODEL DESCRIPTION

3.1. INTRODUCTION

This chapter provides a detailed insight into the double-box aircraft exhaust plume model developed to simulate the non-linear aerosol microphysical processes at plume scale which are otherwise difficult to capture by the global models due to their coarse resolution, resulting in a wide range of uncertainties in the aviation-induced aerosol effects (specifically in ACIs) as discussed in Chapter 1. The development of an aircraft exhaust plume model to address the challenges discussed in the previous chapters has motivated this thesis. The plume model is developed based on the MADE3 microphysical mechanism (Sect. 2.2) to simulate the microphysical transformation of aviation-induced aerosols inside an expanding aircraft plume.

To provide a structured understanding, this chapter is organized into following sections: Sect. 3.2 conceptualizes the initial idea behind the plume model development, introducing the two approaches developed to model the aircraft exhaust plume with the goal to eventually compare them at the end of the dispersion regime. Sect. 3.3 outlines the technical overview of the plume model with all the processes involved in the different plume regimes. These processes are then further described in their respective sections: the technical details involved in the online calculations for the sulfate production rate in the plume model is presented in Sect. 3.4, the one-way interface implemented in the double-box configuration which allows the interaction between the two boxes as well as calculates the diffusion dynamics is described in Sect. 3.5. Sect. 3.6 focuses on the illustration of the aerosol microphysics involved in the vortex regime, before the aviation-induced aerosols enter the dispersion regime. This section discusses the role and impact of short-lived contrail ice crystals on the aviation-induced aerosol microphysics during the first 2 minutes of the simulation. Sect. 3.7 discusses the plume model initialisation methods, which involves the detailed description of the parameters required to calcu-

This chapter is based on Sharma et al. [79]

late the aviation-induced species mass and number concentrations. In order to assess the impact of individual microphysical processes on the aerosols, the tendency diagnostics (Sect. 3.8) is implemented in the model. Sect. 3.9 explains the implementation of the plume model into the MESSy (Modal Earth Submodel System, [53]) framework and the parameters required for model configuration. Finally, Sect. 3.10 highlights some of the numerical tests performed at different stages of the plume model development to validate the model performance.

3.2. PLUME MODEL CONCEPT

The concept of the double-box aircraft exhaust plume model developed in this study is based on Petry et al. [45], who originally introduced it to better account for the plume chemistry of the reactive species inside an aircraft exhaust plume at cruise altitude. The double-box plume model introduced in this study explicitly focuses on simulating the aerosol microphysics and my idea behind this concept is to compare the results of instantaneous mixing of the aircraft exhaust inside a large-scale grid box with a more detailed approach where the diffusion of a dispersing plume within the background is simulated in detail. By comparing the resulting concentration of the species at the end of the plume dispersion, it is possible to estimate the impact of the more accurate plume dispersion approach over the instantaneous dispersion approach. In the present work, the concept of Petry et al. [45] is adapted to account for the aerosol microphysical processes within a dispersing aircraft plume and extended to further include the interactions of aviation-induced aerosol with contrail ice crystals during the vortex regime in the first stages of the plume evolution.

In the instantaneous dispersion approach (Fig. 3.1), usually adopted by global models, the aircraft emissions are instantaneously distributed over the large (~100 km) gridbox and homogeneously mixed at once. This method completely disregards the microphysical processes occurring at plume-scale, thus misrepresenting the impact of key transformation processes (such as particle coagulation and nucleation) taking place during the expansion and dispersion of the plume in the surrounding background. This may in turn lead to inaccurate estimates of the aviation-induced aerosol particle properties at the end of the dispersion, in particular in terms of aviation-induced aerosol number concentration and their lognormal size distribution [34, 39, 41]. These properties are critical in the context of the climate impact of aviation aerosols, as they control the potential perturbation on cloud droplet number concentration in liquid clouds and hence the resulting radiative forcing via ACIs. The approach developed here allows to explicitly simulate the plume-scale processes representing the aerosol microphysics inside a dispersing aircraft plume. Fig. 3.1 schematically describes the approach: a plume model is applied to simulate the dispersion of a single aircraft plume (represented by the single-plume box, hereafter SP) inside a background atmosphere (represented by the background box, BG). This plume approach is then compared with the instantaneous dispersion approach, where the aviation emissions are instantaneously released in the background of a single box (ID box). As mentioned above, the microphysics in all three boxes (SP, BG and ID) is simulated using MADE3. To simulate the dispersion of the plume box (SP) in the background box (BG), a one-way interface is implemented based on the plume diffusion dynamics as in Petry et al. [45]. Furthermore, the double-box plume

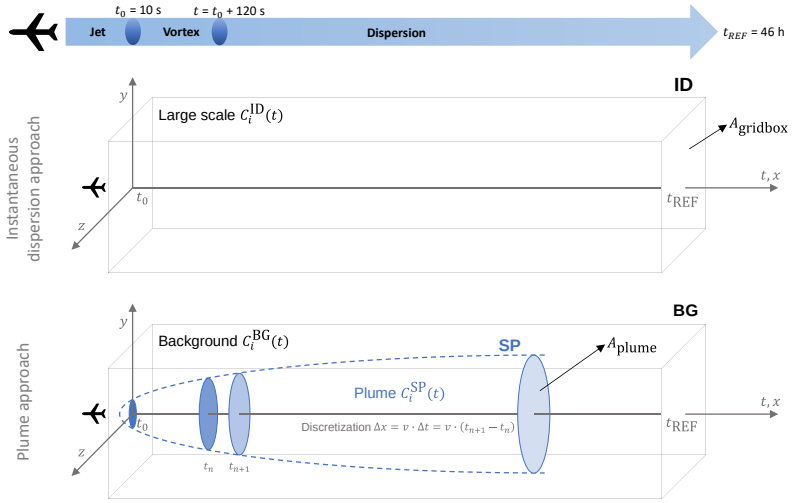

Figure 3.1: Schematic representation of double-box aircraft exhaust plume model highlighting the two modelling approaches; as a) Instantaneous dispersion approach of aircraft emissions in a large-scale grid box (ID box) and b) Double-box plume model accounting for the dispersion of a single aircraft plume (SP box) in the background (BG box). The x-axis represents the flight trajectory. The plume gradually grows and disperses with time t, both vertically (y-axis) and laterally (z-axis). The plume growth is schematically represented by the elliptical cross-section area A_{plume} increasing at each timestep behind the aircraft, while the cross-section area $A_{\text{grid-box}}$ of the large-scale remains constant. Here, t_0 denotes the initial timestep of the simulation, set at the end of the jet regime (~10 seconds behind the aircraft, not accounted for in the model), whereas C_i^{ID}, C_i^{SP} and C_i^{BG} indicate the concentration of a species i in the three boxes, respectively. The arrow on the top symbolizes an aircraft exhaust plume with different regimes based on their time of emission.

model is capable of simulating two scenarios for a single aircraft plume, namely with and without the presence of contrail ice particles in the vortex regime and their coagulation with the aerosol particles. The contrail ice is assumed to sublimate at the beginning of the dispersion regime, releasing the coagulated aerosol particles back in to the SP box.

3.3. PLUME MODEL STRUCTURE

Two model approaches (instantaneous dispersion and plume approach) are applied and compared to quantify the impacts on the particle properties at the end of the dispersion regime due to aviation effects. In the instantaneous dispersion approach (as shown in Fig. 3.1a) aviation emissions are released at time t_0 and instantaneously and homogeneously dispersed in the model grid box (ID box). The evolution of the concentration $C_i^{\text{ID}}(t)$ for each species i is then simulated by MADE3, mimicking the behaviour of the global model for a single box. In the plume approach (Fig. 3.1b), aviation emissions are released at time t_0 within the SP box and their mixing with the BG box during the plume dispersion is explicitly simulated, while also accounting for the aerosol microphysics.

The plume cross-section area expands both laterally (z-axis) and vertically (y-axis) while mixing with the background air. According to Schumann et al. [69], in a stably stratified atmosphere, the aircraft wakes tend to shrink vertically while expanding or stretching horizontally. This anisotropic growth is represented using the elliptical slices (or cross-sections) along the flight track (x-axis) in Fig.3.1b. The expansion of the plume along the flight track is considered negligible. The two boxes, SP and BG, evolve together in time and experience the same microphysical processes in the MADE3 core routines, updating the values of the concentrations $C_i^{\mathrm{SP}}(t)$ and $C_i^{\mathrm{BG}}(t)$. The time integration proceeds until the plume cross-section area (A_{plume}) reaches the same value of the large-scale grid box area ($A_{\mathrm{grid-box}}$), which marks the end of the dispersion regime, i.e. when the plume is completely dispersed within the background. The same time integration is applied to the ID box. In the following, I will refer to this point as the reference time and will compare the results of the two approaches at this point to estimate the impact of the plume processes on simulated aviation aerosol number concentrations. This will be expressed as a plume correction with respect to the instantaneous dispersion.

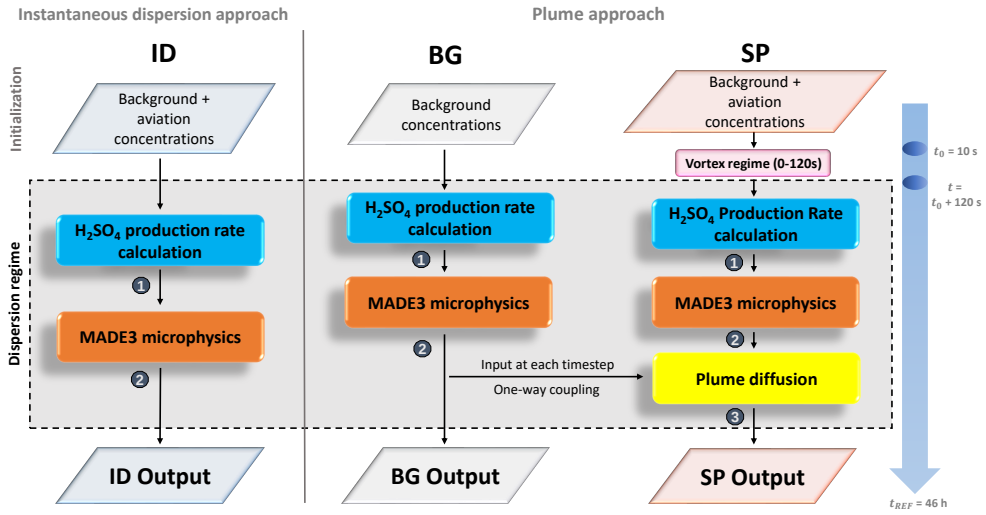

Figure 3.2: Schematic representation of the process flow of the two approaches described in this thesis: the instantaneous dispersion approach (left) and the plume approach (right). Here, the rectangular boxes represent the components highlighting the key processes in the two modelling approaches. The time-loop of the dispersion regime is common to both approaches and proceeds until the cross-section area of the plume in the plume approach is equivalent to the large-scale grid box area in the instantaneous dispersion approach. The numbers (1), (2) and (3) refers to different set of processes tracked by the tendency diagnostics implemented in the model (see Sect. 3.8).

The details of the time integration within each box are shown in Fig. 3.2. At each model timestep, the chemical production rate of H_2SO_4 is calculated before calling the MADE3 microphysical scheme, which integrates the concentrations $C_i(t)$ by solving the aerosol dynamics equations (see Sect. 2.2). The explicit calculation of the H_2SO_4 production rate during the model time integration is an improvement introduced in this

work compared to the MADE3 box-model version by Kaiser et al. [44], who assumed a prescribed constant production rate of H_2SO_4. Here, I opted for a more sophisticated approach, where the production rate is calculated at each timestep from the SO_2 and OH concentrations (see details in Sect. 3.4). The online sulfate production rate calculation is relevant in the context of this thesis, as the H_2SO_4 production rate affects the nucleation of SO_4 particles and the growth of existing particles by condensation, hence affecting the aerosol properties, particularly the number concentrations. The SP box include two additional processes, which are specific to the plume approach namely, the diffusion routine accounting for the mixing of the plume with the entrained background (Sect. 3.5) and the routine for the vortex regime, which simulates the coagulation of the aerosol particles with the ice particles during the vortex regime (10 to 120 s behind the aircraft), representing the aerosol-ice interactions occurring within a short-lived contrail in a simplified manner (Sect. 3.6). I will show that this is a key process in the plume evolution and has a significant impact on the resulting aviation-induced particle number concentrations. The time integration of the dispersion regime is same in all boxes and considers a constant time-step (time resolution) of 60 seconds, while the short vortex regime of the SP box uses a time resolution of 1 second, given the short duration of this regime. The meteorological parameters such as temperature, pressure and relative humidity are kept constant during the whole simulation and are identical in the three boxes. The generated output comprises of temporally resolved mass concentrations for all simulated aerosol species and total aerosol number concentrations per mode and mixing state (as described in Sect. 2.2).

The initial background concentrations of the different tracers use climatological means from the global EMAC simulation of Righi et al. [43] for different regions, while the aviation emissions are calculated offline based on the typical emission indices and other parameters representative of a young aircraft plume. These emissions are then used to initialise the concentration of aviation-induced species for both the SP and the ID box, considering the initial cross-section area of the respective boxes. Further details about the initialisation procedure are given in Sect. 3.7.

3.4. ONLINE SULFATE PRODUCTION RATE

Sulfur dioxide (SO_2) is formed inside the engine combustor as a result of oxidation via hydroxyl radical (OH) and fuel sulfur [26]. The aircraft-emitted SO_2 upon entering the dispersion regime undergoes oxidation with the OH in the downstream plume which then leads to the formation of sulfate aerosols (SO_4) within seconds behind the aircraft. According to the in-situ measurements by Jurkat et al. [80], a small fraction (a few percent) of SO_2 mass is converted into aerosol sulfate (primary SO_4) during the jet regime. The remaining SO_2 mass remains available in the system to form H_2SO_4 gas (see Fig. 3.3), which serve as a precursor gas for the formation of additional SO_4 during the dispersion regime, either via nucleation or by condensation on existing particles.

Sulfate production is a slow process and therefore is calculated only in the dispersion regime and neglected in the vortex regime [81, 82]. The latter is only responsible to perform the aerosol-aerosol and aerosol-ice coagulation processes. The formation of H_2SO_4 in the gas phase occurs via the third-body reaction:

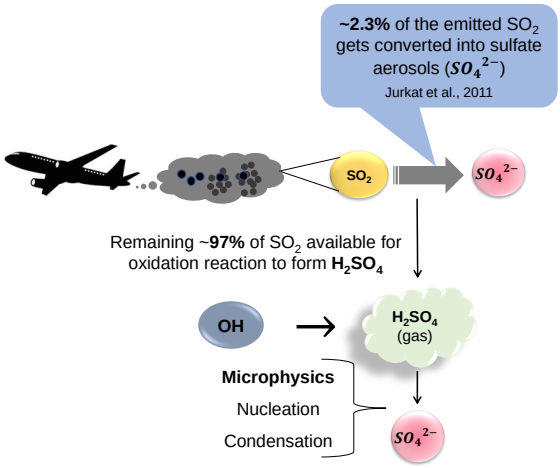

Figure 3.3: Schematic illustration of aviation emitted SO_2 and H_2SO_4 production in the troposphere.

$$P_{H_2SO_4} = k_{3rd}\,[SO_2]\,[OH], \tag{3.1}$$

where the reaction rate k_{3rd} can be calculated as:

$$k_{3rd} = \frac{k_0(T)\,C}{1 + k_{ratio}(T)}\, f_c^{\frac{1}{1+[\log_{10}(k_{ratio}(T))]^2}}, \tag{3.2}$$

using the auxiliary variables:

$$k_{ratio}(T) = \frac{k_0(T)\,C}{k_{inf}(T)}, \tag{3.3}$$

$$k_0(T) = k_0^{300}\left(\frac{300\,K}{T}\right)^n, \tag{3.4}$$

$$k_{inf}(T) = k_{inf}^{300}\left(\frac{300\,K}{T}\right)^m. \tag{3.5}$$

The parameters f_c, k_0^{300}, k_{inf}^{300}, n and m are taken from the MECCA chemical scheme of EMAC based on Burkholder et al. [83, 84] as given in Table 3.1.

In the equations 3.2 and 3.3, the concentration of air molecules C (in units of molecule cm^{-3}) is expressed as a function of temperature T (in Kelvin), pressure p (in Pascal) and specific humidity q (in kg kg^{-1}) as follows:

$$C = 10^6\, N_A\, \frac{p}{R\,T}\, \frac{1-q}{1+q(\frac{1}{\epsilon}-1)} \tag{3.6}$$

where, N_A is the Avogadro number (molecule mol^{-1}) and $\epsilon = M_{H_2O}/M_{air}$ is the ratio of the molecular weight of water and dry air. The additional tracers SO_2 and OH are added

in the plume model as they were not included in the original MADE3 box-model version. Note, however, that OH can only be prescribed with a constant mixing ratio in the current configuration of the double-box plume model. In this thesis, all the simulations are performed with a typical background peak concentration of OH between 1.3 to 3 $\times 10^{-13}$ mol/mol (the value varies for the ensemble boxes based on the EMAC output, Sect. 3.7). The initial values are based on the EMAC output for the ambient background conditions of North Atlantic region representative of the cruising altitude of ~10.5 km. The ambient concentration of OH varies throughout the day, also known as the diurnal variations or diurnal cycle which refers to the daily fluctuation in OH concentrations, which generally peak during the day and decrease at night. The OH radical often termed as the "detergent" of the atmosphere and influences the atmospheric composition by initiating the oxidation of various trace gases. In the troposphere, the production of OH involves the photolysis of O_3 followed by a reaction with water vapour H_2O [85]. The influence of low ambient temperature on the production of OH reaction rates and atmospheric dynamics, contributes to the diurnal variations [86, 87]. Temperature plays an integral role in determining OH levels throughout the day, with higher concentrations during warmer, sunlit hours and a sharp decline at night. A time-varying mixing ratio for OH, reproducing for example its typical daily cycle in the upper troposphere, will be considered for future versions of the model. A daytime peak value is selected for this study based on offline tests conducted to assess the impact of OH concentration on sulfur chemistry, as well as its overall effect on aerosol microphysical processes during plume dispersion.

Table 3.1: K_{3rd} parameters as taken from MECCA based on Burkholder et al. [83, 84].

Parameter	Values	Units
k_0^{300}	3.3×10^{-31}	$cm^6\ molecule^{-2}\ s^{-1}$
k_{inf}^{300}	1.6×10^{-12}	$cm^3\ molecule^{-1}\ s^{-1}$
n	4.3	
m	0	
f_c	0.6	

The production and loss of sulfur mass is calculated independently in the model through the explicit simulation of key chemical reactions and microphysical processes. The sulfur mass budget accounts for the gas-phase oxidation of SO_2 to SO_4 by the oxidants such as OH, as well as subsequent aerosol formation and removal processes like condensation and coagulation. Therefore, a sulfur mass budget closure analysis is performed to track the SO_2 mass concentration in the model and to evaluate the mass conservation of sulfur species (for example: Fig. 3.8, as described in Sect. 3.10.2), which is also verified with the tendency analysis (Fig. 3.8) as described in tendency diagnostics (Sect. 3.8).

3.5. ONE-WAY INTERFACE AND DIFFUSION DYNAMICS

As an integral part of the double-box aircraft exhaust plume model development, a one-way interface is implemented in the double-box configuration (Fig. 3.2; yellow box) to

account for diffusion dynamics and for the entrainment of background air into the growing and dispersing aircraft plume, following the approach of Petry et al. [45]. In their study, the plume is described as a Gaussian plume, assuming the diffusion parameters typical for the upper troposphere as described by Schumann et al. [69] representing the dispersion of chemically passive species in a stably stratified atmosphere with anisotropic turbulent diffusivities. The diffusion dynamics equation is solved as a Gauss function with horizontal (σ_h), vertical (σ_v) and shear (σ_s) standard deviations given by:

$$\sigma_h^2(t) = \frac{2}{3} s^2 D_v\, t^3 + (2D_s + s\sigma_{0v}^2) s\, t^2 + 2D_h\, t + \sigma_{0h}^2, \tag{3.7}$$

$$\sigma_v^2(t) = 2D_v\, t + \sigma_{0v}^2, \tag{3.8}$$

$$\sigma_s^2(t) = sD_v\, t^2 + (2D_s + s\sigma_{0v}^2)\, t. \tag{3.9}$$

These variables are time dependent and determine the rate of plume expansion and dispersion processes within the expanding plume. The diffusion coefficients, namely horizontal diffusion (D_h), vertical diffusion (D_v) and shear (D_s), as well as the initial horizontal (σ_{0h}), vertical (σ_{0v}) and shear (σ_{0s}) standard deviations, along with wind shear (s) are taken from Schumann et al. [69] and shown in Table 3.2.

Eqs. (3.7)-(3.9) assume the plume to expand both laterally and vertically and to grow elliptically over time due to the strong vertical shrink of the wake formed by the wing tips during the vortex regime of the plume expansion. Based on these equations the growth of the plume cross-section area $A_{\text{plume}}(t)$ is calculated as:

$$A_{\text{plume}}(t) = \pi c^2 \sqrt{\sigma_h^2(t)\sigma_v^2(t) - \sigma_s^2(t)}, \tag{3.10}$$

where t is the time elapsed since the beginning of the dispersion regime and c is a free parameter determining the fraction of the initial plume incorporated in Gaussian plume. Here, as in Petry et al. [45], a value of $c = 2.2$ is chosen, representing 98.6% of the exhaust incorporated in the plume. Based on the above equation, the solution to the diffusion equation is implemented in the single plume box (SP) and applied to update the species concentrations $C_i^{\text{SP}}(t)$ after the entrainment of background air in the plume at each timestep t:

$$C_i^{\text{SP}}(t) = \frac{A_{\text{plume}}(t) - A_{\text{plume}}(t-\Delta t)}{A_{\text{plume}}(t)} C_i^{\text{BG}}(t) + \frac{A_{\text{plume}}(t-\Delta t)}{A_{\text{plume}}(t)} C_i^{\text{SP}}(t) \tag{3.11}$$

where t is the current timestep and $t - \Delta t$ is the previous timestep.

In the double-box plume model, the routine implementing Eq. (3.11) is called right after the MADE3 microphysical core, as shown by the yellow box in Fig. 3.2. The time integration continues until the value of the plume cross-section area is equivalent (or larger) to the cross-section area of the large-scale grid box i.e. $A_{\text{plume}} \geq A_{\text{grid-box}}$. In the following, this final timestep is denoted as reference time and is considered when comparing the results of instantaneous dispersion approach and plume approach. Considering a cross-section for a single large-scale grid box of 300 km (horizontal) times 1 km (vertical), typical of the EMAC T42L41DLR resolution used in previous studies on the aviation impact of aerosol [34, 43], results in a large-scale area $A_{\text{grid-box}} = 300\ \text{km}^2$.

Table 3.2: The diffusion and shear coefficients along with the initial standard deviations at the end of the vortex regime as taken from Petry et al. [45] based on Schumann et al. [69] (see text for explanation).

Parameter	Values	Units
D_v	0.3	$m^2\ s^{-1}$
D_h	10.0	$m^2\ s^{-1}$
D_s	1.0	$m^2\ s^{-1}$
s	0.004	s^{-1}
σ_{0v}	50.0	m
σ_{0h}	200.0	m
σ_{0s}	0.0	m

As shown in Sect. 4.2, for the set of diffusion parameters as in Petry et al. [45] this corresponds to a reference time of about 46 hours. Moreover, the double-box plume model can simulate two additional diffusion scenarios by scaling the initial diffusion parameters (D_h, D_v, D_s, and s, Table 3.2) by a factor of 0.75 and 1.5, resulting in a faster and slower plume diffusion with the reference time of 61 h and 30.5 h respectively.

3.6. VORTEX REGIME MICROPHYSICS IN PLUME MODEL

The vortex regime (Sect. 2.3) is initialised 10 seconds after the release of emissions. At this stage, the emitted exhaust gets trapped inside the wake vortices which are formed when the vorticity sheet rolls up around the aircraft wing and wing-tips [52] and it can last up to a few minutes before the dispersion regime starts. During the vortex regime several dynamical processes such as chemical kinetics, turbulence, fluid dynamics occurs. The contrail formation behind the aircraft is determined by the Schmidt-Appleman criterion [25, 73], which is based on several parameters such as aircraft altitude, engine and fuel type, temperatures and relative humidity [37, 88, 89] and may vary with different regions. Studies suggest that 85% of the contrails formed behind an aircraft are short-lived and may last up to a few minutes [75, 77].

The plume model concept outlined above accounts for the aerosol microphysical processes occurring during the dispersion regime of the plume evolution. However, the vortex regime could also be relevant for the aerosol population, especially in the case when a short-lived contrail is present during this regime, since the interactions of the aerosol particle with the ice crystals may impact the properties of the aerosol population. In the plume model, I make the simple assumption that the formation of contrail ice particles occurs in the jet regime and that both ice crystal number concentration and size remain constant during the vortex regime. This simplified assumption is justified since the goal is to characterize the effect of the coagulation of the aerosol particles with the ice crystals in the vortex, mimicking the effect of a short-lived contrail which sublimates at the end of the vortex regime. In the plume approach, the vortex regime is represented as a separate process loop for the first 2 minutes of the simulations in the SP box (see Fig. 3.2; pink box). Please note that t=2 min represents a lower limit for vortex regime simulations in the plume model. This value is flexible and can be easily adjusted in the model configuration to accommodate a longer duration for the vortex regime.

Here, the interaction of aerosols and ice is calculated via Brownian coagulation using the coagulation routine of the MADE3 microphysical core (Sect. 2.2) and implementing a passive tracer representing the ice crystals population. Given the short duration of this regime, the temporal resolution is increased to 1 second for the time integration of the vortex regime.

Mass and number concentrations of short-lived contrail ice crystals are initialised with the typical values corresponding to the end of jet regime [90]. During the vortex regime, no additional ice crystal formation is considered and no ice crystal growth is accounted for. The sedimentation of ice crystals during this regime is also considered negligible based on a simple estimate of the sedimentation velocity of the ice crystals based on the methods by Seinfeld & Pandis [1] and Spichtinger et al. [91]. In the first method, the sedimentation velocity is calculated as:

$$v_s = \frac{\rho_p \, {D_p}^2 \, g \, C_c}{18\mu} \tag{3.12}$$

with:

$$\lambda = \frac{2\mu}{P(\frac{8M}{\pi RT})^{\frac{1}{2}}}, \tag{3.13}$$

$$C_c = 1 + \frac{2\lambda}{D_p}\left[1.257 + 0.4\exp(-\frac{1.1 D_p}{2\lambda})\right], \tag{3.14}$$

$$\mu = 10^{-5}\left[1.718 + 0.0049\,T - 1.2\times10^{-5}\,T^2\right]. \tag{3.15}$$

The calculation for sedimentation velocity of ice crystals require typical ice crystal parameters such as particle density (ρ_p) and particle diameter (D_p), along with the viscosity of air (μ) which is also calculated offline based on the method from the SEDI submodel of MESSy using Eq. 3.15. Eq. 3.12 requires two additional parameters including, the mean free path (λ) and slip correction coefficient (C_c). The mean free path is calculated using Eq. 3.13 which depends on the ambient meteorology such as temperature (T) and pressure (p) along with gas constant (R) and molecular weight of air (M). The slip correction coefficient (C_c) is a size dependent parameter (D_p) and is also calculated offline using Eq. 3.14.

A second approach is also tested using the method from Spichtinger et al. [91] where the particle terminal velocity ($v(m)$) is calculated as:

$$v(m) = \gamma(m)\, m^{\delta(m)} \tag{3.16}$$

This method requires two constant parameter functions which are mass dependent, i.e. $\gamma(m)$ and $\delta(m)$ as 735.4 and 0.42 respectively based Spichtinger et al. [91].

The simple calculation of the ice crystals sedimentation velocity from these two methods i.e. Spichtinger et al. [92] (as in Eq. 3.16) and Seinfeld & Pandis [1] (as in Eq. 3.12), results in a similar value of about 0.1 cm s^{-1} for the typical conditions at cruise altitude. Considering the cross-section area of the plume and the short duration (2 minutes) of the vortex regime in the model, this implies that this velocity is too small for the sedimentation to remove the ice crystals during the vortex regime. This also means that impact

scavenging by sedimenting ice crystal is inefficient for the removal of aerosol particles in the vortex and can be neglected. The ice crystals are assumed to completely sublimate at the end of the vortex regime and the residual aerosol mass is returned to the aerosol tracers of the SP box. To estimate the residual number, I assume that every sublimating ice crystal releases a single aerosol particle, hence the residual aerosol number coincide with the assumed (constant) number of ice crystals, given that ice-ice coagulation is negligible due to the large size (~micron) of the crystals. Based on the residual aerosol mass and number concentrations, a residual diameter is then calculated for a lognormal size distribution and used to determine the target mode to assign the residuals to, consistent with the MADE3 modal structure. The residual particle is assigned to the mixed (insoluble) mode if the soluble mass of the residual is larger (smaller) than 10%, and to the Aitken (accumulation) size mode if its diameter is smaller (larger) than 100 nm. The resulting aerosol mass and number concentration serve then as initial values for the further simulation of the plume evolution in the dispersion regime.

3.7. INITIALISATION

The plume model is initialised with typical background concentrations and with the aviation emissions of ~10 sec behind the aircraft (see Fig. 3.4), considering representative values at cruise altitude of the commercial fleet. Background concentrations, required to initialise the ID box in the instantaneous dispersion approach and the BG box in the plume approach, and meteorological parameters are taken from a global simulation with the EMAC model [43]. The plume model simulations for this study are performed for different regions (Table 5.1), with the reference simulation focusing the North Atlantic region (Table 4.2). For all regions, data from the EMAC model hybrid levels 18 and 19 (corresponding to an altitude of about 10-12 km) are considered. In order to account for the spatial variability of background conditions, the climatological mean values of each of the EMAC model grid-boxes within each region are used to initialise multiple ensemble simulations of the plume model and the ensemble mean of the results is considered for the subsequent analysis. Each of the large-scale grid box has a size of 300 km (horizontal) times 1 km (vertical), corresponding to the EMAC T42L41DLR resolution used in previous studies of aviation impact of aerosols [34, 43].

For the reference setup, two background initialisation methods are tested in this thesis as a) background ensemble and b) background mean. For both methods, the background initialisation data is based on EMAC output for the years between 2006 and 2015 representative of the flight levels of 18 and 19 corresponding to the pressure levels between 21000 to 24000 Pa as shown in Table 4.2. For the reference setup (REF), the North Atlantic region is selected (lat: 40-63 $^{\circ}N$; lon: 70-5 $^{\circ}W$) which comprises of about 432 grid cells. In the second background initialisation method the average of all the climatological means over the North Atlantic region is considered, which eventually consist of a single initialisation file for the model simulation. Although the latter method saves both computational time and resources, the ensemble method is favoured, as it better captures the spatial variability over the region.

The initial concentrations induced by aviation emissions $C_{\text{aviation}}(t_0)$ are calculated offline using aircraft operational parameters and the following equation:

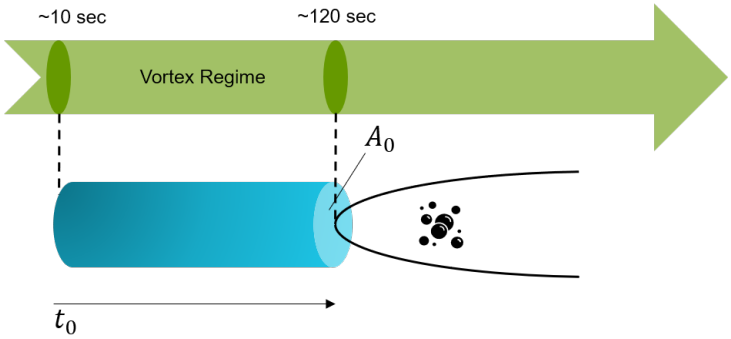

Figure 3.4: Conceptualization of plume model initialisation corresponding to Fig. 3.1. The aviation emissions are initialised at t_0 = 10 seconds behind the aircraft along the flight track. No substantial growth is assumed during the vortex regime with $A_{\text{plume}}(t_0) = 0.15$ km^2. Background entrainment is established during the dispersion regime.

$$C_i^{\text{aviation}}(t_0) = \frac{\text{EI}_i\, f}{A_{\text{plume}}(t_0)\, v}, \tag{3.17}$$

where EI_i is the emission indices of the species i, f the fuel consumption, $A_{\text{plume}}(t_0) = 0.15$ km^2 the initial plume area calculated using Eq. (3.10) and v the aircraft speed. Eq. (3.17) basically converts aviation emissions to concentrations by assuming that the species are released within a given initial volume, determined by the initial plume cross-section area and the aircraft speed. The values for these parameters depend on the aircraft and engine type and may be subject to a large variability. All initial parameters that are considered in this study typically represent the wide-body aircraft types like Boeing 747 [45], Airbus 340 [93] and the DLR ATTAS (a twin-engine aircraft with medium bypass ratio turbofan). The initial size parameters for emitted primary and secondary mode particles are based on Petzold et al. [46] which represents the Rolls Royce/SNECMA M45H Mk501 turbofan of DLR ATTAS (details are shown in Table 3.3).

The aviation emissions are calculated for young plume conditions based on their time of emission as described for the different plume regimes (see Fig. 3.4). In both modelling approaches (instantaneous dispersion and plume), I assume that the emitted exhaust is mixed with the existing background at timestep t_0. In the plume approach, the aerosols are transformed gradually within the dispersing aircraft plume, hence in the plume model the initial concentration of the aviation emissions, $C_i^{\text{aviation}}(t_0)$, is added to the background concentrations $C_i^{\text{BG}}(t_0)$:

$$C_i^{\text{SP}}(t_0) = C_i^{\text{aviation}}(t_0) + C_i^{\text{BG}}(t_0) \tag{3.18}$$

Here, the BG box concentrations initialised from the EMAC simulations undergo an initial spin-up of 6 hours to ensure internal consistency of the different tracers prior to entering the time loop.

In the instantaneous dispersion approach, the ID box is initialised diluting the emissions inside a large-scale grid box with a cross-section area $A_{\text{grid-box}} = 300$ km^2. There-

fore, the emission values are scaled to the grid-box area with respect to the initial plume area $A_{\text{plume}}(t_0)$ within the model and later mixed with the background concentrations:

$$C_i^{\text{ID}}(t_0) = \frac{A_{\text{plume}}(t_0)}{A_{\text{grid-box}}} C_i^{\text{aviation}}(t_0) + C_i^{\text{BG}}(t_0) \tag{3.19}$$

The emission index (EI) represents the mass of a specific pollutant emitted per kilogram of fuel burned, serving as a crucial parameter in calculating total emissions. For the reference case, I use the average EI values for species mass such as SO_2 as provided in Lee et al. [26], which represent the average over the aircraft types and diverse operational conditions to standardize and simplify the estimation of aviation emissions. The initialisation of soot and ice particles, on the other hand, is based on number EI from Bier et al. [90], which represent model based values. I recall that SO_2 is added as a new gaseous species in the MADE3 box- and plume-model version in order to drive the online sulfur chemistry for the production of H_2SO_4 (see Sect. 3.4). To calculate the initial SO_2 mass, I assume an EI value of 0.8 $g(SO_2)\,kg_{\text{fuel}}^{-1}$ based on Lee et al. [26]. Thereafter, the initial aerosol sulfate mass M_{SO_4} is derived as a mass fraction ϵ of emitted SO_2 mass:

$$M_{SO_4} = \epsilon\, M_{SO_2} \frac{\mu_{SO_4}}{\mu_{SO_2}} \tag{3.20}$$

where μ indicates the molecular weight.

Aviation emitted soot is initialised in terms of number concentration, based on the number emission index EI_{soot} by Bier et al. [90]. For the plume scenario with the availability of short-lived contrail ice particles in the vortex regime, I initialise the ice crystals with the available ice number concentration (N_{ice}) corresponding to the EI_{soot} also based on Bier et al. [90].

To convert initialised mass (number) concentrations to number (mass) concentrations for both aerosol and ice particles, I apply the standard equation for lognormal distributions derived from the third moment:

$$N_{i,j} = \frac{6}{\pi} \frac{M_{i,j}}{D_{i,j}^3 \exp(4.5 \ln^2 \sigma_{i,j}) \rho_i} \tag{3.21}$$

where $N_{i,j}$, $M_{i,j}$ and $\rho_{i,j}$ are the number, mass and specific density, respectively, for the aerosol species (or ice) i in the mode j. The choice of the lognormal parameters like the geometric mean diameter $D_{i,j}$ and geometric standard deviation $\sigma_{i,j}$ is based on a literature review and summarized in Table 3.3.

The model is initialised through a namelist file, specifying tracer concentrations as a matrix. This matrix includes the mass of aerosol species and aerosol number concentrations distributed across nine lognormal modes (Fig. 2.2), along with gaseous species (Sect. 2.2). In addition to the above mentioned gas species, NO_x and OH are added as the passive tracers as they do not undergo any chemical process in the model. These initial tracer concentrations are either taken from EMAC (based on available global model inventories) or can be calculated offline (in case of plume model) based on available parameters, such as emission indices of species mass or number. However, in case of availability of particle number concentration (N_i) a corresponding mass concentration

Table 3.3: Parameters used for the calculations of the initial aviation-induced concentrations for the reference simulation in this study. Primary sulfate emissions are assigned to the soluble Aitken mode (ks). Soot emissions are assigned to the Aitken and accumulation modes, with a 80/20% split between the insoluble and mixed modes (ki/km and ai/am). Ice is temporarily assigned to the insoluble coarse mode (ci) during the vortex regime.

Parameter	Description	Units	Reference value	Reference(s)
f	Fuel consumption	$kg\,s^{-1}$	0.426	[46]
$A_{plume}(t_0)$	Initial plume area	m^2	1.5×10^5	[45]
v	Aircraft speed	$m\,s^{-1}$	167	[46]
EI_{soot}	Soot number emission index	kg_{fuel}^{-1}	1.5×10^{15}	[90]
N_{ice}	Ice crystal number concentration	cm^{-3}	222	[90]
EI_{SO_2}	SO_2 mass emission index	$g(SO_2)\,kg_{fuel}^{-1}$	0.8	[26]
EI_{NO_x}	NO_x mass emission index	$g(NO_2)\,kg_{fuel}^{-1}$	14	[26]
ϵ	Primary SO_4 mass fraction	%	2.3	[80]
$D_{soot,k}$; $\sigma_{soot,k}$	Soot lognormal parameters (Aitken)	nm; -	25; 1.55	[46]
$D_{soot,a}$; $\sigma_{soot,a}$	Soot lognormal parameters (accum.)	nm; -	150; 1.65	[46]
$D_{SO_4,ks}$; $\sigma_{SO_4,ks}$	SO_4 lognormal parameters	nm; -	2.5; 1.7	[82]
$D_{ice,ci}$; $\sigma_{ice,ci}$	Ice lognormal parameters	nm; -	2300; 2.2	[93]

(M_i) can be calculated using the volumetric concentration (V_i) of species (i) as shown in Eq. (3.22) and the specific density of the species (ρ_i) with the help Eq. 3.23.

$$V_i = \frac{\pi}{6} N_i D_{i,j}^3 \exp(4.5 \ln^2 \sigma_{i,j}), \tag{3.22}$$

$$M_i = V_i \rho_i \tag{3.23}$$

Here, $D_{i,j}$ stands for the geometric mean diameter and $\sigma_{i,j}$ is the geometric standard deviation of the respective modes. The resulting output, in terms of aerosol mass and number concentration, is further utilized to calculate the lognormal size distributions for both mass and number concentrations (Sect. 4.4.5). These calculations are based on the respective size parameters (D_p) assigned to each mode. The distribution is based on lognormal functions [1] based on the characterization of individual modes (Aitken, accumulation and coarse).

3.8. TENDENCY DIAGNOSTICS

To support the interpretation of the model results and to characterize them at the process level, tendency diagnostics have been implemented in the MADE3 core routines. The aim of these diagnostics is to track the changes in the tracer concentrations resulting from individual microphysical processes. The tracked processes are categorized in three groups:

1. Chemical processes: This component explicitly accounts for the online sulfate production rate (Sect. 3.4) and it helps tracking the reduction in SO_2 gas which contributes to the formation of H_2SO_4 gas, which is a precursor gas for sulfate aerosol. This process plays a key role in the sulfur budget (Sect. 3.10.2).

2. Aerosol microphysics: This component accounts for all the MADE3 microphysical processes (Sect. 2.2) to help understand their contribution to the changes in

aerosol mass and more importantly the particle number concentrations during the simulation.

3. Plume-specific processes: This component explicitly operates for the plume approach (SP box) of the double-box plume model (Sect. 3.5), corresponding to the model schematic described in Fig. 3.2. It helps understand the contribution of diffusion dynamics to the aerosol microphysics.

The tendency diagnostics are computed both in the single-box and in the double-box configuration, except for the tendencies for plume-specific processes, which are only available in the double-box configuration. The model provides a detailed tendency output for all MADE3 species both gases and aerosols (Sect. 2.2), the latter also in the nine lognormal aerosol modes.

Table 3.4: List of all tendency tracers for the both box-model and double-box plume-model configuration.

Tendencies	Group	Description
`i_cond`	MADE3 microphysics	Tracer for condensation process
`i_coag`	MADE3 microphysics	Tracer for coagulation process
`i_nuc`	MADE3 microphysics	Tracer for nucleation process
`i_gtp`	MADE3 microphysics	Tracer for gas-to-particle partitioning
`i_rename`	MADE3 microphysics	Tracer for particle aging (renaming)
`i_micro`	MADE3 microphysics	Sum of all MADE3 microphysical processes
`i_chem`	Chemical processes	Tracer for the chemical production of H_2SO_4 while tracking the corresponding reduction in SO_2 concentration
`i_other`	-	Tracer for other processes in MADE3 (e.g. cloud cover weighting etc.)
`i_rest`	-	Tracer for any numerical artifact
`i_disp`	Plume-specific processes	Tracer for plume dispersion
`i_emiss`	-	Tracer for emissions

3.9. IMPLEMENTATION IN MESSY FRAMEWORK

The plume-model is implemented in the MESSy framework as an extension of the MADE3 single-box model configuration by Kaiser et al. [44]. Numerical tests have been performed to ensure the backward compatibility with MADE3 single-box configuration of Kaiser et al. [44]. The double-box plume model configuration has been further tested to ensure binary identical results when both boxes are initialised with the same parameters and the one-way plume dispersion is deactivated: this ensures that the core microphysical processes of MADE3 are identically represented in both boxes and that no numerical artifacts are introduced by the extension from single- to double-box plume model. A detailed description of numerical tests can be found in Sect. 3.10).

The model configuration can be fully controlled via a single Fortran namelist (`made3.nml`) which allows the user to operate the model either as single-box model or as a plume model. For the latter, it is also possible to choose between the instantaneous dispersion approach and the plume approach. The namelist includes two sections: `BOXINIT` is used to control either the box-model configuration or the BG box of the plume model configuration, whereas `PLUMEINIT` controls the SP and the ID box of the plume model

Table 3.5: List of the namelist parameters for the box-model configuration (BOXINIT) and double-box plume-model configuration (PLUMEINIT). For simplicity, only the parameters which are relevant to this study are listed, for a complete listing of box-model see [44].

Parameter	Units	Description
BOXINIT:		
timesteps	-	Number of timesteps
tmst	s	Timestep length
box_pressure	Pa	Pressure
box_temperature	K	Temperature
box_relhum	-	Relative humidity
box_so4rat	-	False for online calculation of H_2SO_4 production rate (see Sect. 3.4). (if True, a constant value for the rate must be provided in $\mu g\,m^{-3}\,s^{-1}$).
box_tracer	mol mol^{-1}	Initial tracer concentrations for aerosol and gases
l_plume_model	-	True to activate the double-box configuration
PLUMEINIT:		
n_spinup	-	Number of timesteps for the spin-up phase
vortex_timesteps	s	Number of timesteps for the vortex regime
vortex_tmst	-	Timestep length in the vortex regime
N_ice_vortex	m^{-3}	Ice crystal number concentration in the vortex regime
plume_so4rat	-	Equivalent to box_so4rat, but for the second box.
plume_tracer	mol mol^{-1}	Aviation-induced tracer concentrations for aerosol and gases.
l_inst_disp	-	True (False) for the instantaneous dispersion (plume model) approach (this controls the scaling of the aviation tracers, see Sect. 3.7).

configuration. The meteorological parameters, namely temperature, pressure and relative humidity, and the time parameters are initialised only once in the BOXINIT since they are the same in both boxes. A detailed list of the namelist parameters is shown in Table 3.5.

3.10. NUMERICAL TESTS AND QUALITY CHECKS

As discussed above, the double-box aircraft exhaust plume model is based on the well-established aerosol submodel MADE3. Throughout the development of the plume model, several online and offline numerical tests were conducted at various stages to evaluate the performance of individual modules within the plume model. A selection of these tests is listed below:

1. MADE3 box model test: initial test of MADE3 box model to reproduce the box-model results by Kaiser et al. [44].

2. Box model parameters: analysing the impact of individual model parameters such as temperature, pressure, temporal resolution, duration etc. on the model output.

3. Single-box to double-box test: a double-box consistency test which essentially compares two identical boxes as a first stage development of a two-box model.

4. Offline test for diffusion dynamics: testing the diffusion dynamics offline to better understand the process and its impact on aerosols prior to its online implementation integrated in the one-way interface (3.5) in the double-box configuration.

5. Process flexibility and limitation: coagulation process has been tested for its flexibility in terms of temporal resolution, for later implementation into the plume model. The results indicated that numerical instabilities occur when the temporal resolution is below 1 second. Therefore, coagulation rates cannot be reliably calculated below this temporal limit.

6. Offline sulfate chemistry: performing offline calculations for the sulfate chemistry to understand the process before implementing the online sulfate production rate for both model configurations (as shown in Sect. 3.4).

7. Terminal velocity of ice crystals: performing offline calculations for the terminal velocity of ice crystals during the vortex regime to establish whether particle removal via scavenging shall be considered in the plume model (as already discussed in Sect. 3.6).

This section discusses and elaborates only a few of these initial tests performed during the development stage of the plume model including: the first-stage test while extending the MADE3 single-box configuration to a two-box is described in Sect. 3.10.1; the sulfur budget test to verify the sulfur mass conservation is described in Sect. 3.10.2. Additionally, as a technical feature, a spin-up is introduced for the background concentrations which is performed prior to the plume model simulations and is discussed in Sect. 3.10.3.

3.10.1. DOUBLE-BOX CONSISTENCY TEST

To address the research questions outlined in Sect. 1.4, I aimed to develop a modelling approach capable of simulating the aerosol microphysical process inside an aircraft plume in the direction of the flight track as it expands and grows and eventually disperses along the flight track. To achieve this, an existing and well-established aerosol submodel MADE3 is adopted and further expanded to a double-box configuration. As the first stage of development, a single-box configuration of MADE3 is extended to the two-box configuration which should perform identical microphysics and reproduce identical results. As a part of the two-box test, I used initialisation data from Kaiser et al. [44].

Fig. 3.5 highlights the two boxes i.e., Box-1 (left) and Box-2 (right), driven by identical namelist files and producing consistent results in terms of mass concentrations. The figure shows a temporal evolution of aerosol mass concentrations in μg m^{-3} for all 9 MADE3 species (see Sect. 2.2). This test is performed over a time duration of 24 hours with a 30 minutes resolution. Furthermore, a similar test is conducted with the same namelist files for a duration of over 50 hours with a 30 minutes resolution to observe the consistency in the two boxes for a longer time duration duration (Fig. 3.6).

A standard MADE3 output is demonstrated by Fig. 3.6, highlighting the identical results in terms of the temporal evolution of aerosol number concentration (cm^{-3}) in two boxes in the nine modes (see Sect. 2.2), confirming the consistent microphysics performed in the two identical boxes. Note that at this stage, there is no interface implemented for the communication between the two boxes, thus they simply perform independent simulations based on MADE3 core microphysics.

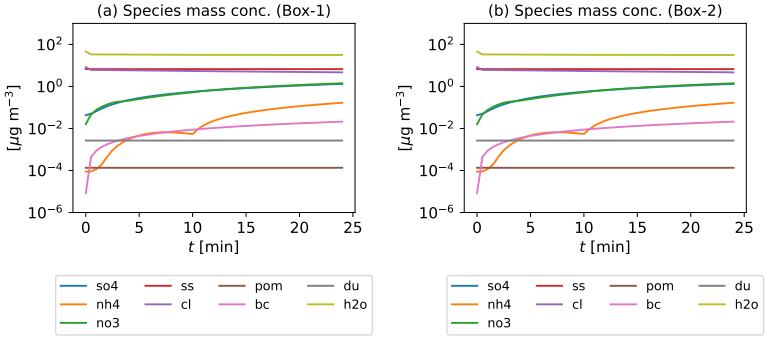

Figure 3.5: Temporal evolution of mass concentrations of all 9 aerosol species in MADE3 [44] for two identical boxes namely, a) Box-1 and b) Box-2. This test is for performed with 24 h time duration.

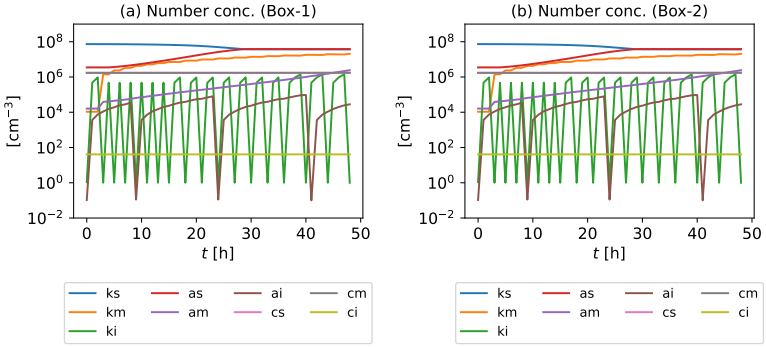

Figure 3.6: Temporal evolution of aerosol number concentrations tested for the consistency of the two identical boxes, namely a) Box-1 and b) Box-2. Here, different colours represent the MADE3 aerosol species (total mass in the nine modes). This test is performed with 24 h time duration.

After confirming the consistency in model output between the two identical boxes, an additional test is carried out to evaluate whether the two boxes exhibit similar behaviour, when initialisation parameters such as the meteorological conditions namely, temperature, pressure and relative humidity, and H_2SO_4 production rate value (note that at this stage the sulfate production rate can only be initialised as a constant), are altered in their respective namelist files. Sulfate production rate is an essential parameter in the model as it plays a key role in the formation of SO_4 aerosol in an aircraft plume (see Sect. 3.4). Table 3.6 shows the tested values of the above mentioned parameters.

Fig. 3.10 illustrates the effects of the aforementioned parameters on the aerosol number concentration in two boxes i.e., Box-1 and Box-2. Meteorological parameters such as pressure (c-d) and relative humidity (RH, e-f), significantly influence the Aitken and accumulation mode particles in all 3 mixing states. Additionally, the sulfate production rate plots (g-h) demonstrate that variations in H_2SO_4 concentrations have an influence on the Aitken mode particle concentrations in the model, which mostly comprises of the SO_4 aerosols and can be supported by Fig. 3.11 (g-h). In terms of species mass concen-

Table 3.6: List of parameters selected for the double-box consistency test along with their units and tested values.

Parameter	units	Values
Temperature	K	295.8
Pressure	Pa	50000
Relative humidity	%	87
H_2SO_4 production rate	$\mu g\,m^{-3}\,s^{-1}$	1.538×10^{-7}

trations (Fig. 3.11) however, changes in pressure shows a notable effect as compared to the reference values as shown in Fig. 3.5. In all cases, the two boxes demonstrate identical results. Therefore, it is concluded that both boxes i.e., Box-1 and Box-2, exhibit a consistent behaviour when subjected to changes in the parametrisation.

However, the sulfate production rate test signifies the importance of the H_2SO_4 production rate value for the model simulations due to its key role in the formation of Aitken mode sulfate aerosol particles. Therefore, additional tests are performed with higher (10^{-8} $\mu g\,m^{-3}\,s^{-1}$) and lower (10^{-10} $\mu g\,m^{-3}\,s^{-1}$) than the average value (10^{-5} $\mu g\,m^{-3}\,s^{-1}$) as assigned by Kaiser et al.(2014) [44]. It is observed that the sulfate production rate values have a direct impact on both SO_4 mass as well as the particle number concentrations in the Aitken mode, which influences the end results as they vary substantially with the changes in sulfate production rate values. This sensitivity study motivated the implementation of the online calculations for the H_2SO_4 production rate in the model, details are discussed in Sect. 3.4.

3.10.2. SULFUR BUDGET CLOSURE

As discussed in Sect. 3.4, the SO_4 aerosol particles are formed via nucleation or condensation of H_2SO_4 (gas) which are chemically produced by SO_2 gas with the help of available OH concentration in the troposphere (see Fig. 3.3). As the sulfate chemistry is implemented in the model, it is essential to understand the developments and changes in different sulfur species and to validate the conservation of sulfur mass in the model.

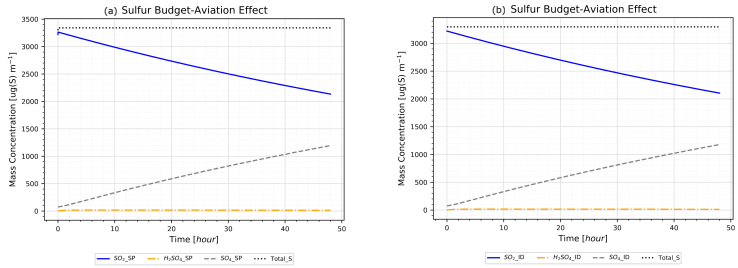

Figure 3.7: Sulfur budget closure test for SP (a) and ID (b) boxes. Sulfur species are represented by different colours such as SO_2 as blue, H_2SO_4 as orange and SO_4 as gray. Black dotted line represent the total sulfur mass. The time duration of this test was about 46 hours with a 30 minutes resolution.

The sulfur budget is tested based on the plume model output comprising of the temporal evolution of different sulfur species mass concentrations along with the tendency

diagnostics. The preliminary test for SP and ID box respectively (Fig. 3.7 a,b) shows the reduction in SO_2 mass concentration, with a corresponding growth in SO_4 mass concentration. The total sulfur mass (black dotted line, Fig. 3.7) is conserved in both SP and ID box. Here, it is observed that both modelling approaches i.e. instantaneous dispersion approach (as shown by ID box) and plume approach (as shown by SP box) display identical behaviour for the sulfur budget test, concluding that the sulfur mass is conserved in both cases.

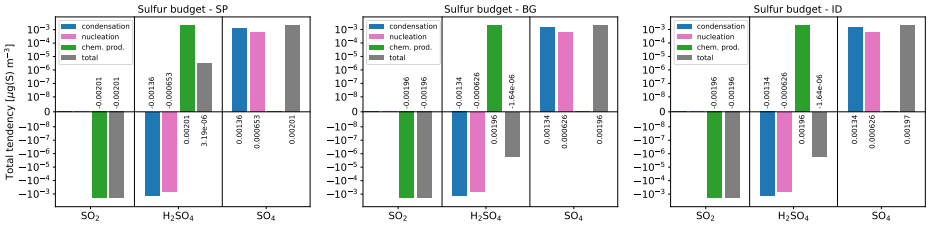

Figure 3.8: Illustration of sulfur budget for the individual boxes in the two modelling approaches namely plume approach (SP and BG box) and instantaneous dispersion approach (ID box) depicting the production of sulfate aerosol (SO_4) through nucleation and condensation processes in the plume model. The formation of H_2SO_4 (gas) is calculated online via the oxidation of sulfur dioxide (SO_2) by hydroxyl radicals (OH).

Please note that the chemical production of H_2SO_4 (gas) and their consumption for the formation of SO_4 aerosol particles, are all taking place simultaneously within a single timestep, therefore a tendency diagnostic is required to follow the whole process including the intermediate steps to assess the sulfur budget. Fig. 3.8 exhibits the processes involved in the online sulfate chemistry (see Sect. 3.4) which influences the sulfur mass concentration in all three boxes i.e., SP, BG and ID in the plume approach. This tendency analysis signifies the key role of SO_2 gas in the chemical formation of H_2SO_4 (gas) (depicted by green bars) in the model. H_2SO_4 act as a precursor for SO_4 aerosol, which is generated either through condensation processes (depicted by blue bars) or nucleation events (depicted by pink bars). The gray bars in all boxes signifies the total sulfur mass which is conserved, thus demonstrating the closure of the sulfur budget test.

3.10.3. BACKGROUND SPIN-UP CALIBRATION

As discussed in Sect. 3.7, the background concentrations play a crucial role and can affect the aerosol microphysics inside the dispersing aircraft plume. Sect. 3.2 elaborates that the emitted aircraft exhaust is mixed with the existing background concentrations upon emission, which is also numerically represented by Eqs. 3.18 and 3.19. This initial mixing is adopted for both modelling approaches i.e., instantaneous dispersion and plume approach. As these background concentrations are taken from the a simulation with the global model EMAC [43], a spin-up time is required to allow the initial concentrations (C_i^{BG}) in the BG box to reach numerical stability prior to entering the process loop, as shown in Fig. 3.2.

Fig. 3.9 shows the results from the spin-up test performed for the background aerosol concentrations, demonstrating the lognormal size distribution of the aerosols in the BG box at the initial timestep (t=0) for different spin-up durations (`n_spinup`) i.e., no spin-

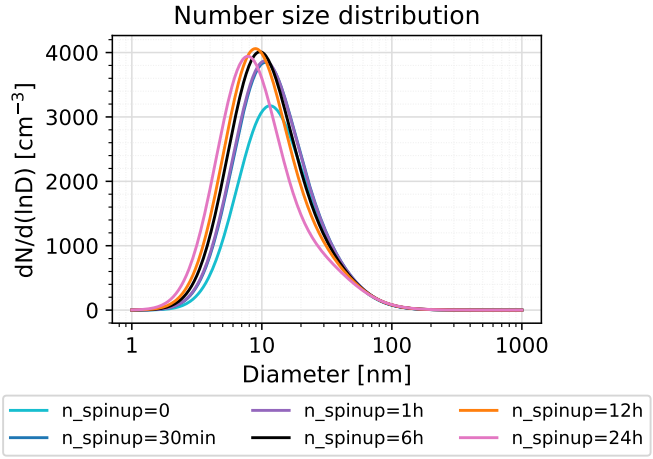

Figure 3.9: Lognormal size distribution of the aerosol particles in the background (BG box) showing the effect of different spin-up durations: no spin-up (cyan), 30 minutes (blue), 1 hour (purple), 6 hours (black), 12 hours (orange) and 24 hours (pink).

up, 30 min, 1 h, 6 h, 12 h, and 24 h. It is important to note that it is a purely numerical test. Its primary goal is to calibrate the spin-up time in the BG box before the actual plume simulation. The optimal duration is chosen when the size distribution reaches a relatively stable value. The spin-up time is a flexible parameter in the model and it can be adjusted with the help of the namelist switch `n_spinup` as described in Sect. 3.9, Table 3.5.

Based on these tests, a stable value for the size distribution is attained at around 6 hours. For longer spin-up durations, the maximum of the size distribution keeps fluctuating around a relatively constant value, with no significant changes for longer spin-up times. Considering the requirements for the plume model, I therefore set the spin-up duration to 6 hours, with a time resolution of 1 minute during the spin-up phase. This setting is used consistently to all simulations performed in this thesis.

3.11. SUMMARY

A double-box aircraft exhaust plume model is developed to explicitly simulate the aerosol dynamics in two different plume regimes namely, vortex and dispersion regime, defined based on their time of emission (Fig. 3.1). Two modelling approaches are considered: the plume approach, which consists of two boxes for the plume and the background, respectively, and accounts for the background entrainment into the plume at each timestep via one-way interface simulating diffusion dynamics (Sect. 3.5); and the instantaneous dispersion approach, in which aircraft emissions are released in a single background box, mimicking the approach of global climate models. In addition to this, online sulfate chemistry is implemented in the model to calculate the sulfate production rate based on SO_2 and OH concentration (Sect. 3.4). The double-box plume model is implemented as an extension of the standard MADE3 single-box model configuration within the MESSy

framework (Sect. 3.9). The plume model is initialized ~10 seconds behind the aircraft (Fig. 3.4) with typical background concentrations representative of the cruise altitude, while the aviation emissions are calculated using aircraft operational parameters such as aircraft fuel consumption and speed, together with the emission indices of the emitted species based on Lee et al. [26] and the size parameters from Petzold et al. [46].

A detailed assessment is carried out for single-box model configuration to reproduce previous results from Kaiser et al. [57], together with some additional diagnostics for initial sensitivities by varying different parameters in the model (Sect. 3.10). The double-box plume model configuration is also tested to ensure binary identical results when both boxes are initialised with the same parameters and the one-way plume dispersion is deactivated, to ensures that no numerical artifacts are introduced by the extension from single- to double-box plume model. As a result of the high flexibility of the MESSy interface, the model is fully configurable via Fortran namelist, allowing to switch between the single-box and double-box configuration, and to run the double-box plume model either in the plume dispersion or in the instantaneous dispersion approach (see Sect. 3.9).

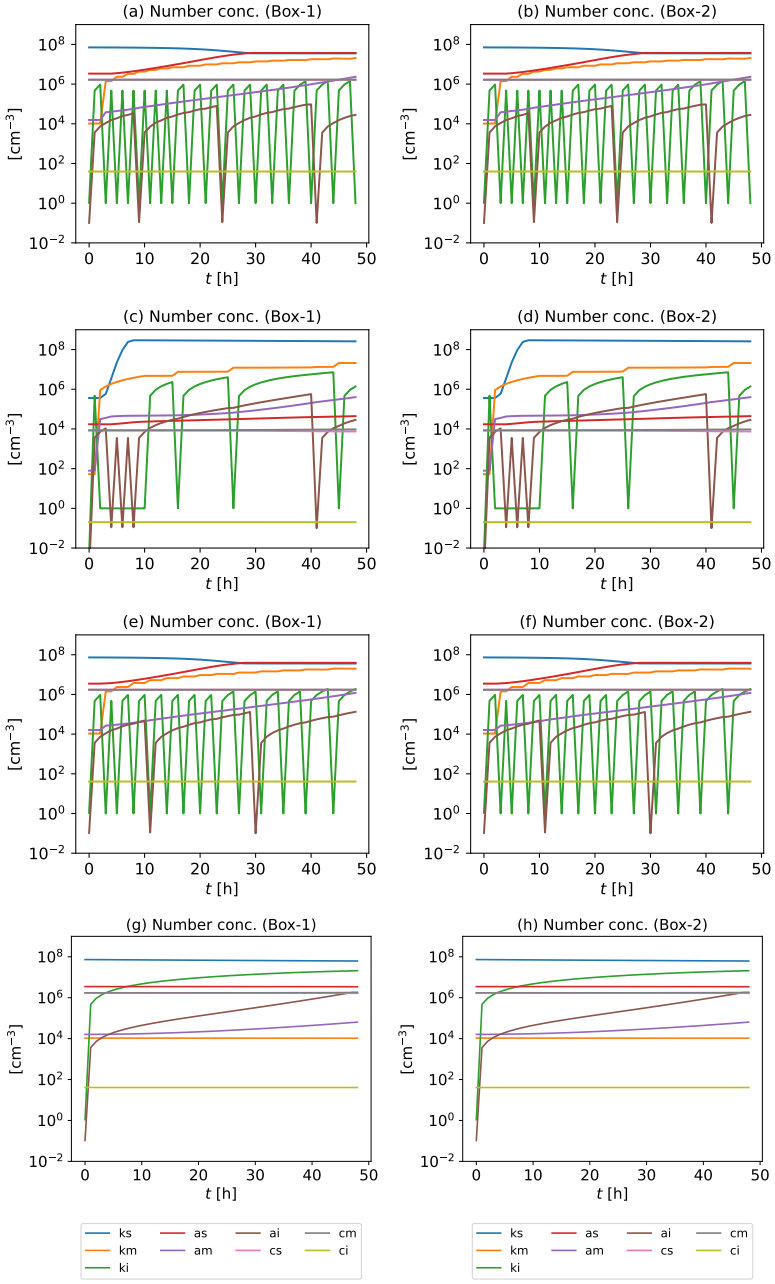

Figure 3.10: Similar to Fig. 3.6, but for the variation of the parameters such as the meteorological conditions i.e., Temperature (a-b), Pressure (c-d), and Relative humidity (e-f), and sulfate production rate (g-h) as compared for Box-1 and Box-2.

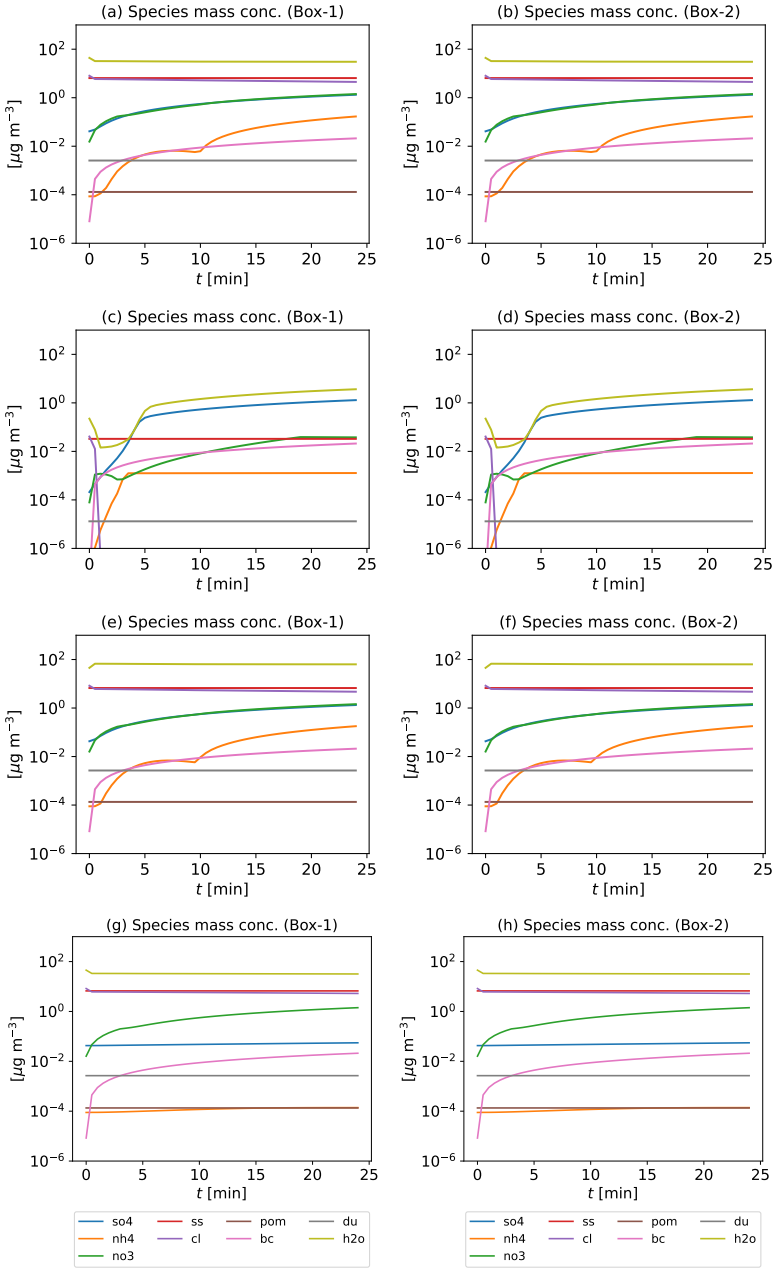

Figure 3.11: Similar to Fig. 3.10, but for the species mass as compared for Box-1 and Box-2.

4

MODEL APPLICATION

4.1. INTRODUCTION

The previous chapter provided a detailed overview of the double-box aircraft exhaust plume model, including the underlying concept, technical framework, and a comprehensive description of all modules implemented in the plume model. It also outlined the methods used to initialise the two different approaches of the plume model. Based on the following details, the current chapter focuses on the application of plume model, highlighting the plume geometry as an essential feature of the model and presenting the plume model results related to aviation-induced aerosol particles.

In this chapter, I first present the plume geometry which sets the physical boundaries within which all microphysical, chemical, and dynamical processes evolve. It comprises of two components, namely "plume age proxy" to determine the age aircraft exhaust plume and the emitted particles and gases that are trapped inside (Sect. 4.2.1), and "plume area evolution" (Sect. 4.2.2) to determine the growth and expansion of aircraft exhaust plume based on diffusion dynamics at the cruise altitude. Sect. 4.3 explains the methods required to assess the plume model results to explicitly highlight the plume effects on the emitted aerosol particles. Furthermore, a detailed analyses of the plume model results for the reference setup (Sect. 4.4, also referred as REF in this thesis), are presented and discussed in the following sections: Sect. 4.4.1 highlights the temporal evolution of the total mass concentration of aerosol species, focusing on SO_4 and soot, and the aviation effects for the species mass concentration are discussed in Sect. 4.4.2. Sect. 4.4.3 exhibits the temporal evolution of total particle number concentrations, and the aviation effects for aviation-induced aerosol number concentrations are demonstrated in Sect. 4.4.4. Moreover, Sect. 4.4.5 explores the lognormal size distribution of the aviation-induced particles at the end of the dispersion regime. In addition

This chapter is based on Sharma et al. [79],
parts of this chapter are based on Mahnke et al. [94](Monica Sharma)

to coagulation, the nucleation process plays a significant role in influencing the aerosol number concentration, but its representation in the model is subject to uncertainties. To further investigate this, an additional sensitivity experiment is conducted i.e., NUC10 (Sect. 4.5), targeting the size of newly nucleated particles in the plume model, which controls the number concentration of newly formed aerosol particles. The setup for NUC10 experiment is same as the REF setup, except the size of newly formed particles, see Table 4.1 for details.

The discussion on the results follow the comparison of two modelling approaches (as described in Chapter 3): the plume approach and the instantaneous dispersion approach. Both approaches are analysed under two distinct plume scenarios, with and without the presence of short-lived contrail ice particles in the vortex regime (referred to as Wice and NOice, respectively). For the reference setup (REF), the North Atlantic region as background is considered (Sect. 3.7), since it has one of the busiest flight corridors in the world. Table 4.2 highlights the boundary conditions for the setup.

Additional regions are further analysed in Chapter 5 to investigate the impact of background conditions on the aerosol microphysical processes. As outlined in Sect. 3.8, the tendency diagnostics are implemented in the model to analyse the contribution of individual microphysical processes to the aerosol properties and will be used throughout the chapter to support the interpretation of the results.

4.2. PLUME GEOMETRY

This section discusses the plume geometry as the temporal evolution of the plume cross-section area, based on the diffusion scheme described in Sect. 3.5, and as an additional feature, the plume model can also calculate a plume age proxy based on the evolution of the NO_y passive tracer (Sect. 4.2.1). This feature was implemented in the model motivated by a collaboration between DLR and Forschungzentrum Jülich (FZJ) in the EU-project ACACIA. The plume age proxy developed here were used to analyse measured data obtained by the IAGOS-Caribic flying laboratory and to constrain the age of the observed plumes based on the measured NO_y concentrations. The results are presented in the publication by Mahnke et al. (2024)[94].

Note that during the dispersion regime the diffusion of an aircraft plume is controlled by the dispersion dynamics as calculated in the plume model (Sect. 3.5) based on the initial diffusion parameters, namely D_h, D_v, D_s and s (Table 3.2). Alternatively, these diffusion parameters are factored by 1.5 and 0.75 based on Petry et al. [45] for a faster and a slower dispersion rate, respectively. This added feature complements the plume diffusion calculation in the model and is illustrated through both features of the plume geometry i.e., plume age proxy and plume area evolution.

4.2.1. PLUME AGE PROXY

The reactive nitrogen NO_y comprises of the sum of all reactive nitrogen species derived from the nitrogen oxides NO_x ($NO_x = NO + NO_2$) [95], and other reactive nitrogen species such as nitric acid (HNO_3), dinitrogen pentoxide (N_2O_5) and peroxyacetyl nitrate (PAN) [45, 96]. Aircraft emission of nitrogen oxides (NO_y) is influenced by a number of parameters such as engine type, engine load, fuel flow, flight velocity, flight altitude and

Table 4.1: Overview of the experiments conducted in this work. Further details on the respective parameters are provided in Table 5.1, 3.3 and 6.1.

Experiment	Description	Contrail ice	Nucleation size	Region	Varied parameter(s)	Section/Chapter
REF(Wice)	Reference	Yes	3.5 nm	North Atlantic	–	Sect. 4.4
REF(NOice)	Reference	No	3.5 nm	North Atlantic	–	
NUC10(Wice)	Sensitivity to nucleation size	Yes	10 nm	North Atlantic	Size of nucleated particles	Sect. 4.5
NUC10(NOice)	Sensitivity to nucleation size	No	10 nm	North Atlantic	Size of nucleated particles	
Europe	Backgr. conditions for Europe	Yes	3.5 nm	Europe	–	Chapter 5
USA	Backgr. conditions for the USA	Yes	3.5 nm	USA	–	
China	Backgr. conditions for China	Yes	3.5 nm	China	–	
North Pacific	Backgr. conditions for North Pacific	Yes	3.5 nm	North Pacific	–	
A1-A4	Sensitivity to contrail ice number	Yes	3.5 nm	North Atlantic	N_{ice}, EI_{soot}	Chapter 6
B1-B4	Sensitivity to soot size	Yes	3.5 nm	North Atlantic	Soot size	
C1-C4	Sensitivity to sulfate size	Yes	3.5 nm	North Atlantic	SO_4 size	
D1-D4	Sensitivity to primary SO_4	Yes	3.5 nm	North Atlantic	Primary SO_4 fraction	
E1-E4	Sensitivity to FSC	Yes	3.5 nm	North Atlantic	FSC	

Table 4.2: Details of reference region considered to initialise background for the REF setup (Sect. 4.4) and nucleation size test (Sect. 4.5) in this thesis. The regional boundaries follow [24] and the resulting parameters are from the reference simulation of Righi et al. [43], representative of 2015 conditions. The vertical selection corresponds to model levels 18 and 19 of EMAC (approx. 10-12 km).

Parameters	Values
Region	North Atlantic
Latitude	40-63° N
Longitude	70-5°W
Temperature [K]	215-220
Pressure [hPa]	210-240
RH [%]	40-70
No. of ensembles	432

ambient atmospheric conditions. These parameters also influence the emission indices of emitted compounds. NO_y emissions are mainly produced as a result of high engine temperature, which converts the molecular nitrogen in the ambient atmosphere into NO_y compounds [97]. In the aircraft plume studies, the minimal difference between NO_x and NO_y in the near-field is neglected, allowing NO_y to be used as a proxy for NO_x [80, 98] to simplify the data interpretation without the significant loss of accuracy. Although NO_y is a family of highly reactive species in the atmosphere, studies suggest that NO_y is relatively stable (i.e. chemically inert) in the early stages of an aircraft plume (first few hours), thereafter it undergoes chemical transformations [99].

Some studies also support the use carbon dioxide (CO_2) tracer as a plume age proxy [96], given its chemical inertness and high atmospheric stability [100, 101]. However, due to its high and uniform atmospheric background concentration, which is primarily driven by combustion emissions, it has a low emission perturbation detection [102]. Therefore, the dynamical properties of the NO_y makes it an appropriate and more reliable tracer for the plume age proxy in the *in-situ* measurements, alternative to the CO_2 tracer.

NO_y is added as a passive tracer to the plume and is initialised at time t_0 = 2 minutes behind the aircraft at the beginning of the dispersion regime (Fig. 3.1). Since the aircraft emitted NO_y is emitted in the form of NO_x [94], the initial NO_y mass concentration (C_{NO_y}) is calculated based on the available emission index value of NO_x from Lee et al. [26] using Eq. 3.17 (see Table 3.3).

The plume model described in this thesis can simulate three dispersion scenarios: slow, medium and fast as shown in Fig. 4.1, thus also providing an uncertainty range in the plume age estimated from the NO_y concentration.

4.2.2. PLUME AREA EVOLUTION

As mentioned in Sect. 3.5, the initial cross-section area of the aircraft plume (A_{plume}) is calculated based on parameters such as diffusion coefficients and wind shear. I assume that during the vortex regime, there is no substantial growth in a aircraft plume, thus the plume area expansion calculations begin after the first 2 minutes of the simulation, which is the beginning of dispersion regime in the plume model (Fig. 3.2). As discussed in Sect. 3.2, since my aim is to compare the plume model approach with the instantaneous dispersion approach, the time integration of the model continues until the value

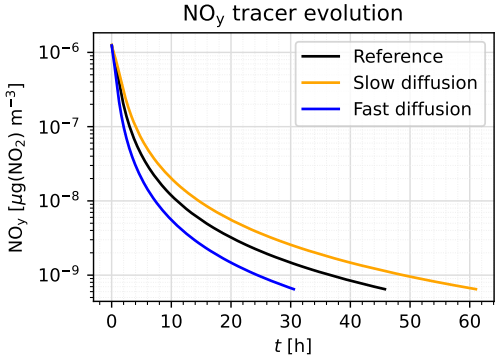

Figure 4.1: Temporal evolution of NO_y mass concentration ($\mu g(NO_2)$ m^{-3}) in the plume model during the dispersion regime. Three dispersion scenarios simulated by the plume model are medium or REF (black), slow (orange) and fast (blue).

of the plume cross-section area is equivalent to the cross-section area of the large-scale grid box i.e. $A_{\text{plume}} = A_{\text{grid-box}} = 300$ km^2. This is the reference area shown in Fig. 4.2 and the time where this cross-section area is reached is the reference time. Unless otherwise stated, the comparison of the model results between the two approaches will be performed at the reference time.

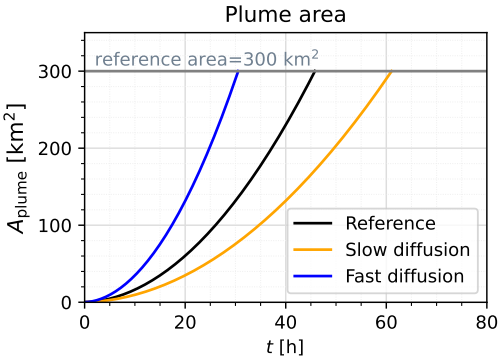

Figure 4.2: Temporal evolution of plume cross-section area (km^2).

As shown in Fig. 4.2, for the set of diffusion parameters as in Petry et al. [45], the reference area corresponds to a reference time of ~46 hours. For the purpose of the studies carried out in this thesis, I have used the medium dispersion scenario i.e. 46 hours, for all my simulations. As discussed in Sect. 3.5, the diffusion process is controlled by the variability in the atmospheric parameters which eventually influence the aerosol microphysics inside the dispersing plume. Thus, plume diffusion can be considered as an additional source of variability in the model results.

4.3. AVIATION EFFECT AND PLUME CORRECTION

Plume model results are evaluated for the mass concentrations of the emitted species inside an aircraft plume as well as the total particle number concentrations. In this thesis, at first, the temporal evolution of aerosol particles in terms of total mass concentrations of species such as SO_4 and soot together with total aerosol number concentrations are analysed with the aim to characterize the overall aerosol transformation throughout the simulation in both modelling approaches. However, the temporal evolution of the total aerosol concentrations alone does not allow to disentangle the impacts on the aviation-induced concentrations, as these are small compared to the overall concentrations (including background), also in consideration of the fact that the plume model tracks the emissions from a single aircraft plume, which has a small impact compared to the background. Moreover, the area-scaling effect due to the mixing of plume in the background environment- which refers to the influence of the geometric plume expansion on the dilution and distribution of a quantities such as aerosol concentration and number density, adds further complexity to assessing the aviation effect on the aircraft emitted aerosols. Therefore, in order to isolate the plume scale effect on the aviation emissions, as a next step the aviation effect $\mathscr{E}$ is calculated for particle masses, numbers and lognormal size distributions, and their values are compared in the two approaches at the end of the dispersion regime, i.e. at the reference time where the plume cross section area reaches the value of the large-scale grid box (~46 h).

This aviation effect, $\mathscr{E}$, is calculated offline by subtracting the background concentration from the concentration in the SP and in the ID box, for the plume and instantaneous dispersion approach, respectively. In order to obtain and isolate the effect of microphysical processes at the plume-scale on the concentration of the species i at the scale of the grid box, the aviation effect in the plume approach is scaled with the ratio of the cross-section areas:

$$\mathscr{E}_i^{\text{plume}}(t) = \left[C_i^{\text{SP}}(t) - C_i^{\text{BG}}(t)\right] \frac{A_{\text{plume}}(t)}{A_{\text{grid-box}}}, \tag{4.1}$$

$$\mathscr{E}_i^{\text{inst.disp.}}(t) = C_i^{\text{ID}}(t) - C_i^{\text{BG}}(t), \tag{4.2}$$

for the plume and instantaneous dispersion approach, respectively. Note that at the reference time the scaling has no effect, as the two areas are identical by definition ($A_{\text{plume}}(t = 46\text{ h}) = A_{\text{grid-box}}$). Based on Eqs. (4.1) and (4.2), I further define a plume correction, $\mathscr{P}(t)$ (Eq. 4.3), as the difference in the aviation effect calculated with the plume approach with respect to the instantaneous dispersion approach:

$$\mathscr{P}(t) = \frac{\mathscr{E}_i^{\text{plume}}(t) - \mathscr{E}_i^{\text{inst.disp.}}(t)}{\mathscr{E}_i^{\text{inst.disp.}}(t)}. \tag{4.3}$$

Smaller spatial scales provide an opportunity for higher collision rates and more rapid phase changes compared to the larger spatial scales. Hence, microphysical processes such as coagulation, nucleation and condensation are expected to be more efficient at the plume-scale than over a larger grid-box area, which eventually affect the

overall aerosol number concentrations at the end of the dispersion regime of an aircraft plume. The effect on the aerosol mass is expected to be negligible, as the total mass is conserved, although minor differences may arise due to difference in the condensation and nucleation rates in the two approaches affecting the partitioning between the gas and aerosol phase. These aspects will be explained by analysing the tendency diagnostics available in the plume model output. A significant deviation is expected under different plume scenarios upon comparing the two modelling approaches.

4.4. REFERENCE CASE: NORTH ATLANTIC REGION

4.4.1. AEROSOL MASS IN AN AIRCRAFT PLUME

This section discusses the the plume model results in terms of total mass concentrations of SO_4 and soot in the two modelling approaches, explicitly highlighting the values from SP and ID boxes, for the reference case study of the North Atlantic region. Fig. 4.3 shows the temporal evolution of total SO_4 mass concentration for the reference setup and two plume scenarios i.e. REF(Wice) and REF(NOice). Fig. 4.3 shows the microphysical transformation of total SO_4 mass concentrations in two different regimes of an aircraft plume, i.e. vortex (violet-shaded area, first 120 seconds) and plume dispersion (white area). The initial difference at time t_0 between the solid and dashed lines is due to the fact that the same mass is initialised in both boxes, but scaled over different cross-section areas (initial plume area vs. large-scale grid box). Thereafter no change is observed during the vortex regime, as the only process active in this phase is coagulation, which is mass conserving.

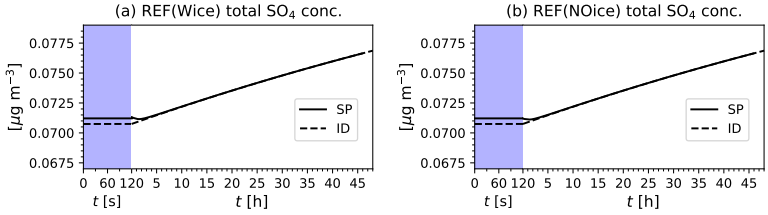

Figure 4.3: Temporal evolution of SO_4 mass concentration (μg m^{-3}) in two modelling approaches with SP box (solid) and ID box (dashed) for two plume scenarios in the reference setup as REF(Wice) and REF(NOice). Here, the violet-shaded area represents vortex regime (time in seconds) of an aircraft exhaust plume while the dispersion regime is shown by white background (time in hours).

However, at the end of the vortex regime as the ice particles undergo total sublimation, some residual mass (see Sect. 3.6) is released back to the aerosol phase which can be seen as the small jump at the beginning of the dispersion regime of REF(Wice) only (Fig. 4.3 a). In case of SO_4 however, an approximately constant growth is observed for both modelling approaches during the dispersion regime, resulting from the formation of SO_4 particles via the oxidation of SO_2 into H_2SO_4 (gas) and subsequent condensation and nucleation into SO_4. This is shown by the sulfur budget analysis in Fig. 3.8, where the increasing SO_4 mass corresponds to either the formation of new particles and/or the condensation of H_2SO_4 (gas) which are chemically produced via the oxidation of SO_2 gas and OH concentration as calculated explicitly in the model. At the end of the dispersion

regime (46 h), both approaches show almost identical values for the mass of SO_4. Similar conclusion can be drawn for the REF(NOice) scenario.

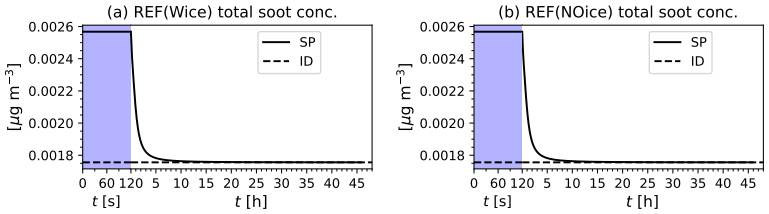

Figure 4.4: As in Fig. 4.3, but for the temporal evolution of aviation-emitted soot mass concentration in the two modelling approaches with SP box (solid) and ID box (dashed) for two plume scenarios in the reference setup as REF(Wice) and REF(NOice).

In case of soot (Fig. 4.4), a similar behaviour is observed from both modelling approaches, with no changes during the vortex regime. However, during the first few hours of the dispersion regime, an exponential reduction is observed in soot mass resulting from the plume diffusion. Unlike SO_4, after the emission no further sources of soot are included in the model which may lead to an increased mass concentration. Hence, the soot mass concentration decreases in the SP box due to plume diffusion, while it remains constant in the ID box. As for the reference time, the total concentration of aviation emitted soot remains same at the end of the dispersion regime in both modelling approaches.

4.4.2. AVIATION EFFECT ON SPECIES MASS

In order to highlight the effect of plume-scale processes on the aviation-induced SO_4 mass in the two approaches, the aviation effect is calculated based on Eqs. (4.1) and (4.2) as described in Sect. 4.3. Fig. 4.5 shows the temporal evolution of the aviation-induced SO_4 mass concentration in the two approaches for the REF(Wice) and REF(NOice) scenario. SO_4 is controlled by the availability of SO_2 gas concentration in the model. Therefore, the concentration of SO_2 depletes as it gets chemically converted into H_2SO_4 gas via the oxidation with OH as explicitly calculated in the model (Sect. 3.4). As H_2SO_4 is produced in the gas phase it eventually contributes to the aerosol SO_4 via nucleation and/or condensation, resulting in the almost linear growth observed in both approaches during dispersion regime. Due to its slow chemical production [82], the oxidation of SO_2 in H_2SO_4 is not accounted for during the vortex regime and starts at the beginning of dispersion regime at t=120 s. Hence, no changes in aviation-induced SO_4 mass occur during the vortex regime. Since the only active process during the vortex regime is coagulation, the aviation-induced SO_4 mass is conserved during this regime. At the end of the vortex regime (Sect. 3.6), I assume the complete sublimation of the short-lived contrail, releasing the residual aerosol particles back to the plume (SP box). As the sulfate production rate is initiated at the beginning of the dispersion regime, H_2SO_4 becomes immediately available for nucleation and condensation. In the early phases of the dispersion regime, however, nucleation is favoured over condensation due to the low availability of condensation sinks, as shown by the tendency time-series in Fig. 4.6.

This is not the case in the REF(NOice) scenario (Fig. 4.6 b), since no efficient reduc-

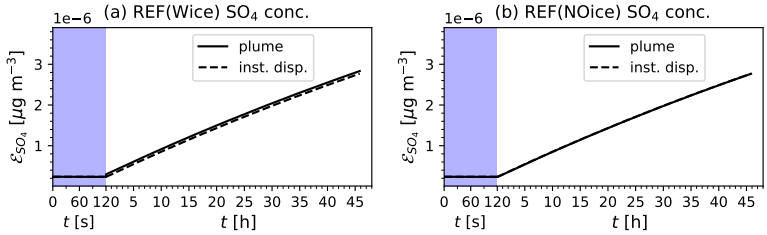

Figure 4.5: Aviation effect ($\mathscr{E}$) of microphysical processes at the plume-scale on the concentration of SO_4 in the two modelling approaches: plume (solid) and instantaneous dispersion (dashed) in the reference case with (a) and without the short-lived contrail ice (b). The shaded area represent the vortex regime. Note the different units for time on the horizontal axis for the vortex and dispersion regime.

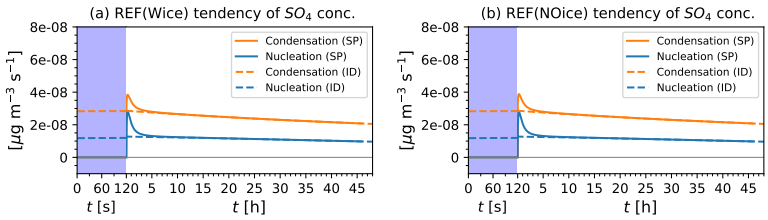

Figure 4.6: Tendency diagnostics of aerosol SO_4 mass concentration (μg m^{-3} s^{-1}) integrated over the dispersion regime in the SP (solid) and ID box (dashed) for the two plume scenarios with (a) and without (b) contrail ice formation showing the two dominant processes condensation (orange) and nucleation (blue).

tion of particle number takes place during the vortex regime, leaving enough condensation sinks available at the beginning of the dispersion regime. The sulfur budget analysis as shown in Fig. 3.8 (Sect. 3.10.2), demonstrates the production of SO_4 mass dominantly due to the condensation of H_2SO_4 (gas) in all the three boxes SP, BG and ID. This is responsible for an approximately linear growth of SO_4 mass during the dispersion regime (see Fig. 3.8). This applies to both Wice and NOice scenarios.

4.4.3. AEROSOL NUMBER IN AN AIRCRAFT PLUME

The particles emitted by an aircraft are generally smaller than those from other combustion sources, due to the higher combustion efficiency of aircraft turbines. Hence, even for the relatively small emissions of aerosol mass, the corresponding particle number emission can be large, which is reflected in my assumptions for the initialisation of particle number (see Sect. 3.7 and Table 3.3). The temporal evolution of total particle number concentration in the two modelling approaches is shown in Fig. 4.7. Considering the critical roles of coagulation and nucleation processes in aerosol number concentration, the comparison of the two plume scenarios offers valuable insights, particularly highlighting the impact of aerosol-ice coagulation in the Wice scenario relative to the NOice scenario. In the REF(Wice) scenario, the SP box shows a strong almost linear reduction in the total particle number concentration during the vortex regime. This is the result of both, aerosol-aerosol and aerosol-ice coagulation during this phase, with the latter be-

ing the dominant one, given the large relative difference in size between aerosol particles (~10 nm) and ice crystals (~1 μm), which maximizes the coagulation rates.

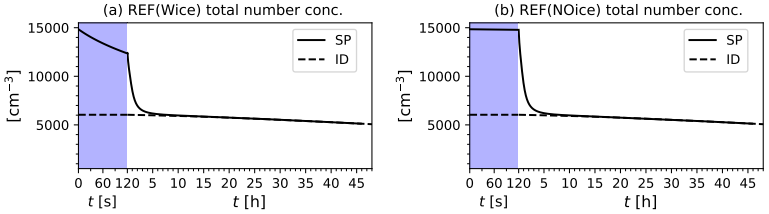

Figure 4.7: Temporal evolution of total aerosol number concentration (cm^{-3}) for two modelling approaches, i.e. SP box (solid) and ID box (dashed) in two plume scenarios, a) REF(Wice) and b) REF(NOice). The two regimes of an aircraft plume represented here are vortex regime (violet) and dispersion regime (white).

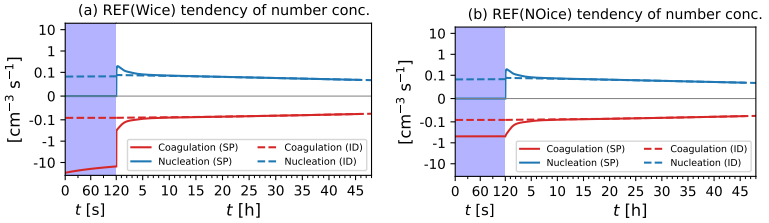

Figure 4.8: Tendency diagnostics of aerosol number concentration in both vortex (violet) and the dispersion regime (white) in the SP (solid) and ID box (dashed) for the two plume scenarios with (a) and without (b) contrail ice formation showing the two dominant processes coagulation (red) and nucleation (blue).

Notably, this process leads to a ~20% reduction in total particle number concentration in the plume approach already within the first 2 minutes in REF(Wice) scenario (Fig. 4.7 a). At the end of the vortex regime (Fig. 3.2), I assume that the short-lived contrail completely sublimates, releasing the residual aerosol particles (Sect. 3.6) back to the plume and they enter the dispersion regime. During the dispersion regime, I observe a strong exponential decay in the total aerosol number concentration within the first few hours of simulation in case of the SP box, which is due to the enhanced coagulation process in the plume approach as compared to the instantaneous dispersion approach and is explained by the tendency diagnostics for the aerosol number concentration in Fig. 4.8. As the simulation proceeds and the plume expands further, the coagulation process becomes less effective and a slower but steady reduction in total particle number concentrations is observed. In the ID box, however, the total aerosol number concentration remains constant during the first two minutes (Fig. 4.7, dashed line), as there are no ice particles in the vortex regime and hence no aerosol-ice coagulation involved, while only a slow reduction is visible during the dispersion regime, due to a much less effective coagulation process than in the SP box (Fig. 4.7).

In the REF(NOice) scenario (Fig. 4.7 b), the total particle number reduction in the SP box during the vortex regime is negligible due to the absence of short-lived contrail ice crystals, and the reduction due to aerosol-aerosol interaction is far less efficient and

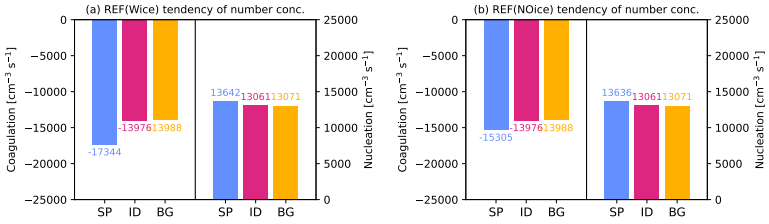

Figure 4.9: Tendency diagnostics of aerosol number concentration (cm^{-3} s^{-1}) for the two plume scenarios i.e., with and without the presence of contrail ice in the vortex regime as shown by a) REF(Wice) and b) REF(NOice) respectively. The plots demonstrate an overall impact of the two dominant microphysical processes namely, coagulation (left axis) and nucleation (right axis) on the aerosol number concentrations in all three boxes; SP (blue bar), BG (orange bar) and ID (pink bars). Note the different scales on the vertical axes for coagulation (left axis) and nucleation (right axis).

for such short duration (~2 minutes) is insignificant. This demonstrates the impact of short-lived contrail ice crystals on the aerosol population during the vortex regime. The tendency diagnostics reveal the role of both nucleation and coagulation processes in controlling the particle number concentration. Fig. 4.8 highlights a critical aspect that in addition to coagulation, nucleation is also a key process in controlling the particle number concentrations in the plume, especially in the early stages (first 8 hours).

Additionally, Fig. 4.9 signifies the overall efficiencies of the two dominant processes controlling the particle number concentrations i.e., coagulation (left axis) and nucleation (right axis), in all three boxes namely, SP, BG and ID. Here, it is clearly observed that the coagulation process is more efficient in the SP box (blue bar) especially in case of REF(Wice) scenario due an effective collision between the small-sized aerosol particles and larger ice crystals in the vortex regime as compared to REF(NOice) scenario. The efficiency of nucleation is also comparatively high in SP box for both plume scenarios.

4.4.4. AVIATION EFFECT ON AEROSOL NUMBER

While Sect. 4.4.3 explores the total aerosol number concentration, in this section the aviation effect is analysed similar to the Sect. 4.4.2, but for the aviation-induced aerosol number concentrations to isolate the effect of microphysical processes from the plume dispersion (Fig. 4.10). Here, a clear difference between the plume and the instantaneous dispersion approach can be distinguished, in both scenarios. In the REF(Wice) scenario, the aviation-induced number concentration is considerably reduced during the vortex regime: due to their much larger size (~1 μm), the ice crystals effectively remove the Aitken-sized (~10 nm) aerosol particles via coagulation within the first 2 minutes of the simulation. After contrail sublimation at the end of the vortex regime, the residual aerosol numbers are then returned to the aerosol phase (assuming one residual particle is left for each ice crystal), which can be seen as the slight increase in the aviation-induced number concentration at t=120 s in Fig. 4.10 a (solid line). During the dispersion regime, the aviation-induced number concentration is further reduced in both approaches, due to the coagulation process, which is more efficient in the plume approach. At the same time, nucleation events occur during the dispersion regime contribute to an increase in the aviation-induced number concentration by forming new sulfate parti-

cles from the gas phase. Given the small size (3.5 nm) of the particles assumed by the nucleation scheme of MADE3 [62], even a few nucleation events might have large contributions to the particle number. Hence, coagulation and nucleation act in opposite directions to affect particle number concentrations. The analysis of the respective tendencies (Fig. 4.8) shows that both processes are more efficient in the SP than in the ID box due to the higher aerosol concentrations over a smaller spatial scale, especially in the early phase of the plume dispersion (first 8 hours), while they evolve similarly at later stages, as the plume cross-section area gradually expands.

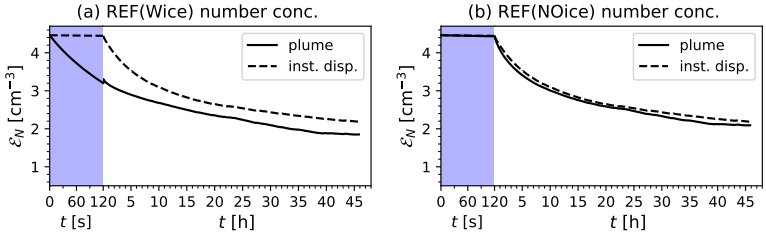

Figure 4.10: Aviation effect ($\mathscr{E}$) of microphysical processes at the plume-scale on aviation-induced particle number concentration in the two modelling approaches in the reference case with (a) and without the short-lived contrail ice (b). The shaded area represent the vortex regime. Note the different units for time on the horizontal axis for the vortex and dispersion regime.

The difference in the concentration of aviation-induced aerosol numbers in plume approach relative to the instantaneous dispersion approach varies during the simulation based on the availability of the aerosol numbers and the predominant processes in the plume model. After the first two hours of the simulation the plume correction ($\mathscr{P}$) is about –23% in the REF(Wice) scenario, as a result of the coagulation during the vortex regime (Fig. 4.10 a). As the simulation proceeds, $\mathscr{P}$ reduces to about –17% after 6 hours and further to –12% after 12 hours. At the end of the dispersion regime, the plume correction is –15% with a ±1 standard deviation range of [–30; –0.7]%. In absolute terms this corresponds to –0.33 [–0.65; –0.02] cm^{-3}.

In the REF(NOice) scenario (Fig. 4.10 b), no significant change can be seen in aviation-induced aerosol number concentrations in the vortex regime and the concentrations of the aviation-induced aerosol number concentration remain almost identical in both boxes, as the only active process in this regime is the aerosol-aerosol coagulation. As the dispersion regime begins, the two dominant processes i.e., nucleation and coagulation contributes towards the significant reduction of the aviation-induced number concentration in both modelling approaches, as shown by the tendency analysis (Fig. 4.8 and 4.9). In case of REF(Wice), however, they are mostly effective during the early stages of the plume dispersion. The nucleation process has a similar tendency as in the REF(Wice) scenario, while the coagulation is more efficient, possibly due to the higher number concentration in the REF(NOice) scenario resulting from the absence of aerosol-ice coagulation during the vortex regime. The plume correction in this scenario (Fig. 4.10 b) is significantly lower and varies from –3.4% after 2 hours to –3.3% at 6 hours and –2.7% at 12 hours, reaching a value of –4.2% [–20; 11]% (–0.09 [–0.43; 0.25] cm^{-3}) at the reference time.

4.4.5. AVIATION EFFECT ON AEROSOL SIZE

To further characterize the the aviation effect ($\mathscr{E}$) to the aviation-induced particle number concentrations and the different results obtained with the two modelling approaches, I analyse in this section the lognormal size distribution (Eq. 2.3) of the aviation effect on particle number concentrations based on the number concentrations and particle dry diameters in the 9 aerosol modes of MADE3 at the reference time (Sect. 4.2.2, t = ~46 hours).

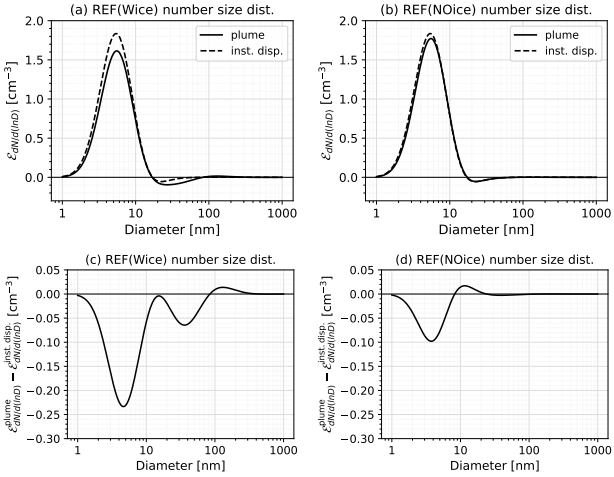

Figure 4.11: Aviation effect ($\mathscr{E}$) at the reference time on the lognormal size distribution calculated from aviation-induced aerosol number concentrations and dry diameters at the reference time in the two approaches (plume and instantaneous dispersion) and for the two scenarios REF(Wice) (a) and REF(NOice) (b). Panels (c) and (d) show the difference between the aviation effects in the two approaches.

As discussed in Sect. 3.7, aviation aerosol emissions are initialised with a particle size of 2.5 nm for aerosol sulfate and in two modes of 30 and 150 nm for soot. During the plume dispersion, processes such as coagulation and condensation contribute to the growth in particle size as the total number concentration reduces. The lognormal size distribution at the final timestep (t = ~46 hours) of the aviation effect shows a peak around 5-6 nm in both modelling approaches, while the amplitude at the peak of the distribution is lower in the plume approach than in the instantaneous dispersion approach, both for the REF(Wice) and REF(NOice) scenarios respectively. This result clearly indicates an overestimation by the instantaneous dispersion approach which is consistent with the results shown in Fig. 4.10 for the aviation-induced aerosol number concentration. The comparison between Fig. 4.11a and b highlights again the effectiveness of the aerosol-ice coagulation in the REF(Wice) scenario, significantly reducing the particle number concentration during the vortex regime, with a clearly visible effect at the end of the dispersion regime. The plume correction to the aviation-induced aerosol number concentration discussed above mostly concerns the Aitken mode particles, which are predominantly comprised sulfate aerosol particles initialised with 2.5 nm size. Another mode is visible around 30-50 nm and is due to soot particles, which are initialised

around this size range, and also show a reduced number concentration in the plume approach. In terms of the difference between the aviation effects in two approaches (Fig. 4.11c,d) the REF(Wice) scenario is characterized by a reduction in Aitken size particles (4-5 nm) of about 0.22 cm^{-3} (about –15%) for REF(Wice), whereas this value reduces to about 0.10 cm^{-3} (–4%) in for REF(NOice). Although small in absolute terms, due to the fact that it represents the effect of a single plume, the relative difference between the two approaches is very relevant, implying that plume effects need to be considered in global models and corrected for when initialising aviation emissions in these models. Initialising emissions with an instantaneous dilution approach may otherwise lead to a significant overestimates of the aviation-induced particle number concentration and in turn to an overestimated impact on cloud droplet number concentration. The presence of short-lived contrails in the vortex regime makes this correction even more significant.

4.5. SENSITIVITY TO THE NUCLEATION PROCESS

The results discussed for the reference case demonstrated that the plume correction to the aviation-induced particle number concentration is determined by the concurrence of two microphysical processes, nucleation and coagulation, and their different effectiveness in the SP and ID box. While the coagulation process is represented by the model solving the classical equations for coagulation rates within and between each mode (intramodal and intermodal coagulation, respectively, based on Kaiser et al. [44]) (see Sect. 2.2), the nucleation process is much more uncertain and needs to be parametrised. MADE3 uses the parametrisation by Vehkamaeki et al. [62], which calculates the nucleation rate as a function of temperature, relative humidity and H_2SO_4 concentration. A critical free parameter in this parametrisation is the initial size of the newly nucleated particles, assumed to be 3.5 nm in diameter. In a global model study with MADE3, however, Kaiser et al. [57] showed that assuming a larger diameter of 10 nm allows for a better model performance for aerosol number concentrations and size distributions in the free troposphere, where nucleation is the major source of ultrafine particles. Motivated by their results, I perform here an additional sensitivity test (hereafter NUC10; Sect. 4.5.1) by repeating the above analysis with this alternative assumption. Note that the EMAC model simulation output used to initialise the background concentrations in the plume model simulations also consider this assumption in a consistent way, i.e. a global simulation assuming 3.5 nm and 10 nm for the size of newly nucleated particles has been used to initialise the REF and NUC10 cases, respectively.

4.5.1. SENSITIVITY OF AVIATION EFFECTS TO NUCLEATION PROCESS

This section explores the influence of nucleation parametrization on the evolution of aviation-induced aerosol number concentration and SO_4 mass concentration. It is important note that, for a given mass, the total aerosol number decreases as particle size increases. In this sensitivity analysis (NUC10), the size of newly-nucleated particles are increased from 3.5 to 10 nm which contributes a factor of $(10/3.5)^3 \simeq 23$ less particles. Therefore, for the same mass concentration, the initial concentration of total aerosol number (Fig. 4.12) is different than in the REF setup (Fig. 4.7) due to the assumption on the size of newly-nucleated particles. The microphysics functions identical in both

cases, thus a similar temporal evolution is observed, with an exponential decrease of the total aerosol number concentration here as well. In case of NUC10(Wice), the initial reduction in total aerosol number concentration in the SP box is due to the aerosol-ice coagulation in the vortex regime which reduces the total number concentration by up to ~14% within the first 2 minutes of the simulation. Afterwards, upon the sublimation of short-lived contrail ice crystals, the residual mass and numbers are added to the total aerosol population (as discussed in Sect. 3.6). The total aerosol number concentration is exponentially reduced via the effective coagulation process within the first few hours (~3 to 5 hours) into the dispersion regime. As there is no vortex regime included in the ID box (see Fig. 3.2), the total aerosol number concentration in this case remains unchanged, however the particle numbers are gradually reduced during the dispersion regime.

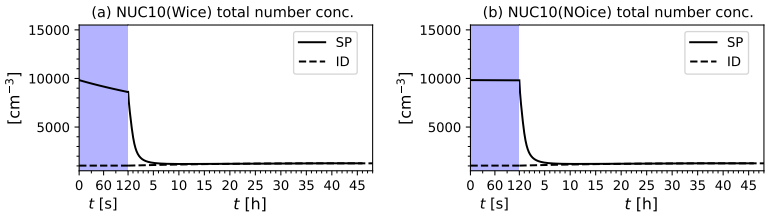

Figure 4.12: Temporal evolution of total aerosol number concentration, as in Fig. 4.7, but with the alternative assumption of 10 nm for the size of newly nucleated particles.

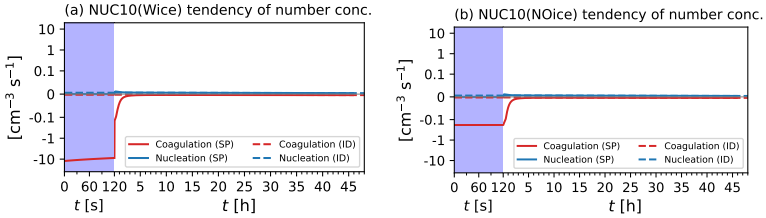

Figure 4.13: Tendency diagnostics of the aerosol number concentration, as in Fig. 4.8, but with the alternative assumption of 10 nm for the size of newly nucleated particles.

It is difficult to disentangle the aviation effect in terms of total aerosol number concentration, therefore the area-scaling effect is removed to isolate the effect of plume-scale aerosol microphysics, similar to Sect. 4.4.4 based on Eqs. 4.1 and 4.2. The aviation effect on the number concentration (Fig. 4.14) shows the same temporal evolution as in the REF case (Fig. 4.10): a very strong reduction in the vortex regime in the REF(Wice) scenario and a monotonic decrease during the dispersion phase. This decrease is much smoother than in the REF case, as the nucleation events in NUC10 produce fewer particles due to their larger size. Furthermore, as a result of the different initialisation backgrounds, a lower number of particles is entrained in the plume in the NUC10 case, hence also the reduction during the vortex regime is relatively smaller than in REF case. Nevertheless, the plume correction at the reference time is comparable to the REF case,

about –13% [–77; 55]% (–0.24 [–1.45; 0.95] cm^{-3}) and –4.2% [–9.1; 1.2]% (–0.07 [–0.17; 0.02] cm^{-3}), in the NUC10(Wice) and NUC10(NOice) scenarios, respectively. The tendency analysis (Fig. 4.13 and 4.15) shows an overall reduction in the efficiency of both microphysical processes in the NUC10 case as compared to the REF case, indicating that a reduced efficiency of the nucleation has an impact also on the coagulation, due to the reduced number of particle available in the plume.

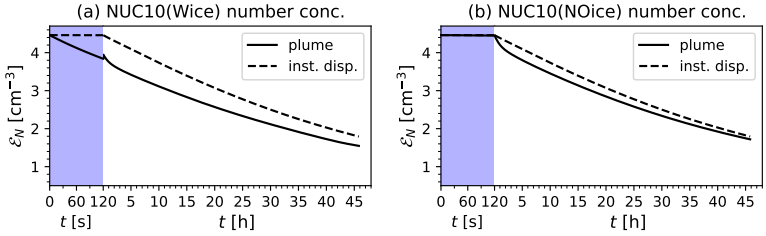

Figure 4.14: Aviation effect ($\mathcal{E}$) of microphysical processes at the plume-scale for the aerosol number concentration in the two modelling approaches, as in Fig. 4.10, but with the alternative assumption of 10 nm for the size of newly nucleated particles. The two scenarios represent the case with (a) and (b) without the short-lived contrail ice. The shaded area represent the vortex regime. Note the different units for time on the horizontal axis for the vortex and dispersion regime.

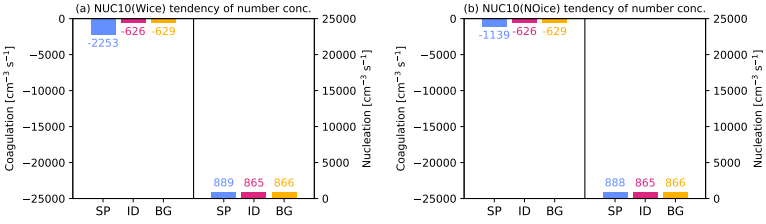

Figure 4.15: Tendency diagnostics of aerosol number concentration highlighting the overall efficiency of the microphysical processes in respective boxes, as in Fig. 4.9, but with the alternative assumption of 10 nm for the size of newly nucleated particles.

Furthermore, the aviation effect calculated for SO_4 mass concentration (Fig. 4.16) also shows the same temporal evolution as the REF case (Fig. 4.5). In NUC10(Wice) scenario (Fig. 4.16 a), no change is observed in both boxes (SP and ID) during the vortex regime as the only process active here is coagulation which is mass conserving. At the end of the vortex regime, as the ice crystals undergo total sublimation, a residual mass is added back to the aerosols based on the assigned parametrisation as discussed in Sect. 3.6 which is also observed as the slight jump at t = 120 s, also discussed in REF case (Sect. 4.4.2). At the end of the dispersion regime (t = ~46 hours), a slight deviation can be seen in the two modelling approaches which is negligible. In both plume scenarios, the sulfate production rate (see Sect. 3.4) functions identical during the dispersion regime which can be seen as a constant and steady growth in the SO_4 mass, identical to REF case.

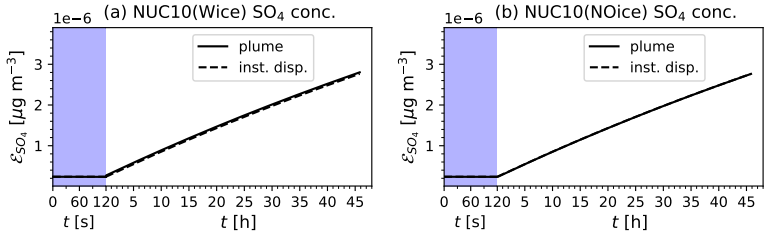

Figure 4.16: Aviation effect ($\mathscr{E}$) for the SO_4 mass concentration, same as Fig. 4.5, but for NUC10 sensitivity test in the two modelling approaches: plume (solid) and instantaneous dispersion (dashed), and in two plume scenarios Wice and NOice.

4

4.5.2. RESPONSE OF LOGNORMAL AEROSOL DISTRIBUTIONS TO CHANGES IN NUCLEATION

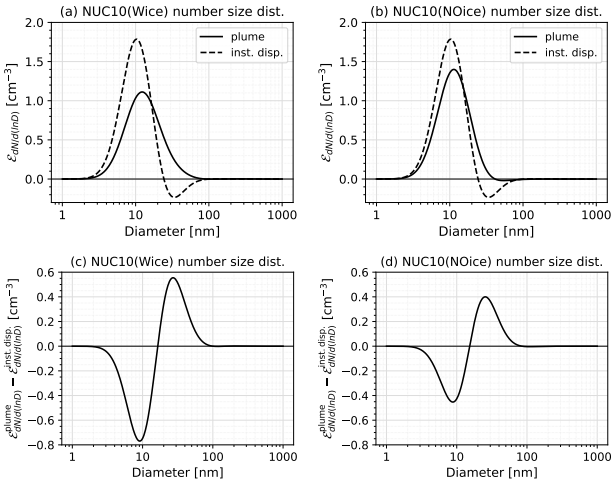

Figure 4.17: Aviation effect ($\mathscr{E}$) at the reference time (t = ~46 hours) on the lognormal size distribution in two modelling approaches (plume and instantaneous dispersion), as in Fig. 4.11, but with the alternative assumption of 10 nm for the size of newly nucleated particles. Panels (c) and (d) show the difference between the aviation effects in the two approaches.

This section presents the influence of the larger nucleation size (10 nm) of newly-nucleated particles on the lognormal size distribution of the aviation-induced aerosol particles, especially at the reference time (t = ~46 hours). Fig. 4.17 (a,b) shows the aviation effect on the size distribution at the reference time for the NUC10 study peaks at 10-15 nm for both scenarios i.e., Wice and NOice which is at a larger size as compared to the REF case, that peaks at 5-6 nm (Fig. 4.11 a,b). This is due to the increased size of newly nucleated particle, which corresponds to the particles with relatively larger size (~20 nm) surviving towards the end of the dispersion regime. The maximum of the distribution in the instantaneous dispersion approach remains higher than in the plume approach for both

scenarios (with and without ice), especially for the particles around 10-20 nm size, which are mostly SO_4 particles.

The difference between the aviation effects in two approaches for the size distribution (Fig. 4.17) further shows that the instantaneous dispersion approach overestimates the survival of the Aitken mode particles between at 8-10 nm and underestimates the 20 nm particles, which results from the less efficient coagulation process in the instantaneous dispersion approach as compared to the plume approach (Fig. 4.13). Although the size of newly nucleated particle is an important parameter in the model, no significant changes in the plume correction at the reference time between the REF and the NUC10 case is found.

4.6. SUMMARY

This chapter presented the plume model results for the reference case over the North Atlantic and a sensitivity study on the role of the aerosol nucleation process. The reference study (Sect. 4.4) demonstrates the overestimation of the aviation-induced aerosol number concentration by the instantaneous dispersion approach (Fig. 4.10) adopted by the global models. The plume approach simulates a lower aviation-induced particle number concentration at the end of the plume dispersion than the instantaneous dispersion approach: this is the so-called plume correction and is −15% for the reference case. This may have important implications for the quantification of the climate impact of aviation-induced aerosols on low clouds. Moreover, the comparison between two scenarios with and without contrail ice in the vortex regime highlights the importance of aerosol-ice interactions in this regime and its impact on the aviation-induced particle number concentration. The plume correction for the sensitivity of the assumed size of newly nucleated particles is found to be quite small, with similar results to the reference case in both scenarios, with and without contrail ice, despite aerosol nucleation being one of the key microphysical processes in the plume.

In addition to particle number concentration, the chapter also discussed the mass concentrations of aviation-induced aerosol species such as SO_4 and soot. The online sulfate production behaves similarly in both modelling approaches, resulting in a comparable sulfate mass concentrations (Fig. 4.5), i.e. with negligible differences in the gas-particle partitioning for the sulfur species. As no additional sources of soot are included in the model, the soot mass concentration decreases during the first few hours of the dispersion regime due to plume dilution, as captured by the plume approach, and show negligible differences with the instantaneous dispersion approach.

A key takeaway from this chapter is that global models need to account for the plume processes and to correct for the overestimated aviation-induced particle number concentrations resulting from missing subgrid-scale processes in these models. Such plume correction can be quantified with the plume model presented here at different stages of the plume evolution.

5

REGIONAL SENSITIVITY OF AVIATION EFFECTS

5.1. INTRODUCTION

The previous chapter (Ch. 4) presented the aviation effects for typical conditions over the North Atlantic region as a reference case application of the plume model, however, these conditions may of course vary over other regions. This is especially important when considering the background concentrations and the way they influence the aerosol microphysical processes in the plume, following the entrainment of background air inside the gradually expanding aircraft plume. As shown in Ch. 4, the aerosol lognormal size and number concentrations are strongly influenced by the nucleation and coagulation processes, while the condensation process contributes significantly to the aerosol mass concentration. In the atmosphere, new particles are formed through the nucleation process; thereafter, condensable vapours such as sulfuric acid or low-volatility organic compounds contribute to the growth of newly formed particles. This process helps stabilize the particles, preventing them from evaporating. Nucleation events, for instance, are favoured in cleaner backgrounds, due to the lower availability of aerosol particles that serve as condensation sinks (i.e. the particle surface sink for condensable gases) [103]. Given the key importance of the nucleation processes for the plume correction demonstrated in chapter 4, it is important to examine the influence of different background conditions on the plume corrections. In this thesis, I consider four highly trafficked regions in the Northern Hemisphere, characterized by the different background properties than the North Atlantic: Europe, USA, China, and the North Pacific (see Table 5.1 for details). The plume simulations are performed using the same parameters of the reference setup (Table 3.3) under the REF(Wice) scenario considering the presence of short-lived contrail ice crystals in the vortex regime. The only initialisation parameter varied in the

This chapter is based on Sharma et al. [79]

Table 5.1: Definition of the regions considered to initialise background conditions in this chapter. The regions boundaries follow Teoh et al. [24]. The resulting parameters are from the reference simulation by Righi et al. [43], representative of 2015 conditions along with the number of ensembles used in each regional study. Note that the vertical selection is identical in all regions and correspond to model levels 18 and 19 of EMAC (approx. 10–12 km).

Region	Latitude	Longitude	Temp. [K]	Press. [hPa]	RH [%]	Ensembles
Europe	35-60° N	12°W-20°E	213-220	210-240	48-70	240
USA	23-50° N	126-66°W	214-225	210-240	49-70	460
China	18-53.5° N	73.5-135°E	212-230	210-240	50-76	644
North Pacific	35-65° N	140°E-120°W	214-220	210-240	49-66	864

set of simulations discussed in this chapter are the initial background concentrations $C_i^{\mathrm{BG}}(t_0)$ for the respective regions, where i represents different MADE3 species (Sect. 2.2).

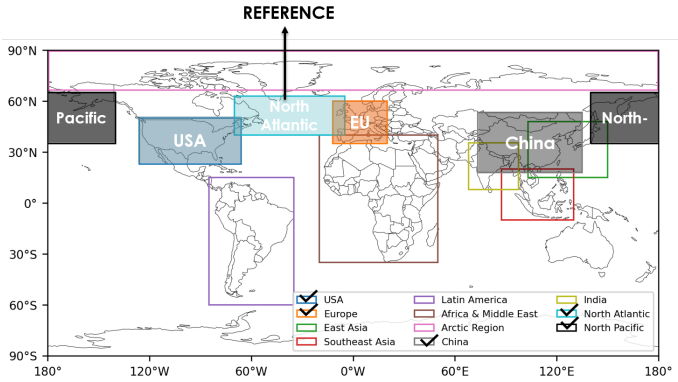

Figure 5.1: Illustration of regional boundaries selected for this chapter as described in Table 5.1. This figure is taken from Teoh et al. [24] and is further modified for the purpose of this thesis to highlight the investigated regions.

The boundaries (latitude and longitude) of the regions selected for this chapter are sourced from Teoh et al. [24] (see Fig. 5.1). As outlined in Sect. 3.7, the ensemble grid boxes varies across regions (see Table. 5.1). The background initialisation employed for the regional study in this chapter is the same as in Ch. 3 (Sect. 3.7), with two vertical levels at cruise altitudes but for the different regions. The meteorological data necessary to initialise the plume model – specifically pressure, temperature, and relative humidity – are also derived from the EMAC output, which varies between different grid boxes, as shown in Table 5.1. As described earlier in Sect. 3.7, in order to simulate the spatial variability of background conditions, the climatological mean values of each of the EMAC model grid-boxes within each region are used to initialise multiple ensemble simulations of the plume model and the model output from the ensemble boxes is analysed by calculating their weighted mean.

Given the importance of regional emission distributions, particularly at cruise altitudes, this chapter investigates how varying regional background aerosol concentrations influence microphysical processes at the plume scale, and how these, in turn, affect the plume model results during the dispersion regime. In the following, Sect. 5.2 presents the

temporal evolution of total aerosol number and SO_4 mass concentration inside a dispersing aircraft plume and discusses the variability resulting from various background conditions as defined by the regions in Table 5.1. Furthermore, Sect. 5.3 discusses the corresponding aviation effects to highlight the impact of non-linear plume-scale processes on the aviation-induced aerosol number as well as mass concentration. Sect. 5.3.3 analyses the aerosol lognormal size distribution based on the aviation-induced aerosol number concentrations at the reference time, along with the corresponding absolute differences that highlight the plume correction, and discusses the impact of regional variability.

5.2. EFFECT OF BACKGROUND CONDITIONS ON PLUME MICROPHYSICS

As discussed, in Sect. 3.7, in the plume model the background concentrations are entrained inside a dispersing aircraft plume (Eqs. 3.18 and 3.19) at each timestep which alters the total particle concentration (both mass and number) inside the dispersing plume. This can influence the aerosol microphysical processes at the plume scale, eventually affecting the plume model results. In this section, I first discuss the temporal evolution of aerosols in terms of total SO_4 mass concentration and total number concentration inside the dispersing plume with background conditions typical of different regions representative of the cruise altitude.

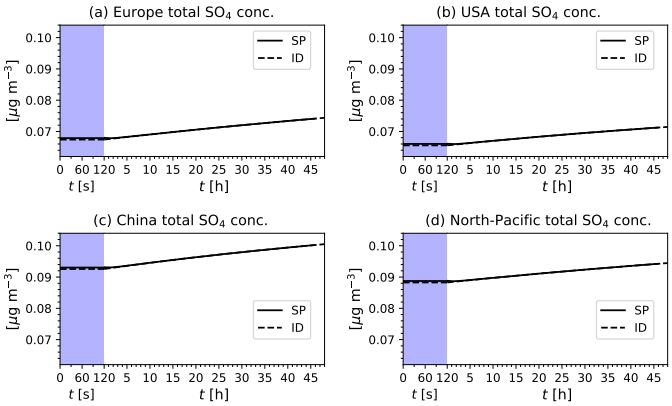

Figure 5.2: Temporal evolution of total SO_4 mass concentration (μg m^{-3}) in two modelling approaches with SP box (solid) and ID box (dashed) for different regions: Europe (a), USA (b), China (c) and North Pacific (d). Here, the violet-shaded area represents vortex regime (time in seconds) of an aircraft exhaust plume while the dispersion regime is shown by white background (time in hours)

In Fig. 5.2, a variation in the initial SO_4 mass is observed in different regions at time t_0, which is due to different background concentrations, given the other parameters and aviation concentrations are identical in all cases. Similar to Fig. 4.3, each region shows a slight difference between the two approaches due to the area-scaling effect between the boxes (SP and ID). Moreover, at time t=2 minutes, the vortex residual effect also observed

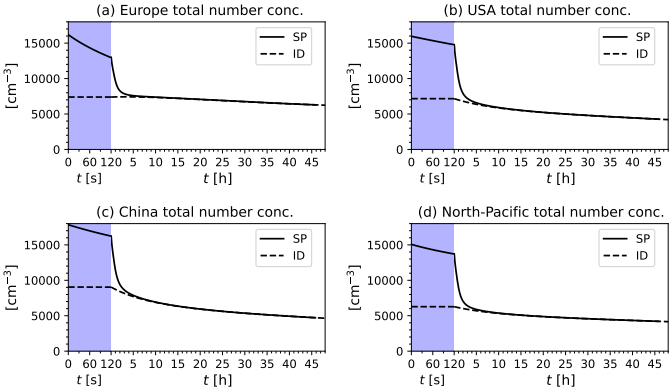

Figure 5.3: Temporal evolution of total aerosol number concentration (cm^{-3}) for different regions, as in Fig. 5.2.

in all four regions due to the total sublimation of ice crystals, as discussed in Sect. 4.4.1. At reference time (t = ~46 hours), no difference can be observed in the two approaches.

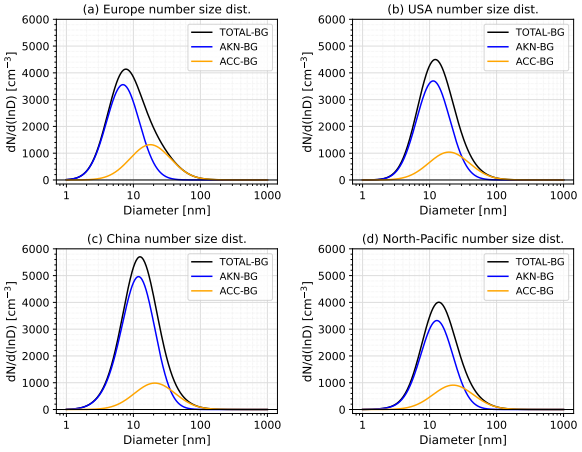

Figure 5.4: Representation of total aerosol lognormal size distribution in the background (BG box) at the initial timestep (t = 0) comprising two aerosol modes i.e. Aitken and accumulation.

Fig. 5.3 shows total aerosol number concentration over different regions. Similar to Fig. 5.2, note that, the initial particle numbers vary in different regions due to the background effect. Furthermore, in case of total aerosol number concentration (Fig. 5.3) also, the initial differences observed between the two boxes SP and ID is due to the area-scaling effect, which can be observed in all regions. As the Wice plume scenario (Sect. 4.1) is considered for this regional study, a reduction is clearly visible in the aerosol numbers as a result of aerosol-ice interaction for all the regions. It is interesting to note that this process lead to ~25% of reduction in the total particle number concentration in

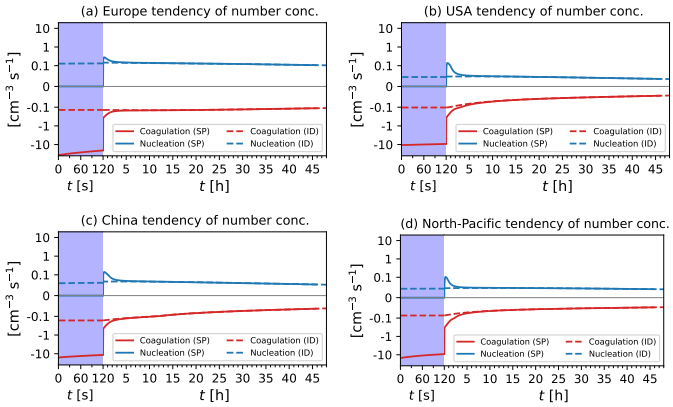

Figure 5.5: Tendency diagnostics of aerosol number concentration, as in Fig. 4.8, but for the regional studies with Wice scenario only, showing the two dominant processes coagulation (red) and nucleation (blue).

5

Europe, ~8% in USA, 10% in China and North Pacific, even if the number concentration of ice crystals in the vortex regime is the same for all cases (222 cm^{-3}). As the only difference between the four regional setups is their respective background concentrations, the variability in the reduction rate of the particle numbers during the vortex regime is due to their different sizes, resulting from the mixing of different background concentrations. The regions with larger particle size display a smaller reduction in the particle number concentration due to a much lower efficiency of coagulation process and vice-versa. Fig. 5.4 exhibits that the polluted regions comprises of particles with larger size as compared to the cleaner backgrounds.

After the vortex regime, a strong reduction is observed in the SP box within the first few hours of the dispersion regime, which is explained by the enhanced coagulation process in the plume approach as shown in tendency diagnostics as well (Fig. 5.5). However, as the plume is fully mixed with the background, no difference is observed at the reference time due to the area-scaling effect (explained in Sect. 4.3).

5.3. AVIATION EFFECT IN DIFFERENT REGIONS

As described in Sect. 3.7, the background concentrations are mixed with the emitted plume at the initial timestep, indicating the importance of various background aerosol concentrations which influence not only the initial aerosol levels but also the initial particle size distribution. These changes alter the aerosol microphysical processes inside an aircraft plume, eventually affecting the plume model results. The aviation effect ($\mathscr{E}$) (Sect. 4.3) calculated using Eqs. 4.1 and 4.2 highlights the plume-scale effect on aviation aerosols. The primary goal of this section is to isolate the effect of microphysics from the plume diffusion (Sect. 3.5) and to assess the changes in aviation aerosol concentrations such as SO_4 mass concentration (Sect. 5.3.1), aerosol number concentration (Sect. 5.3.2) and their corresponding lognormal size distribution (Sect. 5.3.3), under various background aerosol concentrations over different regions (Fig. 5.1) at the cruise altitude.

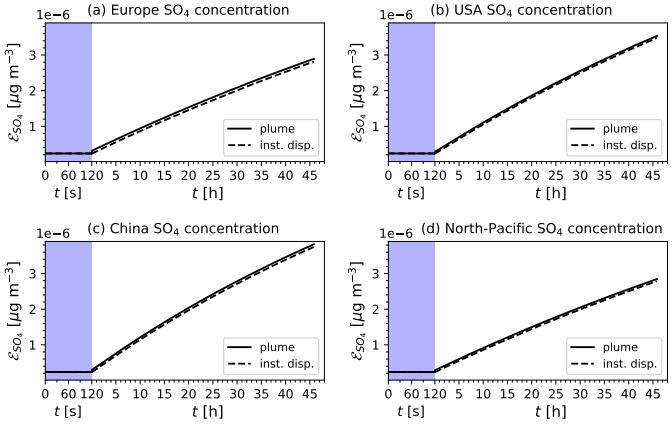

Figure 5.6: Aviation effect ($\mathscr{E}$) for SO_4 mass concentration as in Fig. 4.5, but for different regions.

5

5.3.1. BACKGROUND EFFECT ON AVIATION SULFATE MASS

The aviation effect ($\mathscr{E}$) isolates the effect of microphysics from the plume diffusion (Sect. 3.5). By comparing the aviation effects for SO_4 mass concentrations from the two approaches, it is observed that at time t_0 the initial concentration in the two boxes are same. The only process active during the vortex regime is coagulation, thus no change is observed in the mass during the first 2 minutes of the simulation. As already discussed in the previous section, at the end of the vortex regime some residual mass is added back to the aerosol mass which can be seen as a slight jump in Fig. 5.6. During the dispersion regime, a steady growth is observed in the SO_4 mass in both approaches which is due to the online sulfate production rate (Sect. 3.4) and as this process works the same in both modelling approaches, thus the difference between the SP and ID box at the reference time is negligible. The tendency diagnostics performed on SO_4 mass (Fig. 5.7) shows the two competing processes namely condensation (orange) and nucleation (blue) that play key role in sulfate mass production. The production of SO_4 aerosols via the condensation of H_2SO_4 (gas) is the dominant process and can be observed in most of the regions. In the polluted regions, such as USA (b) and China (c), the condensation process becomes dominant due to the availability of adequate particle surface area. However, in case of the cleaner backgrounds the formation of new particles via nucleation is favoured due to the scarcity of condensation sinks.

5.3.2. BACKGROUND EFFECT ON AVIATION-INDUCED AEROSOL NUMBER CONCENTRATION

Comparing the aviation effect on particle number concentrations for the different regions in Fig. 5.8, a large variation is clearly observed. The plume correction at the reference time is reduced to –12% [–14; –9.4]% (–0.27 [–0.34; –0.21] cm^{-3}) over Europe, while it is larger than for the North Atlantic over all other regions, ranging from –29% [–28; –30]% (–0.69 [–0.61; –0.76] cm^{-3}) over USA, –43% [–66; –28]% (–0.69 [–0.82; –0.56] cm^{-3}) over China to about –39% [–58; –22]% (–0.73 [–1; –0.43] cm^{-3}) over North Pacific. As all the

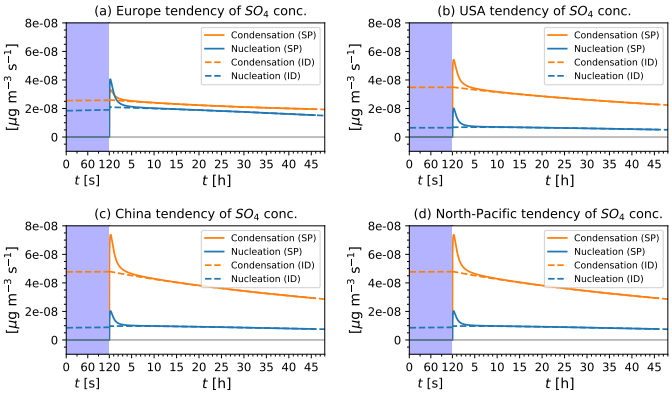

Figure 5.7: Tendency diagnostics for SO_4 mass concentration for the two boxes i.e. SP (solid) and ID (dashed). The two key competing processes that affect SO_4 mass are highlighted as blue (nucleation) and orange (condensation).

5

other parameters are not varied, the resulting variability in the aviation effect of aerosol number concentrations is due to the different background conditions which eventually affect the nucleation and coagulation processes (this is confirmed by the tendency analysis in Fig. 5.5). Especially in the polluted background conditions, the coagulation process tends to effectively reduce the aviation-induced aerosol number concentration, however, the competition between nucleation and coagulation is ubiquitous. The concentration of aviation-induced aerosol numbers is substantially affected by nucleation especially during first few hours of the simulation in all four regions as also shown by the tendency diagnostics in Fig. 5.5. In addition to this, a rather enhanced condensation tendency is observed in the SO_4 mass over the highly polluted regions such as China and USA (Fig. 5.7): this might lead to an efficient depletion of H_2SO_4 at the expenses of nucleation, thus reducing the particle number with respect to other regions. Fig.5.8 and 5.5 also shows that as both USA (b) and China (c) are characterized by polluted background conditions and a relatively high number of large size particles (as discussed above, Fig. 5.3 and 5.4), therefore a rather efficient coagulation process is observed here, leading to a larger plume correction. In the North Pacific (d), the background is slightly cleaner, i.e. less background particle number concentration but with a smaller lognormal size (Fig. 5.4) leading to an effective coagulation during the vortex regime inside an aircraft plume which effectively reduces the particle numbers within the first 2 minutes. Thereafter, due to a low availability of condensation sinks, the new particles are formed via nucleation within the first few hours and once adequate surface is available the coagulation process becomes effective again.

5.3.3. BACKGROUND EFFECT ON AEROSOL SIZE

The regional background concentrations not only have an impact on the particle number concentrations, but they can also influence particle size and composition. In terms of aerosol lognormal size distribution of aviation-induced particles, Europe shows a peak around 5 nm, similar to the North Atlantic case (Fig. 5.9a), while this is shifted to larger

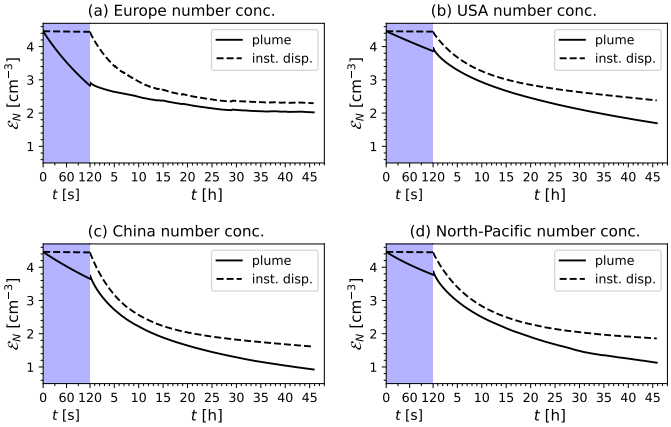

Figure 5.8: Aviation effect ($\mathcal{E}$) on aerosol number concentration in the four regions (a) Europe, (b) USA, (c) China and (d) North Pacific. All simulations are performed based on the Wice scenarios, i.e. considering a short-lived contrail in the vortex regime.

particles, around 7 nm, in both USA and China, which supports the hypothesis of an enhanced condensation process leading to particle growth, while limiting new particle formation via nucleation. In Europe and USA, the size distributions retain the same shape in both approaches, with a lower amplitude in the plume approach as for the North Atlantic case. Over China, however, a bimodal size distribution is observed with two peaks in the plume approach at 6 nm and 30 nm which evidently indicates the survival for a broad range of particles towards the end of the regime. This is supported by the tendency analyses (see Fig. 5.5 and Fig. 5.7), which clearly shows enhanced coagulation and condensation processes in the polluted background conditions.

Additionally, a similar bimodal distribution is observed in the North Pacific region with the two peak values around 5 nm and 20 nm possibly due to the two dominant processes such as nucleation and condensation, where the formation of new particles via nucleation is favoured due to the cleaner background conditions. At the later stage however, these particles are effectively reduced by coagulation processes in the plume approach (Fig.5.9d). This overestimation by the instantaneous dispersion approach is also confirmed by the absolute difference plot (Fig. 5.10), demonstrating an overall overestimation in final size distribution of the Aitken size particles with a substantial variability between the regions due to the background effect (Fig. 5.11).

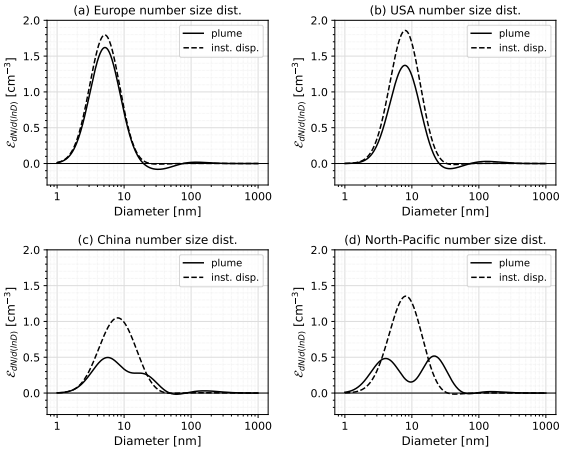

Figure 5.9: Aviation effect ($\mathscr{E}$) at the reference time in terms of lognormal size distribution for the four regions (a-d) and the respective differences between the aviation effects in two approaches (e-h).

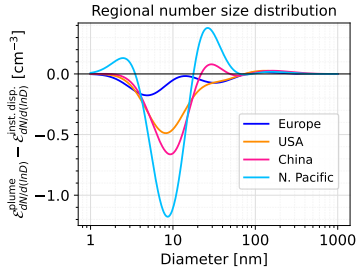

Figure 5.10: Absolute difference between the aviation effects (Fig. 5.9) for the four regions (a-d).

5.4. SUMMARY

This chapter investigated how varying background aerosol concentrations affect plume model results by modifying the aerosol composition within the aircraft plume via the entrainment of background air, thereby influencing aerosol dynamics. Four regions with different characteristics are investigated in addition to the reference case for the North Atlantic presented in the previous chapter: Europe, USA, China and North Pacific. The instantaneous dispersion approach overestimates the aviation-induced particle number concentrations in all investigated regions (Fig. 5.8), however the plume correction varies significantly across the regions between –12% in Europe and –43% in China. This large variability in the plume correction also depends on the initial background particle size (Fig. 5.4) which can substantially influence the aerosol microphysical processes such as coagulation and condensation inside the plume. These results are supported by the processes-based tendency analysis performed on the aerosol number concentrations (Fig. 5.5). The properties of the aerosol population at the end of the dispersion regime are also very diverse in the investigated regions, which highlight the importance of properly

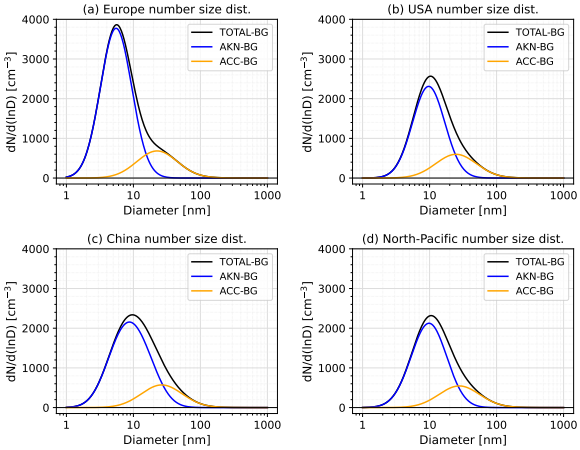

Figure 5.11: Total size distribution from the background (BG box) at the reference time (t = ~46 hours) comprising of two prime modes i.e. Aitken and accumulation.

accounting for different background conditions (Fig. 5.11) when simulating the impact of aviation emissions on aerosol particle number. This needs to be taken into account for future application of the plume model in the context of global model studies of the aviation-aerosol indirect effect and for the development of parametrisations targeting the subgrid-scale aerosol processes in the aircraft plumes.

6

PARAMETRIC SENSITIVITY OF AVIATION EFFECTS

6.1. INTRODUCTION

The double-box aircraft exhaust plume model is initialised with aircraft emissions, background conditions and meteorological parameters. The plume model results are sensitive to these initialisation parameters, as already described in Sect. 3.7 and summarized in Table 3.3. These initialisation parameters largely depend on the aircraft operations, aircraft and engine efficiency, combustion technology and fuel characteristics. They determine the emission indices of emitted components, initial particle size in the young exhaust plume and, in the short-lived contrail scenario, also the properties of the ice crystals. In this Chapter, I explore the model sensitivity towards those parameters, in order to identify the most sensitive parameters with respect to the aviation effects discussed in Chapter 4 and 5.

Table 6.1 shows a detailed list of the parameters chosen for this variation study and their tested values together with their respective literature references. I test their impact by altering one parameter at a time, while keeping the others at their reference value, in order to facilitate the interpretation of the results. The reference setup in this chapter is the REF(Wice) simulation for the North Atlantic region under the short-lived contrail scenario (see Ch. 4). In this chapter, I will refer to it as REF (see Table 6.1), as no variations are performed for the NOice scenario and thus there is no ambiguity. The values shown in the results for each parametric study are the ensemble mean of the 432 grid-boxes used to initialise the background for this region, as discussed in Sect. 4.4. The following sections in this Chapter discusses in detail the results from the parametric study, in which the following parameters are systematically varied: (A) ice crystal number concentration and number emission index of soot (Sect. 6.2), (B) initial soot size (Sect. 6.3),

This chapter is based on Sharma et al. [79]

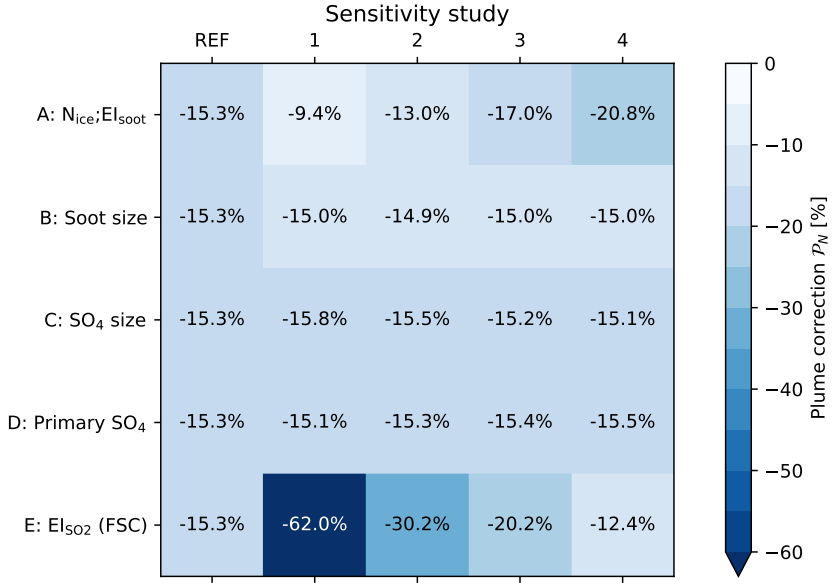

Figure 6.1: Plume correction ($\mathcal{P}_N$) to the aviation-induced particle number concentration for the five variation studies discussed in this chapter. The horizontal axis represent the REF(Wice) configuration and the four variations, the vertical axis the varied parameters in the respective variation studies (see Table 6.1). The REF column exhibits the reference value discussed in Sect. 4.4 for REF(Wice) setup. FSC stands for fuel sulfur content.

6

(C) initial SO_4 size (Sect. 6.4.1), (D) primary SO_4 fraction (Sect. 6.4.2), (E) fuel sulfur content (Sect. 6.4.3).

Table 6.1: List of parameters shortlisted for the parametric study. Each set of variations of a given parameter is identified by an index (A-E) and the different values of the parameters by a number (1-4) in addition to the reference (REF).

Set	Parameter	Units	1	2	REF	4	5	
A	N_{ice}	cm^{-3}	90	163	222	268	350	[90]
	EI_{soot}	kg_{fuel}^{-1}	0.5	1	1.5	2	3	
B	$D_{soot,k}$; $\sigma_{soot,k}$	nm; -	26.3; 1.68	28; 1.68	25; 1.55	27; 1.63	32.5; 1.71	[104]
	$D_{soot,a}$; $\sigma_{soot,a}$	nm; -	-	-	150; 1.65	-	-	
C	$D_{SO_4,ks}$; $\sigma_{SO_4,ks}$	nm; -	2; 1.7	2.2; 1.7	2.5; 1.7	2.7; 1.7	3; 1.7	[82]
D	ϵ	%	1.2	1.9	2.3	2.6	2.8	[80]
E	EI_{SO2}	$g(SO_2)\ kg_{fuel}^{-1}$	0.2	0.4	0.8	0.6	1	[26]

Fig. 6.1 shows the result from the parametric studies performed on the values given in Table 6.1. The values represent the calculated plume corrections for aviation-induced aerosol number concentration. The REF case implies a plume correction of –15% on the aviation-induced aerosol number concentration under the reference set of parameters (Table 6.1). The variation study A (Sect. 6.2) addresses the initial assumptions on number of ice crystals in a short-lived contrail (N_{ice}) and the corresponding soot num-

ber emission index that are derived from the modelling study by Bier et al. [90], which used the simulations from ECHAM5-CCMod model at 240 hPa. To investigate the sensitivity on the initial size of emitted soot particles, Study B (Sect. 6.3) considers different measurements performed during the ACCESS flight campaign on the size distributions parameters of emitted soot particles [104]. Here, I consider the measurement performed with the HEFA 50:50 fuel blend, at medium thrust (simulation B1) and high thrust (B2), and with the standard Jet-A fuel, at medium thrust (B3) and high thrust (B4). Study C (Sect. 6.4.1) targets the initial size of aerosol sulfate particles. Due to the small size of these particles, mostly below the size detection limit of the available instruments, no measurements are available for this parameter, but theoretical studies showed that at 10 seconds behind the aircraft the particles exist in the size range of 1 nm and they are mostly comprised of a molecular clusters of organics. These particles are either consumed or scavenged through Brownian coagulation by the ions of the size range 2-3 nm, which are presumably the SO_4 particles [49, 82, 105]. Hence, I vary the sulfate size within this range for study C. The fraction of SO_2 mass converted into aerosol sulfate (primary SO_4) is explored in study D (Sect. 6.4.2), based on the measurements on the exhaust from different aircraft and engine types during the CONCERT campaign [80]. The emission index of SO_2 (i.e., the fuel sulfur content, study E (Sect. 6.4.3)) is varied based on the range of values provided by Lee et al. [26], which are representative of the fleet average.

6.2. STUDY A: VARIABILITY OF ICE CRYSTAL NUMBERS IN SHORT-LIVED CONTRAILS

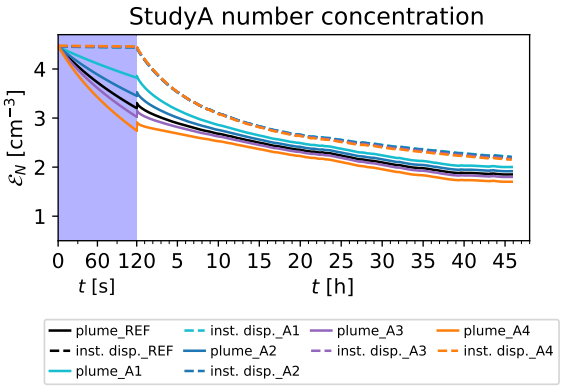

Figure 6.2: Aviation effect ($\mathcal{E}$) on aviation-induced particle number concentration in the two modelling approaches i.e. plume (solid) and instantaneous dispersion (dashed), as in Fig. 4.10, showing the impact of changing N_{ice} in study A. The black line represent the REF case. The two regimes of an aircraft plume represented here are vortex regime (violet) and dispersion regime (white).

Parametric study A focuses on the initialisation of ice crystal number concentration in the vortex regime for the effect of Wice (with- contrail ice) scenario. The aim of this study is to investigate the effect of varying initial ice crystal number concentration (N_{ice}) on the plume model results especially in terms of particle number concentration and

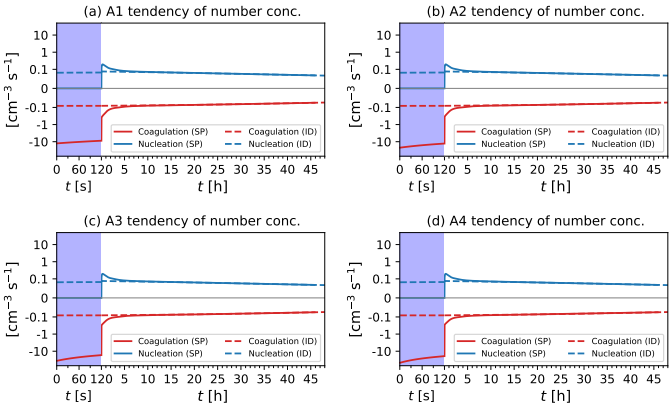

Figure 6.3: Tendency analysis of aerosol number concentration as in Fig. 4.8, but for parametric study A (A1 to A4).

their corresponding lognormal size distribution. Since ice formation in short-lived contrails is driven by soot particles, this parameter is initialised together with a corresponding soot number emission indices. In the model, the emitted soot particles are split between the Aitken insoluble and the accumulation insoluble modes of the MADE3 aerosol scheme. These initial assumptions are based on the modelling results by Bier et al. [90]. The results in term of aviation effect ($\mathscr{E}$) on particle number concentration are shown in Fig. 6.2 for five combinations of the two parameters.

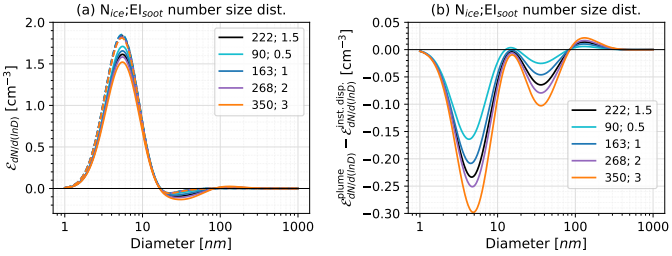

Figure 6.4: Aviation effect ($\mathscr{E}$) for study A in terms of lognormal size distribution at the reference time (a) and the respective difference between the aviation effects in two approaches (b). The two modelling approaches shown in (a) are depicted as plume approach (solid) and instantaneous dispersion approach (dashed).

Study A shows an almost linear relationship between the assumed ice crystal number concentration in the vortex regime (N_{ice} and the associated variation of $\mathrm{EI}_{\mathrm{soot}}$) and the plume correction for aviation-induced number concentration, which varies between –9.4% [–25; 5.6]% (–0.21 [–0.54; 0.13] cm^{-3}) for N_{ice}=90 cm^{-3} and –21% [–35; –7.0]% (–0.45 [–0.74; –0.15] cm^{-3}) for N_{ice}=350 cm^{-3} at the reference time (t = ~46 hours). This is due to the aerosol-ice coagulation in the vortex regime, which increases in efficiency as the number of ice crystals increases, as also demonstrated by the tendency analysis in Fig. 6.3. This leads to an even larger reduction of aerosol particles in the vortex regime

with the plume correction of –14% (for N_{ice} = 90 cm^{-3}) and –38% (for N_{ice} = 350 cm^{-3}) within the first 2 minutes of the simulation, thus confirming once more the importance of this regime for the plume effects, as already concluded in Sect. 4.4.

The tendency analyses shown in Fig. 6.3 (a-d) and Fig. 6.16 (A1-A4) illustrate a steady increase in the coagulation process in SP box with the increasing N_{ice} values which eventually corresponds to the plume correction values as shown in Fig. 6.1 (row A), demonstrating again the importance of the vortex regime in the plume model. Moreover, the final size distribution as shown in Fig. 6.4 (a,b) demonstrates a strong sensitivity of the aviation-induced number concentration to the number of ice crystals in the plume approach (solid lines), while no significant sensitivity is seen in the instantaneous dispersion approach (dashed lines), which does not include a vortex regime.

6.3. STUDY B: INITIAL SIZE OF AVIATION SOOT PARTICLES

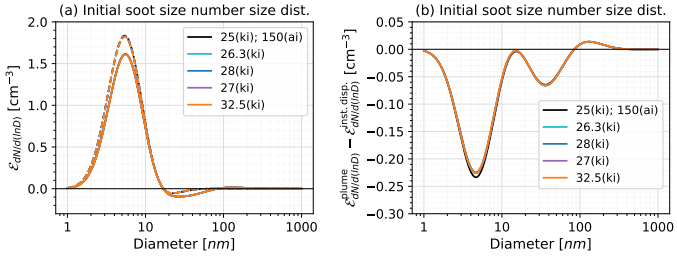

Figure 6.5: As in Fig. 6.4, but for study B depicting the impact of initial soot size on lognormal size distribution of aviation aerosols.

The non-volatile (soot) size distribution parameters are examined for their possible impact on the aviation-induced aerosol number concentrations and size. The results, however, show no remarkable variations in the plume correction (row B in Fig. 6.1). Even in terms of size (Fig. 6.5 a,b) no substantial changes across the different simulations are observed. This is due to the relatively high consistency of the in situ measurements on the soot size distribution parameters [46][104], which generally agree on a diameter of about 25-30 nm for the soot particles, with a moderate dependency on the fuel type. These size distribution parameters were recently confirmed by the large-scale and long-term measurements of the IAGOS experiment by Mahnke et al. [94].

This sensitivity study further reveals that the role of soot on the aviation-induced particle number concentration is marginal, as this is mostly affected by the smaller sulfate aerosol particles in the nanometer size range. The tendency diagnostics performed on the aerosol number concentrations (Fig. 6.16, B1-B4) show only very small changes in terms of total coagulation contribution. The impact of soot size is therefore negligible in terms of plume correction, which remains almost constant around -15% for all investigated cases of Study B (Table 6.1).

6.4. SENSITIVITY ANALYSIS FOR SULPHUR-RELATED PARAMETERS

As discussed in Sect. 3.4, only a small fraction (2.3%) of emitted SO_2 gas contributes to the formation of sulfate aerosols SO_4 within the first few seconds after the emission. Several physio-chemical properties of sulfate aerosol in the atmosphere make it one of the most effective cloud condensation nuclei (CCNs) for low clouds [11]. The reason for this, in particular, is the hygroscopic nature of sulfate particles, which facilitates their activation into cloud droplets [106–108]. Moreover, sulfate often mixes with organic and inorganic compounds in the atmosphere, forming mixed-phase aerosol particles and improving their ability to act as CCNs [15, 109]. Due to their smaller size and high number concentrations, sulfate aerosols can effectively contribute to the formation of smaller but more numerous cloud droplets, which increase cloud albedo (reflectivity). This is known as the Twomey effect (Sect. 1.1), where clouds containing a greater number of smaller droplets reflect more sunlight, resulting in a cooling effect.

Several recent aviation regulations aimed at reducing both CO_2 and non-CO_2 emissions from the aircraft with the focus on curbing emissions which contribute to aviation climate impacts. For an instance, European Union's RefuelEU initiative [110] mandates gradual SAF (Sustainable Aviation Fuel) blending, with the goal of reducing the aviation-induced CO_2 emissions and as an additional feature, it also reduces the aviation emissions of sulfate and soot. SAF, such as hydro-processed esters and fatty acids (HEFA), emits fewer sulfur compounds than conventional jet fuel. These initiatives align with global efforts to mitigate the climate impact of aviation, like the ICAO Carbon Offsetting and Reduction Scheme for International Aviation (CORSIA)[111]. However, one of the recent study [112] argues that although the emissions targets for aviation as per the ICAO's CORSIA are in line with the Paris Agreement goals, there is a high likelihood that the climate impact of aviation will not meet these goals.

6.4.1. STUDY C: INITIAL SIZE OF AVIATION SULFATE PARTICLES

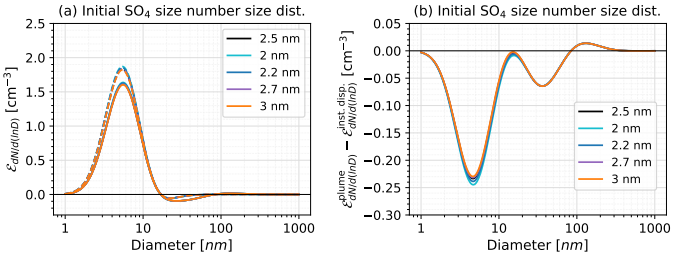

Figure 6.6: As in Fig. 6.4, but for study C depicting the impact of initial SO_4 size on lognormal size distribution of aviation aerosols.

The variation of the initial SO_4 size has no significant impact on the plume correction (row C in 6.1). This is quite surprising, given the overwhelming importance of sulfate for the aviation number concentration discussed in the previous chapters. A decrease in the initial sulfate size leads to only a slight increase of the aviation effect in both approaches

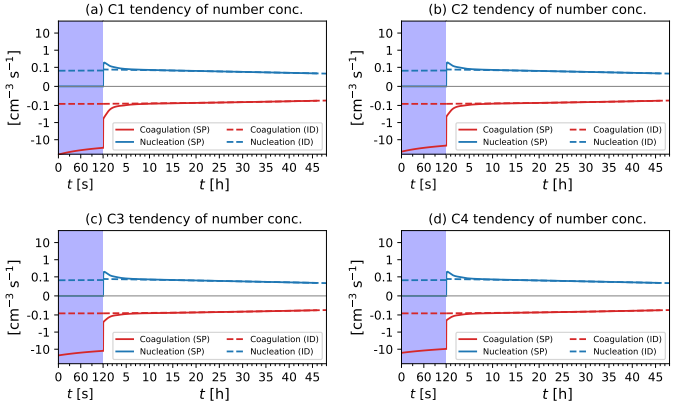

Figure 6.7: Tendency analysis of aerosol number concentration as in Fig. 4.8, but for parametric study C (C1 to C4).

and to a slightly more negative plume correction, from –15% [–30; –0.67]% (–0.33 [–0.64; –0.01] cm^{-3}) to –16% [–31; –1.2]% (–0.35 [–0.68; –0.03] cm^{-3}) when reducing the initial size of sulfate aerosol from 3 to 2 nm (Fig. 6.6a,b). According to the tendency analysis of the aerosol number concentration (Fig. 6.7a-d), this can be explained with the coagulation process increasing its effectiveness as the initial size is reduced and hence more sulfate particles are emitted. This is particularly the case during the vortex regime, where the coagulation-driven reduction in the aviation effect becomes stronger as the initial number increases. This is also explained by the tendency analysis in Fig. 6.16 (C1-C4) highlighting the total coagulation contribution, which is highest for the smallest size and decreases monotonically as particle size increases. At the end of the dispersion process (t = ~46 hours), however, the plume correction converges towards a similar value as in the REF case (Fig. 6.8), regardless of the initial number concentration of sulfate particles. This would suggest that an increase in the emitted number of particles also increases the coagulation efficiency in the plume, hence resulting in a similar aviation effect at the end of the dispersion, more or less regardless of the sulfate particle initial size (and number).

The aviation effect ($\mathscr{E}$) calculated for number concentration in Fig. 6.8 shows the initial variations in aviation-induced aerosol number concentration in both SP and ID boxes, which is due to the initial SO_4 size. The SP box shows reduction in the number concentration within the first 2 minutes due to aerosol-ice coagulation. During the dispersion regime, the higher particle number concentration enhances the coagulation efficiency. This phenomenon is evident as a reduction in particle count is observed within the first few hours of the simulation in both approaches. Fig. 6.8 demonstrates the plume correction ($\mathscr{P}$), defined as the aviation effect in the plume approach relative to the instantaneous dispersion approach (Eq. 4.3), which varies between –29% (for D_{SO_4}=2 nm), –26% (for D_{SO_4}=2.2 nm), –21% (for D_{SO_4}=2.7 nm) and –18% (for D_{SO_4}=3 nm), after the first 2 hours of the simulation. It is important to note that the observed variation is highly influenced by the contrail ice during the vortex regime. The difference observed between the two approaches at the reference time is negligible. Hence, this confirms the above

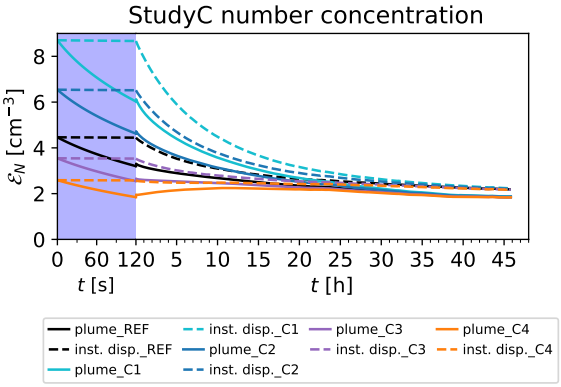

Figure 6.8: As in Fig. 6.2, showing the impact of initial SO_4 size in study C where black line represent the reference value.

statement, that increased particle number emissions (by reduced particle size) leads to an increase in the coagulation process in the plume (Fig. 6.16 C1-C4), especially during the vortex regime (Fig. 6.7), resulting in a similar correction at the end of the dispersion (Fig. 6.8).

6

6.4.2. STUDY D: FRACTION OF PRIMARY SULFATE EMISSIONS

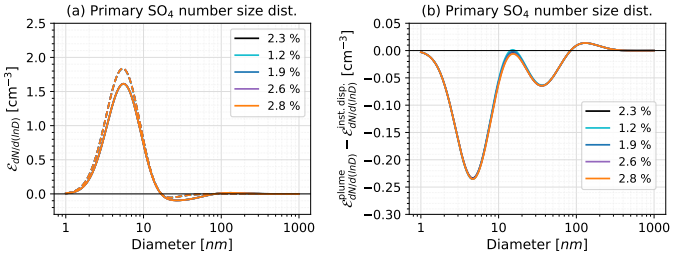

Figure 6.9: As in Fig. 6.4, but for study D depicting the impact of primary SO_4% (ϵ) on lognormal size distribution of aviation aerosols.

As discussed in Sect. 3.4, only a small fraction of emitted gas-phase SO_2 contribute to the formation of primary SO_4 aerosols. The sensitivity of the results to the fraction of emitted primary sulfate (ϵ) is explored here in study D based on the values measured by Jurkat et al. [80]. The results are similar to what is also observed in study C, with the plume correction remaining almost constant at the value of the REF experiment for the whole range of tested values of this parameter (row D in Fig. 6.1) and no changes in the size distributions (Fig. 6.9a,b). The reason is also similar as for study C: an increase in the primary SO_4 fraction results in an increase of the emitted sulfate mass and hence of number of emitted particles. Also in this case, however, the increase in number concentration is compensated by a more effective coagulation process, predominantly in the

vortex regime (Fig. 6.10a-d), reducing the number of particles.

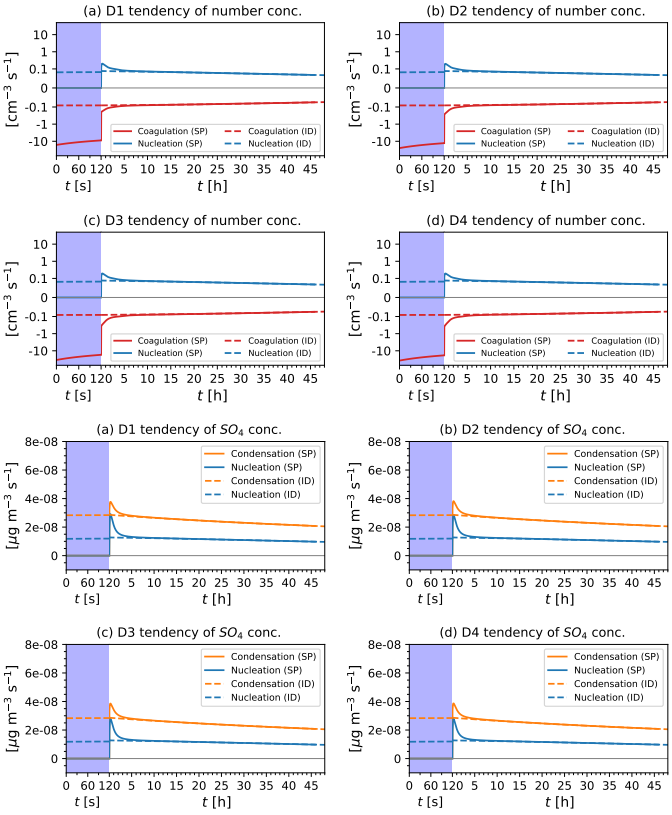

Figure 6.10: Tendency analysis of aerosol number concentration and SO_4 mass concentration as in Fig. 4.8 and 4.6, but for parametric study D (D1 to D4).

A further reason could be that increasing the primary SO_4 fraction slightly reduces the availability of SO_2 gas which is the primary source of H_2SO_4 (gas) in the aircraft plume, thus eventually reducing the impact of nucleation on particle number as shown by the tendency diagnostics in Fig. 6.10 (a-d), with a corresponding effect of condensation process on SO_4 mass concentration (e-h).

Fig. 6.16 (D1-D4) also shows similar results. This would explain the smaller variability in study D as compared to study C, although both result in a similar impact on the initial particle number concentration, as shown in Fig. 6.11. This can be confirmed by the plume correction ($\mathscr{P}$) calculated after first 2 hours of the simulation, which decreases as the primary sulfate fraction (ϵ) increases, i.e., –19% (for ϵ=1.2), –21% (for ϵ=1.9), –23% (for ϵ=2.6) and –24% (for ϵ=2.8). However, the plume correction ($\mathscr{P}$) observed at the reference time remains fairly constant (row D in Fig. 6.1), concluding that the primary sulphate% (ϵ) is not a sensitive parameter in the plume model.

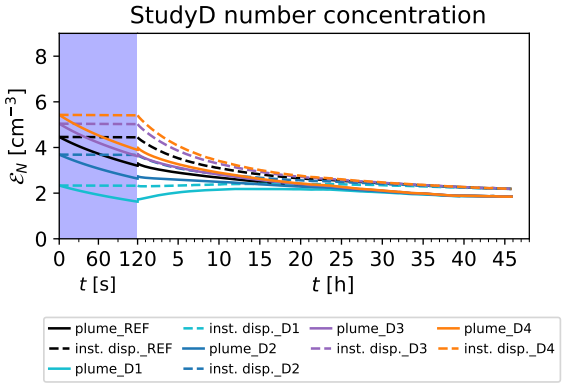

Figure 6.11: As in Fig. 6.2, demonstrating the impact of primary SO_4 % (ϵ) in study D, where black line represent the reference value.

6.4.3. STUDY E: FUEL SULFUR CONTENT

As discussed earlier, the sulfur content in aviation fuel plays a crucial role in the formation of SO_4 aerosols, primarily through the oxidation of sulfur (S) in the fuel to sulfur dioxide (SO_2) during combustion, which then further oxidizes into sulfuric acid (H_2SO_4) and then forms sulfate aerosol via condensation or nucleation. This parametric study reveals that the plume model is highly sensitive to the emission index of SO_2, i.e. to the fuel sulfur content (row E in Fig. 6.1). The plume correction ($\mathscr{P}$) at the reference time shows a large variation across the range of reported literature values (Table 6.1) for this parameters, from –62% [–125; –2.0]% (–0.32 [–0.63; –0.01] cm^{-3}) for a low fuel sulfur content of 0.2 g(SO_2) kg$^{-1}_{\text{fuel}}$ to –12% [–24; –0.8]% (–0.34 [–0.66; –0.02] cm^{-3}) for a high fuel sulfur content of 1.0 g(SO_2) kg$^{-1}_{\text{fuel}}$. This large variation in the plume correction is related to the strong variation in the aviation effect increases in both approaches, while the absolute difference between the aviation effects in two approaches remains fairly constant (Fig. 6.12a,b).

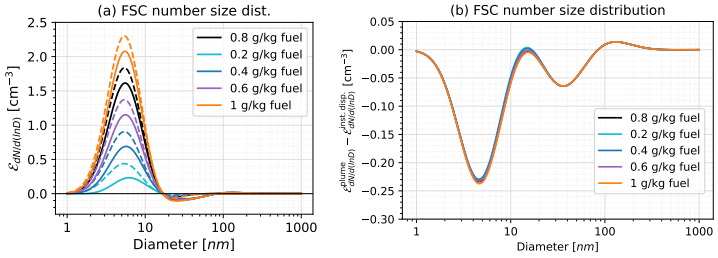

Figure 6.12: As in Fig. 6.4, but for study E depicting the impact of fuel sulfur content on lognormal size distribution of aviation-induced aerosols.

As the fuel sulfur content controls both the SO_2 and the sulfate initial concentrations in the model (via the primary SO_4 fraction ϵ), the nucleation tendency gains impor-

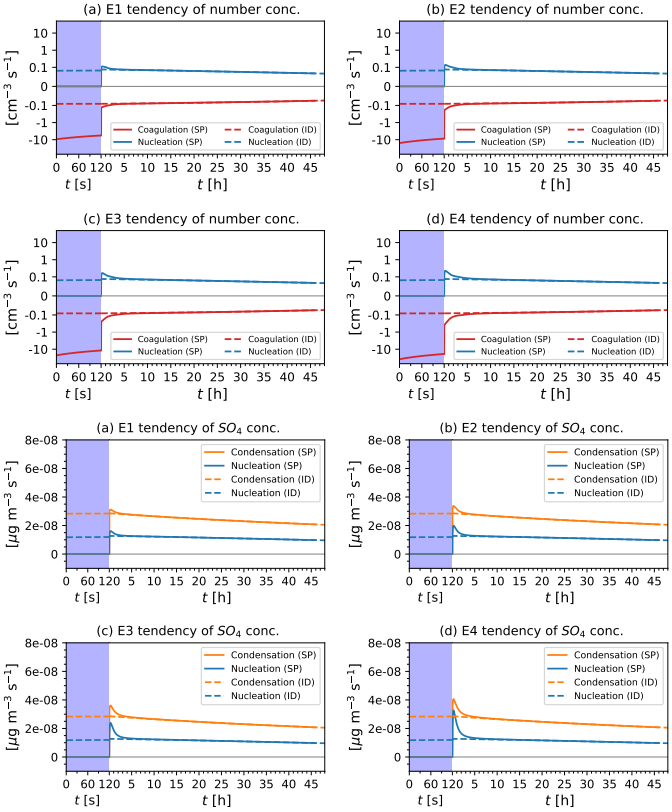

Figure 6.13: Tendency analysis of aerosol number concentration and SO_4 mass concentration as in Fig. 4.8 and 4.6, but for parametric study E (E1 to E4).

tance as more SO_2 and eventually H_2SO_4 become available with increasing fuel sulfur content, although the number tendency is still controlled by coagulation (Fig. 6.13a-d), whereas the SO_4 mass is predominantly controlled by condensation process (Fig. 6.13e-h). This makes fuel sulfur content one of the most sensitive parameters for the plume model. This study also concludes that besides coagulation, nucleation also proves to be a highly effective yet uncertain process (Fig. 6.16, E1-E4), and it can strongly influence the aviation-induced aerosol number concentration inside an aircraft plume.

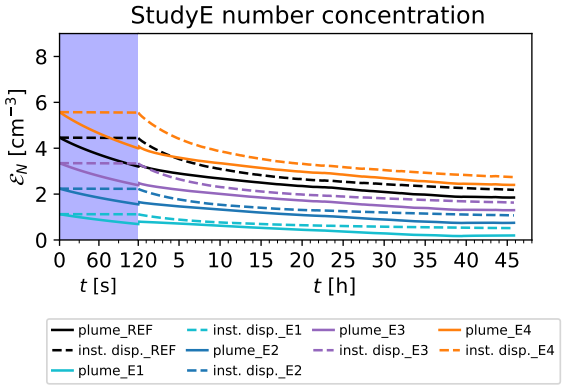

Figure 6.14: As in Fig. 6.2, showing the impact of fuel sulfur content in study E where black line represent the reference value.

6.5. SUMMARY

This chapter provided a comprehensive sensitivity analysis of the plume model dependency on various initial parameters. Study A demonstrated the importance of ice crystal number concentration N_{ice} during the vortex regime, resulting in an approximately linear relation between the plume correction and N_{ice} (Fig. 6.15), varying between –14% (for N_{ice} = 90 cm^{-3}) and –38% (for N_{ice} = 350 cm^{-3}) only after the first 2 minutes of the simulation and –9.4% (for N_{ice} = 90 cm^{-3}) and –21% (for N_{ice} = 350 cm^{-3}) at the end of the dispersion (t = ~46 hours). Another critical parameter is the fuel sulfur content (Study E), as it controls the initial SO_2 concentration in the plume, thereby affecting the online sulfate production rate and ultimately the SO_4 concentration. In this case, however, a non-linear relation is observed between the plume correction and the FSC values (Fig. 6.15) with a variation between –62% for low sulfur fuel and –12% for high sulfur fuel.

The other investigated parameters have a smaller impact on the results. Study C showed that the initial SO_4 size D_{SO_4} does not affect the plume correction, as it remains consistent with the reference case, although it plays a significant role during the early stages of the plume evolution. A strong impact is observed during the vortex regime, primarily due to effective interactions between ultrafine aerosol particles and coarse-mode ice crystals, simulated explicitly in the plume approach. This effect is further amplified by the cumulative effects of microphysical processes during the initial hours of the dispersion regime with a variation between –29% (for D_{SO_4} = 2 nm) and –18% (for D_{SO_4} = 3 nm) after the first 2 hours of the simulation. Similar considerations can be done for the primary SO_4 fraction ϵ in study D as well, with a variation between –19% (for ϵ = 1.2%) and –24% (for ϵ = 2.8%) after the first 2 hours of the simulation, however the values at the end of the dispersion regime remains same as the reference case. Study B which examined the the initial soot size values based on Moore et al. [104] shows no impact on the plume model results and it remains consistent with the reference case.

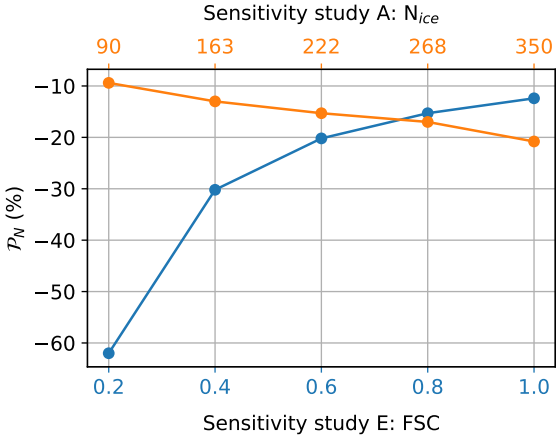

Figure 6.15: Comparing the calculated plume corrections $\mathscr{P}_N$ (%) for their corresponding sensitivity study values. The two x-axes represent the values for study E as fuel sulfur content i.e., FSC (bottom, blue) and study A as the ice crystal number concentration i.e., N_{ice} (top, orange), respectively.

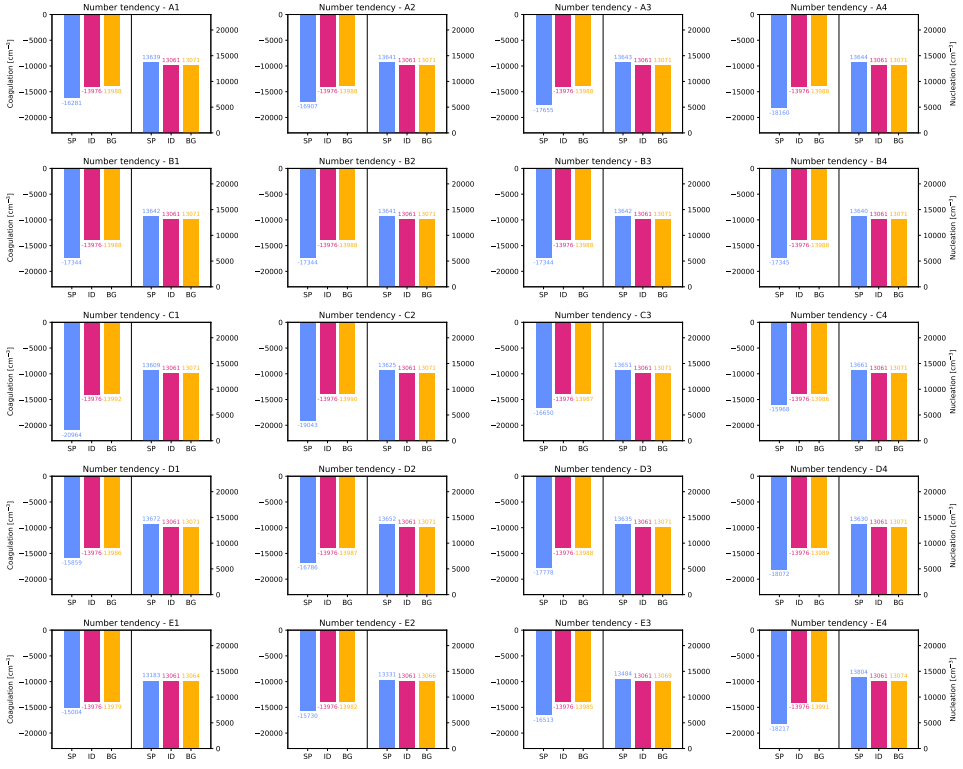

Figure 6.16: Total contribution of microphysical processes, specifically coagulation (left) and nucleation (right), represented as time-integrated number tendencies for the three boxes i.e., SP, BG, and ID, and for the parametric studies A-E.

7

FUTURE APPLICATIONS AND MODEL LIMITATIONS

7.1. APPLICATION IN GLOBAL MODEL STUDIES

The plume model results presented in the previous chapters highlight a strong dependence of aviation-induced effects ($\mathscr{E}$) and plume corrections ($\mathscr{P}$) on various initialisation parameters. These include aviation operational parameters, fuel type (which governs the emission of species like SO_2 and soot), initial particle size distribution of the emissions, background atmospheric conditions during cruise, and key meteorological variables. The observed variability in aerosol number concentration, species mass concentration, and particle size distribution within the dispersing aircraft plume underscores the sensitivity of these parameters to initial conditions. Therefore, to accurately assess the climate impact of aviation aerosols, it is imperative to employ a detailed initialisation process that incorporates plume-scale dynamics in global model simulations.

The aviation inventories required to initialise global aerosol-climate models, such as EMAC, for assessing the climate impact of aviation emissions usually provide the mass of emitted species, but no information about particle number, particularly for volatile particles, which are much more relevant for the aviation impact on low clouds. Converting mass to particle number typically involves assumptions about the size distribution of the emitted particles. A major limitation of existing methods is the scarcity of accurate data for this initialisation, particularly on the number and size of the emitted particles, which introduces uncertainty and potential biases in the representation of aviation-induced aerosols in these models [27, 32, 42]. A further complication derives from the fact that the particle size distribution is not constant in time and depends on the time after the emission, with younger plumes typically characterized by smaller particles, but the global models cannot resolve the plume evolution due to their coarse resolution.

The double-box aircraft exhaust plume model introduced in this thesis can be applied to analyse aviation-induced particle number and mass concentrations, categorized by size mode and mixing state, at different stages of the plume evolution and thus

provide input to global model to initialise aviation emissions. The plume model output allows to calculate a number-to-mass ratio for each aerosol mode, also accounting for the regional variations (Chapter 5) and the parametric uncertainties (Chapter 6). These ratios can be used to derive number emissions from the mass emissions provided by global emission inventories. The number-to-mass ratio R for a species i in the mode j can be written as:

$$R_{i,j}(t) = \frac{N_{i,j}(t)}{M_{i,j}(t)} \tag{7.1}$$

where N and M are the number and mass concentrations of aviation-induced particles at time t in the plume evolution. Here, different stages of the plume evolution may be considered for the initialisation of aviation emissions in the global model. As shown in this thesis, sulfate and soot are the most relevant aerosol species for aviation, so $R_{i,j}$ would need to calculated only for these species. Since the MADE3 microphysical scheme, on which the plume model is based, does not resolve the number concentration for each species but only provides the number concentration in each mode (N_j), further assumptions are required to derive N_{ij} from N_j. I suggest considering sulfate to dominate the Aitken mode and soot to dominate the accumulation mode. The coarse mode can be ignored given the small size of the aviation emitted aerosols. Similar assumptions can also be made for the different mixing states.

This approach can be easily generalized to any global aerosol model, provided that the MADE3 modal scheme can be mapped to the aerosol schemes of other models, which may pose further challenges, although modal aerosol schemes usually share similar features. Given the detailed output of the plume model, more sophisticated methodologies can also be explored, for example by the application of statistical techniques, sensitivity analyses, or machine learning algorithms to enhance the accuracy and reliability of the results. As discussed in the previous chapters, the plume model can also be employed as an online parametrisation to explicitly calculate aviation-induced particle number concentration in global model simulations, thus more accurately accounting for the impact of local conditions. These approaches will help to achieve an improved assessment of the climate impact of aviation aerosols.

To further enhance the accuracy of the plume model, future measurement campaigns can provide useful constrains and should focus on measuring ultrafine particles (<5 nm), particularly their number concentrations and size, at very early stages (e.g., 10 seconds) of an aircraft plume. Initial parameters characterizing the size distribution of the emitted particles would be beneficial. These improvements will enable the plume model to better simulate the dynamics of aerosol formation and their microphysical transformation in the aircraft plumes. Another key application of the plume model is the study of aerosol emissions and their impact on climate from future aircraft technologies, including various combustion engine types (such as lean burn and rich burn) and alternative fuel blends (such as Sustainable Aviation Fuel, SAF). Such assessments would provide a critical insight into the climate impact of aviation aerosol, which will help in developing more sustainable aviation technologies.

7.2. MODEL LIMITATIONS AND FUTURE IMPROVEMENTS

The double-box aircraft exhaust plume model introduced in this thesis captures the plume-scale aerosol microphysical processes in a detailed way, while following the plume expansion with the entrainment of background air, thus improving over the simple instantaneous dispersion approach adopted by global models. As demonstrated in this work, this allows for an improved quantification of the aviation-induced aerosol number concentration. Given the targeted application scope of the plume model, its development has focused on the aerosol microphysics and on specific aspects of the plume dynamics, whereas other processes have been addressed in a simplified way, resulting in limitations and uncertainties that need to be considered when applying the plume model results for application studies:

- **plume dynamics**: complex plume dynamic processes such as turbulence, processes inside primary and secondary wakes, contrail formation, evolution and decay of contrails are beyond the capabilities of the model presented here. Dedicated models, for example, the LES model by Unterstraßer et al. [93] are available which explicitly simulate these complex dynamic processes.

- **short-lived contrail ice**: the representation of short-lived contrail ice in the plume model is very simplified, as the goal is to represent ice crystals as a coagulation sink for aerosol particles and to estimate the reduction in aerosol number concentration during the vortex regime. To this purpose, I considered a simple scenario mimicking a short-lived contrail represented by a passive tracer for ice crystals with a constant number concentration. More realistic representations are of course possible, for instance taking advantage of existing EMAC submodels dealing with contrails.

- **constant meteorology**: parameters such as temperature, pressure and relative humidity are initialised as a constant in the model. Provided the very short duration of the vortex regime (t = 120 seconds), this is well justified in this regime. For the dispersion regime, [69] showed that the vertical diffusivity is negligible compared to the horizontal one, hence it is reasonable to assume that there is no temperature gradient and to assume constant meteorological parameters for the plume.

- **sulfate production rate**: the third-body reaction (3.1) assumes a constant OH concentration and I prescribed an average value for it representative for the upper troposphere. This is of course a simplification, as OH is a short-lived compound characterized by a strong temporal and spatial variability. Since the plume model does not account for detailed gas phase chemistry, this simplification is justified. It can, however, be improved in future version, e.g. by considering the implementation of a daily cycle for OH or using online chemistry if the plume model is coupled to a global model. This can be relevant given the importance of OH in the troposphere as shown by other studies [113–115].

- **sensitivity analyses for multiple parameters**: in this thesis, I performed sensitivity analyses by varying one parameter at a time in order to understand the impact of individual parameters on the model results. While the current approach

provided valuable insights, future analyses may benefit from exploring more advanced techniques, such as the Perturbed Parameter Ensemble (PPE) method, which systematically alters the values of multiple parameters to provide a multi-dimensional insight into their combined impacts on the model results and support the further investigation of model uncertainties.

7.3. SUMMARY

The plume model introduced in thesis is not designed to represent the detailed aspects of the plume dynamics, but it has been specifically developed to target the aerosol microphysical processes in an aircraft plume at a scale that cannot be resolved by the global models, aiming at improving over the instantaneous dispersion approach usually assumed in these models. It helps to calculate the changes in specific parameters of the aerosol population such as mass, number and size, between the time of emission (i.e. the end of jet regime) and the end of the dispersion regime, in order to provide the global models with refined and more physically motivated assumptions to initialise aviation emissions in global simulations, thus account for the plume-scale processes that these models cannot resolve. This chapter outlined a possible approach to calculate the number of emitted particles from the mass using a conversion factor calculated based on the plume model output for each aerosol mode, to help improve the representation of aviation emissions in the global models. These conversion factors can also account for the variability in plume corrections, as estimated through regional and sensitivity studies, and for different stages of the plume evolution.

8

CONCLUSION

Existing studies highlight significant uncertainties regarding the indirect effects of aviation-induced aerosol particles, particularly sulfate aerosols, due to the complex, non-linear aerosol microphysical processes occurring at the plume scale. These processes are challenging to represent accurately in global climate models because their coarse spatial resolution cannot resolve the subgrid-scale processes. Motivated by the challenges outlined above and to conclude the work presented in this thesis, I now recall and answer the research questions:

1. How are aviation-induced aerosols dispersed and transformed in the vortex and dispersion regime of an aircraft exhaust plume?
2. What are the typical concentrations and size distributions of aviation-induced aerosol particles at the end of the plume dispersion?
3. On which parameters and initial conditions do these typical concentrations depend?
4. How can the existing uncertainties surrounding the aerosol indirect effect, particularly with regard to aviation-induced sulfate aerosols and aerosol number concentrations, be reduced?

To answer these questions, I developed a plume model based on the MADE3 aerosol microphysical scheme, which allowed me to simulate the non-linear aerosol microphysical processes for the aviation-induced aerosol particles inside an expanding and dispersing aircraft plume within the upper-tropospheric background. The plume model is realized by extending the MADE3 box model configuration to a double-box configuration representing the plume and the background, respectively, with a one-way interface to simulate the dispersion of the plume into the background. The plume model also features a simplified representation of the vortex regime, which mimics the formation of a short-lived contrail ice in the early stage of the plume and allows to estimate the impact of the interactions between aerosol particles and ice crystals via coagulation.

I employed the plume model to evaluate and compare the two methodological approaches: the plume approach, explicitly resolving the expansion of the aircraft plume into background air, and the instantaneous dispersion approach commonly adopted by global models, in which aviation emissions are instantaneously dispersed in the background without accounting for plume processes. I quantified the impact of aviation emissions on aerosol in the two approaches, considering both particle mass and number concentrations along with particle size distributions. By comparing the results of the two approaches, I defined a plume correction to characterize the impact of the plume-scale processes on aviation-induced particle concentrations at the end of the dispersion phase of the plume, with a particular focus on particle number and size, given the relevance of these quantities for the assessment of the impact of aviation aerosol on clouds.

I undertook extensive plume model simulations to comprehensively assess the model sensitivity to a range of parameters and underlying assumptions. This systematic investigation allowed me to enhance the understanding of model behaviour and the overall impact of these parameters on the aviation aerosols especially at the end of the dispersion regime.

The main conclusions of this Thesis can be summarized as follows:

1. For typical upper-tropospheric conditions over the North Atlantic, the plume approach simulates a lower (–15%) aviation-induced particle number concentration at the end of the plume dispersion than the instantaneous dispersion approach. This is regarded as a plume correction. (→ research questions 1, 2)

2. The bulk of this reduction is due to the very efficient coagulation of aerosol particle with the (larger) ice crystal particles during the vortex regime. An alternative scenario without short-lived contrail ice particles resulted in a much smaller plume correction of –4.2%. (→ research questions 1, 2, 3)

3. The effect on aerosol sulfate and soot mass was found to be negligible, as the total mass is conserved, although minor differences in the condensation and nucleation rates in the two approaches were found, affecting the partitioning between the gas and aerosol phase and resulting in minor difference in the total sulfate mass. (→ research questions 3, 4)

4. A detailed process-level analysis was performed thanks to the tendency diagnostics I implemented in MADE3 as part of this thesis. This analysis showed that coagulation and nucleation are identified as the most relevant processes controlling the aviation-induced particle number concentration during the plume dispersion regime and the resulting plume correction with respect to the instantaneous dispersion approach. A sensitivity study showed that reducing the efficiency of nucleation is compensated by a reduced efficiency of coagulation, so that the plume correction at the end of the dispersion phase is only weakly affected. (→ research questions 3)

5. The properties of the background where the plume is released have a considerable impact on the results. Simulations performed over different regions of the Northern Hemisphere show large variations in the plume correction, from –12%

over Europe to –43% over China, as a result of the different properties of the background aerosol in these regions. (→ research questions 3, 4)

6. Variation studies on several aviation emission parameters used for model initialisation showed a strong sensitivity of the model to the assumed ice crystal number concentration in the scenario with a short-lived contrail in the vortex regime (controlling the efficiency of the nucleation with aerosol particles and thus their number reduction) and to the fuel sulfur content (impacting the formation of the sulfuric acid precursor, eventually driving new particle formation via nucleation). Despite the dominant importance of aviation-induced sulfate particles over soot particles, the model showed a weak sensitivity to sulfate parameters, such as size and primary sulfate fraction, due to the modulation effect of the nucleation process. (→ research questions 1, 2, 3, 4)

Overall, the plume model that I developed in this thesis demonstrated that the aerosol microphysical processes, in particular coagulation and nucleation, are more efficient at the plume-scale compared to the large-scale grid boxes simulated by global models, and that accounting for these subgrid-scale effects has an important impact on the aviation-induced aerosol number concentrations at the end of the dispersion regime of an aircraft plume. Thanks to its flexibility and its very low computational demand, the plume model is suitable for both offline and online applications in global models, and will allow to achieve a more refined representation of the aviation-induced particle properties in the early stages after the emissions. The many sensitivity simulations that I performed in this study will help to narrow the number of parameters to be considered when applying the model for global applications, also providing hints to future measurement campaigns targeting aviation emissions.

9

OUTLOOK

As elaborated in this thesis, the double-box aircraft exhaust plume model aims to tackle the large uncertainties behind the current estimates of the climate impact of aviation aerosol. To advance in this area, an improved understanding of the microphysical processes occurring at the plume scale, and how these processes affect the aviation-induced aerosols within a gradually dispersing aircraft plume, is essential. The plume model developed in this thesis addresses these challenges by providing a framework to simulate and assess the interactions and impacts of these microphysical processes on aviation aerosols in terms of species mass concentration (mainly sulfate and soot), particle number concentration, and their size distribution, inside an aircraft plume. The plume model simulates the aerosol microphysics in two aircraft plume regimes: the vortex regime (10-120 s after the emissions) and the dispersion regime (120 s to several hours after the emission). For the dispersion regime, the plume model is designed to simulate three distinct aerosol dispersion scenarios, enabling a comprehensive analysis of varying diffusion dynamics on aerosol microphysics. In order to understand the aviation effect on aerosols, the two modelling approaches i.e., plume approach and instantaneous dispersion approach are compared. Here, the plume approach consists of a double-box model configuration, which represents the entrainment of background air into a gradually dispersing plume. The instantaneous dispersion approach on the other hand, represents a large-scale grid box, which accounts for a homogeneous and instantaneous dispersion of an aircraft plume, as being followed by global climate models. In this thesis, the two aforementioned approaches are compared to quantify the aviation effect on the particle number concentration and their respective lognormal sizes. The studies performed in this thesis clearly shows a significant role of parameters such as initial ice crystal number concentration (N_{ice}), fuel sulfur content (FSC) as well as the background aerosol concentrations at the cruise altitude.

The calculated plume corrections provide a comprehensive understanding of the key parameters influencing aerosol dynamics by altering microphysical processes within an aircraft-emitted plume. This insight forms a critical foundation for future advancements in the model development and refinement, such as using the existing model outcome for

global model studies. In order to proceed in this direction, the first step is the development of conversion factors based on the existing aviation effects and plume corrections for aerosol mass and number. This will help enable the users to initialise the aviation inventories in the global climate models (such as EMAC) as the future applications of the plume model, providing a possibility of online parametrisation to account for the unresolved plume-scale processes.

One of the advantages of the plume model, is its low computational cost and very short simulation time (~minutes) which renders it particularly useful for process understanding and targeted parametric studies. Future estimates of the aviation-induced impact on climate via aerosol-cloud interactions may benefit from this model to include more robust assumptions on the properties of aviation aerosol upon and shortly after emissions, with important consequences for the simulations of the life cycle of aviation-induced aerosol particles and their interactions with clouds.

As this study advances in exploring aerosol dynamics and their direct and indirect effects on climate, I anticipate further testing utilizing both the current version of MADE3 (V4.0) and future model developments. These efforts aim to deepen our understanding of the micro-scale processes driving changes in aerosol behaviour, which, in turn, influence low cloud formation and properties, and ultimately impact the global radiation budget. Future studies will focus on refining the plume model, also exploring new parametrisation to improve the representation of specific processes:

1. **future scenarios**: based on the current development stage of the plume model MADE3, the model simulations can also be performed for different scenarios (e.g., under the Shared Socioeconomic Pathways, SSPs, [116]), representing different background concentrations in the future,

2. **alternative fuels**: aircraft emissions from alternative fuels, such as Sustainable Aviation Fuel (SAF), can be evaluated for their impact on aviation-induced aerosols using the plume model. This would allow for a detailed assessment of the influence of SAF on the aerosol formation, aging and dispersion inside an aircraft plume as compared to conventional jet fuels.

3. **overlapping plumes**: the current version of plume model simulates a single aircraft plume in individual ensemble boxes, however future extensions could enable the examination of scenarios involving multiple plumes traversing in the model grid-box, thus mimicking the partial overlapping of the aircraft plumes.

While this study primarily focuses on the aerosol properties towards the end of the dispersion regime, it is important to consider that once the aerosols are emitted from the aircraft engine, they begin to interact with the incoming solar radiation, even as they undergo microphysical transformation within a dispersing aircraft plume. This interaction may contribute to the direct impact of aviation aerosols on the Earth's radiation budget. Thus, the plume model results can also be applied to assess the direct impact of aviation aerosols on climate.

The initialisation parameters are essential to produce accurate estimates of aviation-induced aerosol during the plume dispersion, which can be used to correct for unresolved subgrid-scale processes in global model studies. However, these initialisation pa-

rameters are also uncertain and in this work have partly been derived from relatively old measurement data, also because real-time or in-situ measurements of the aerosols properties in the early plume stages (~10 seconds after the emissions) behind aircraft are extremely challenging, due to several safety and aerodynamic considerations, primarily related to wake turbulence. In addition to this, measuring the ultra-fine volatile particles ($\leq$ 5 nm) immediately after their formation (within seconds behind the aircraft) remains a challenge due to rapid transformation processes like coagulation and condensation in the young plumes which, as shown in this thesis, have a potentially large impact on aviation-induced particle number concentrations. Thus, the current equipments need to improve their accuracy, especially in capturing volatile fractions shortly after emission [96, 117], which can provide more accurate information on the size of emitted particles from the engine exhaust. This will in turn help to improve the plume model results and eventually a refined quantification of the climate impact of aviation aerosol.

In conclusion, the insights gained from this study based on the plume model output are expected to contribute substantially to an improve quantification of climate impact of aviation aerosol, both for the present day and for future scenarios, providing critical input that can inform climate policy and strategies for mitigating aerosol impacts. I am optimistic about the significant advancements this study can contribute to both the scientific community and society at large. As the aviation industry continues to grow, so does its impact on our climate, particularly through aerosol emissions that influence the cloud microphysics and Earth's radiation budget. Understanding the intricate microphysical processes at plume scales is essential for accurately predicting their impact on aerosol transformation, aerosol-cloud interactions, on cloud properties, and the resulting radiative forcing. By enhancing the research in this area, we can develop innovative solutions that not only mitigate the climate impacts of aviation but also contribute to the broader goal of achieving a sustainable future, therefore continued investments in this research area are essential for effectively addressing the existing and future challenges.

BIBLIOGRAPHY

[1] J. H. Seinfeld and S. N. Pandis. *Atmospheric Chemistry and Physics: From Air Pollution to Climate Change, 3rd Edition*. Wiley, Apr. 2016. ISBN: ISBN: 978-1-118-94740-1.

[2] N. Riemer, A. P. Ault, M. West, R. L. Craig, and J. H. Curtis. "Aerosol Mixing State: Measurements, Modeling, and Impacts". In: *Rev. Geophys.* 57.2 (May 2019), pp. 187–249. DOI: 10.1029/2018rg000615. URL: https://doi.org/10.1029%2F2018rg000615.

[3] J. E. Penner, D. H. Lister, D. J. Griggs, D. J. Dokken, and M. (McFarland. "Aviation and the Global Atmosphere". In: *A Special Report of the Intergovernmental Panel on ClimateChange Working Groups I and III* (1999).

[4] P. Forster, V. Ramaswamy, P. Artaxo, T. Berntsen, R. Betts, D. Fahey, J. Haywood, J. Lean, D. Lowe, G. Myhre, J. Nganga, R. Prinn, G. Raga, M. Schulz, and R. V. Dorland. "Changes in Atmospheric Constituents and in Radiative Forcing". In: *In: Climate Change 2007:The Physical Science Basis. Contribution of Working Group I to the Fourth Assessment Report of the Intergovernmental Panel on Climate-Change* (2007).

[5] S. J. Smith, J. van Aardenne, Z. Klimont, R. J. Andres, A. Volke, and S. Delgado Arias. "Anthropogenic sulfur dioxide emissions: 1850–2005". In: *Atmospheric Chemistry and Physics* 11.3 (Feb. 2011), pp. 1101–1116. ISSN: 1680-7324. DOI: 10.5194/acp-11-1101-2011.

[6] Z. Klimont, S. J. Smith, and J. Cofala. "The last decade of global anthropogenic sulfur dioxide: 2000–2011 emissions". In: *Environ. Res. Lett.* 8.1 (Jan. 2013), p. 014003. DOI: 10.1088/1748-9326/8/1/014003. URL: https://doi.org/10.1088%2F1748-9326%2F8%2F1%2F014003.

[7] R. M. Hoesly, S. J. Smith, L. Feng, Z. Klimont, G. Janssens-Maenhout, T. Pitkanen, J. J. Seibert, L. Vu, R. J. Andres, R. M. Bolt, T. C. Bond, L. Dawidowski, N. Kholod, J.-i. Kurokawa, M. Li, L. Liu, Z. Lu, M. C. P. Moura, P. R. O'Rourke, and Q. Zhang. "Historical (1750–2014) anthropogenic emissions of reactive gases and aerosols from the Community Emissions Data System (CEDS)". In: *Geosci. Model Dev.* 11.1 (Jan. 2018), pp. 369–408. DOI: 10.5194/gmd-11-369-2018. URL: https://doi.org/10.5194%2Fgmd-11-369-2018.

[8] W. Aas, A. Mortier, V. Bowersox, R. Cherian, G. Faluvegi, H. Fagerli, J. Hand, Z. Klimont, C. Galy-Lacaux, C. M. B. Lehmann, C. L. Myhre, G. Myhre, D. Olivié, K. Sato, J. Quaas, P. S. P. Rao, M. Schulz, D. Shindell, R. B. Skeie, A. Stein, T. Takemura, S. Tsyro, R. Vet, and X. Xu. "Global and regional trends of atmospheric sulfur". In: *Scientific Reports* 9.1 (Jan. 2019). ISSN: 2045-2322. DOI: 10.1038/s41598-018-37304-0.

[9] V. Vestreng, G. Myhre, H. Fagerli, S. Reis, and L. Tarrasón. "Twenty-five years of continuous sulphur dioxide emission reduction in Europe". In: *Atmospheric Chemistry and Physics* 7.13 (July 2007), pp. 3663–3681. ISSN: 1680-7324. DOI: 10.5194/acp-7-3663-2007.

[10] O. Boucher and D. Randall. "Chapter-7, Clouds and Aerosols". In: *IPCC, Fifth Assessment Report* (2013).

[11] U. Lohmann, F. Lüönd, and F. Mahrt. *An Introduction to Clouds: From the Microscale to Climate*. Cambridge University Press, Apr. 2016. ISBN: 9781139087513. DOI: 10.1017/cbo9781139087513.

[12] M. B. Baker and T. Peter. "Small-scale cloud processes and climate". In: *Nature* 451.7176 (Jan. 2008), pp. 299–300. ISSN: 1476-4687. DOI: 10.1038/nature06594.

[13] T. Chen, W. B. Rossow, and Y. Zhang. "Radiative Effects of Cloud-Type Variations". In: *J. Climate* 13.1 (Jan. 2000), pp. 264–286. DOI: 10.1175/1520-0442(2000)013<0264:reoctv>2.0.co;2. URL: https://doi.org/10.1175%2F1520-0442%282000%29013%3C0264%3Areoctv%3E2.0.co%3B2.

[14] G. McFiggans, P. Artaxo, U. Baltensperger, H. Coe, M. C. Facchini, G. Feingold, S. Fuzzi, M. Gysel, A. Laaksonen, U. Lohmann, T. F. Mentel, D. M. Murphy, C. D. O'Dowd, J. R. Snider, and E. Weingartner. "The effect of physical and chemical aerosol properties on warm cloud droplet activation". In: *Atmos. Chem. Phys.* 6.9 (July 2006), pp. 2593–2649. DOI: 10.5194/acp-6-2593-2006. URL: https://doi.org/10.5194%2Facp-6-2593-2006.

[15] M. Andreae and D. Rosenfeld. "Aerosol–cloud–precipitation interactions. Part 1. The nature and sources of cloud-active aerosols". In: *Earth Sci. Rev.* 89.1-2 (July 2008), pp. 13–41. DOI: 10.1016/j.earscirev.2008.03.001. URL: https://doi.org/10.1016/j.earscirev.2008.03.001.

[16] S. M. Kreidenweis, K. Koehler, P. J. DeMott, A. J. Prenni, C. Carrico, and B. Ervens. "Water activity and activation diameters from hygroscopicity data - Part I: Theory and application to inorganic salts". In: *Atmos. Chem. Phys.* 5.5 (June 2005), pp. 1357–1370. DOI: 10.5194/acp-5-1357-2005. URL: https://doi.org/10.5194%2Facp-5-1357-2005.

[17] D. Archer, M. Eby, V. Brovkin, A. Ridgwell, L. Cao, U. Mikolajewicz, K. Caldeira, K. Matsumoto, G. Munhoven, A. Montenegro, and K. Tokos. "Atmospheric Lifetime of Fossil Fuel Carbon Dioxide". In: *Annual Review of Earth and Planetary Sciences* 37.1 (May 2009), pp. 117–134. ISSN: 1545-4495. DOI: 10.1146/annurev.earth.031208.100206.

[18] D. Lee, D. Fahey, A. Skowron, M. Allen, U. Burkhardt, Q. Chen, S. Doherty, S. Freeman, P. Forster, J. Fuglestvedt, A. Gettelman, R. D. León, L. Lim, M. Lund, R. Millar, B. Owen, J. Penner, G. Pitari, M. Prather, R. Sausen, and L. Wilcox. "The contribution of global aviation to anthropogenic climate forcing for 2000 to 2018". In: *Atmos. Environ.* 244 (Jan. 2021), p. 117834. DOI: 10.1016/j.atmosenv.2020.117834.

[19] D. S. Lee, M. R. Allen, N. Cumpsty, B. Owen, K. P. Shine, and A. Skowron. “Uncertainties in mitigating aviation non-CO2 emissions for climate and air quality using hydrocarbon fuels”. In: *Environ. Sci. Atmos.* 3.12 (2023), pp. 1693–1740. ISSN: 2634-3606. DOI: 10.1039/d3ea00091e.

[20] B. Kärcher. “Formation and radiative forcing of contrail cirrus”. In: *Nat. Commun.* 9.1 (May 2018). DOI: 10.1038/s41467-018-04068-0.

[21] I. P. on Climate Change (IPCC). “The Earth’s Energy Budget, Climate Feedbacks and Climate Sensitivity”. In: *Climate Change 2021 – The Physical Science Basis: Working Group I Contribution to the Sixth Assessment Report of the Intergovernmental Panel on Climate Change*. Cambridge University Press, 2023. Chap. 7, pp. 923–1054.

[22] K. Esmeijer, M. den Elzen, and H. van Soest. *Analysing international shipping and aviation emission projections*. Tech. rep. PBL publication number: 4076. The Hague: PBL Netherlands Environmental Assessment Agency, 2020.

[23] A. Petzold, J. A. Ogren, M. Fiebig, P. Laj, S.-M. Li, U. Baltensperger, T. Holzer-Popp, S. Kinne, G. Pappalardo, N. Sugimoto, C. Wehrli, A. Wiedensohler, and X.-Y. Zhang. “Recommendations for reporting ”black carbon” measurements”. In: *Atmos. Chem. Phys.* 13.16 (Aug. 2013), pp. 8365–8379. DOI: 10.5194/acp-13-8365-2013. URL: https://doi.org/10.5194%2Facp-13-8365-2013.

[24] R. Teoh, Z. Engberg, M. Shapiro, L. Dray, and M. E. J. Stettler. “The high-resolution Global Aviation emissions Inventory based on ADS-B (GAIA) for 2019–2021”. In: *Atmos. Chem. Phys.* 24.1 (Jan. 2024), pp. 725–744. ISSN: 1680-7324. DOI: 10.5194/acp-24-725-2024.

[25] U. Schumann. “On conditions for contrail formation from aircraft exhausts”. In: *Meteorol. Z.* 5.1 (Mar. 1996), pp. 4–23. DOI: 10.1127/metz/5/1996/4.

[26] D. Lee, G. Pitari, V. Grewe, K. Gierens, J. Penner, A. Petzold, M. Prather, U. Schumann, A. Bais, and T. Berntsen. “Transport impacts on atmosphere and climate: Aviation”. In: *Atmos. Environ.* 44.37 (Dec. 2010), pp. 4678–4734. DOI: 10.1016/j.atmosenv.2009.06.005. URL: https://doi.org/10.1016%2Fj.atmosenv.2009.06.005.

[27] A. Gettelman, H. Morrison, C. R. Terai, and R. Wood. “Microphysical process rates and global aerosol–cloud interactions”. In: *Atmos. Chem. Phys.* 13.19 (Oct. 2013), pp. 9855–9867. DOI: 10.5194/acp-13-9855-2013. URL: https://doi.org/10.5194%2Facp-13-9855-2013.

[28] J. Hendricks, B. Kärcher, U. Lohmann, and M. Ponater. “Do aircraft black carbon emissions affect cirrus clouds on the global scale?” In: *Geophys. Res. Lett.* 32.12 (June 2005), n/a–n/a. DOI: 10.1029/2005gl022740. URL: https://doi.org/10.1029%2F2005gl022740.

[29] J. E. Penner, Y. Chen, M. Wang, and X. Liu. “Possible influence of anthropogenic aerosols on cirrus clouds and anthropogenic forcing”. In: *Atmos. Chem. Phys.* 9.3 (Feb. 2009), pp. 879–896. DOI: 10.5194/acp-9-879-2009. URL: https://doi.org/10.5194%2Facp-9-879-2009.

[30] D. S. Lee, D. W. Fahey, P. M. Forster, P. J. Newton, R. C. Wit, L. L. Lim, B. Owen, and R. Sausen. "Aviation and global climate change in the 21st century". In: *Atmos. Environ.* 43.22-23 (July 2009), pp. 3520–3537. DOI: 10.1016/j.atmosenv.2009.04.024. URL: https://doi.org/10.1016%2Fj.atmosenv.2009.04.024.

[31] J. Hendricks, B. Kärcher, and U. Lohmann. "Effects of ice nuclei on cirrus clouds in a global climate model". In: *J. Geophys. Res. Atmos.* 116.D18 (Sept. 2011). DOI: 10.1029/2010jd015302. URL: https://doi.org/10.1029%2F2010jd015302.

[32] M. Righi, J. Hendricks, U. Lohmann, C. G. Beer, V. Hahn, B. Heinold, R. Heller, M. Krämer, M. Ponater, C. Rolf, I. Tegen, and C. Voigt. "Coupling aerosols to (cirrus) clouds in the global EMAC-MADE3 aerosol–climate model". In: *Geoscientific Model Development* 13.3 (Mar. 2020), pp. 1635–1661. ISSN: 1991-9603. DOI: 10.5194/gmd-13-1635-2020.

[33] M. Righi, J. Hendricks, and C. G. Beer. "Exploring the uncertainties in the aviation soot–cirrus effect". In: *Atmos. Chem. Phys.* 21.23 (Nov. 2021), pp. 17267–17289. DOI: 10.5194/acp-21-17267-2021. URL: https://acp.copernicus.org/articles/21/17267/2021/.

[34] M. Righi, J. Hendricks, and R. Sausen. "The global impact of the transport sectors on atmospheric aerosol: simulations for year 2000 emissions". In: *Atmos. Chem. Phys.* 13.19 (Oct. 2013), pp. 9939–9970. DOI: 10.5194/acp-13-9939-2013. URL: https://doi.org/10.5194%2Facp-13-9939-2013.

[35] G. Brasseur, R. Cox, D. Hauglustaine, I. Isaksen, J. Lelieveld, D. Lister, R. Sausen, U. Schumann, A. Wahner, and P. Wiesen. "European scientific assessment of the atmospheric effects of aircraft emissions". In: *Atmos. Environ.* 32.13 (1998), pp. 2329–2418. ISSN: 1352-2310. DOI: https://doi.org/10.1016/S1352-2310(97)00486-X. URL: https://www.sciencedirect.com/science/article/pii/S135223109700486X.

[36] D. Cariolle, D. Caro, R. Paoli, D. A. Hauglustaine, B. Cuénot, A. Cozic, and R. Paugam. "Parameterization of plume chemistry into large-scale atmospheric models: Application to aircraft NOx emissions". In: *J. Geophys. Res. Atmos.* 114.D19 (Oct. 2009). DOI: 10.1029/2009jd011873. URL: https://doi.org/10.1029%2F2009jd011873.

[37] R. Paoli, D. Cariolle, and R. Sausen. "Review of effective emissions modeling and computation". In: *Geosci. Model Devel.* 4.3 (2011), pp. 643–667. DOI: 10.5194/gmd-4-643-2011.

[38] T. M. Fritz, S. D. Eastham, R. L. Speth, and S. R. H. Barrett. "The role of plume-scale processes in long-term impacts of aircraft emissions". In: *Atmos. Chem. Phys.* 20.9 (May 2020), pp. 5697–5727. DOI: 10.5194/acp-20-5697-2020.

[39] K. N. Tait, M. A. H. Khan, S. Bullock, M. H. Lowenberg, and D. E. Shallcross. "Aircraft Emissions, Their Plume-Scale Effects, and the Spatio-Temporal Sensitivity of the Atmospheric Response: A Review". In: *Aerospace* 9.7 (July 2022), p. 355. DOI: 10.3390/aerospace9070355.

[40] S. K. Meilinger, B. Kärcher, and T. Peter. "Microphysics and heterogeneous chemistry in aircraft plumes - high sensitivity on local meteorology and atmospheric composition". In: *Atmos. Chem. Phys.* 5.2 (Feb. 2005), pp. 533–545. DOI: 10.5194/acp-5-533-2005.

[41] A. Gettelman and C. Chen. "The climate impact of aviation aerosols". In: *Geophys. Res. Lett.* 40.11 (June 2013), pp. 2785–2789. DOI: 10.1002/grl.50520. URL: https://doi.org/10.1002%2Fgrl.50520.

[42] Z. Z. Kapadia, D. V. Spracklen, S. R. Arnold, D. J. Borman, G. W. Mann, K. J. Pringle, S. A. Monks, C. L. Reddington, F. Benduhn, A. Rap, C. E. Scott, E. W. Butt, and M. Yoshioka. "Impacts of aviation fuel sulfur content on climate and human health". In: *Atmos. Chem. Phys.* 16.16 (Aug. 2016), pp. 10521–10541. DOI: 10.5194/acp-16-10521-2016. URL: https://doi.org/10.5194%2Facp-16-10521-2016.

[43] M. Righi, J. Hendricks, and S. Brinkop. "The global impact of the transport sectors on the atmospheric aerosol and the resulting climate effects under the Shared Socioeconomic Pathways (SSPs)". In: *Earth Syst. Dyn.* 14.4 (Aug. 2023), pp. 835–859. DOI: 10.5194/esd-14-835-2023.

[44] J. C. Kaiser, J. Hendricks, M. Righi, N. Riemer, R. A. Zaveri, S. Metzger, and V. Aquila. "The MESSy aerosol submodel MADE3 (v2.0b): description and a box model test". In: *Geosci. Model Dev.* 7.3 (June 2014), pp. 1137–1157. DOI: 10.5194/gmd-7-1137-2014. URL: https://doi.org/10.5194%2Fgmd-7-1137-2014.

[45] H. Petry, J. Hendricks, M. Möllhoff, E. Lippert, A. Meier, A. Ebel, and R. Sausen. "Chemical conversion of subsonic aircraft emissions in the dispersing plume: Calculation of effective emission indices". In: *J. Geophys. Res. Atmos.* 103.D5 (Mar. 1998), pp. 5759–5772. DOI: 10.1029/97jd03749. URL: https://doi.org/10.1029%2F97jd03749.

[46] A. Petzold, A. Döpelheuer, C. A. Brock, and F. Schröder. "In situ observations and model calculations of black carbon emission by aircraft at cruise altitude". In: *J. Geophys. Res. Atmos.* 104.D18 (Sept. 1999), pp. 22171–22181. DOI: 10.1029/1999jd900460. URL: https://doi.org/10.1029%2F1999jd900460.

[47] C. Voigt, U. Schumann, A. Minikin, A. Abdelmonem, A. Afchine, S. Borrmann, M. Boettcher, B. Buchholz, L. Bugliaro, A. Costa, J. Curtius, M. Dollner, A. Dörnbrack, V. Dreiling, V. Ebert, A. Ehrlich, A. Fix, L. Forster, F. Frank, D. Fütterer, A. Giez, K. Graf, J.-U. Grooß, S. Groß, K. Heimerl, B. Heinold, T. Hüneke, E. Järvinen, T. Jurkat, S. Kaufmann, M. Kenntner, M. Klingebiel, T. Klimach, R. Kohl, M. Krämer, T. C. Krisna, A. Luebke, B. Mayer, S. Mertes, S. Molleker, A. Petzold, K. Pfeilsticker, M. Port, M. Rapp, P. Reutter, C. Rolf, D. Rose, D. Sauer, A. Schäfler, R. Schlage, M. Schnaiter, J. Schneider, N. Spelten, P. Spichtinger, P. Stock, A. Walser, R. Weigel, B. Weinzierl, M. Wendisch, F. Werner, H. Wernli, M. Wirth, A. Zahn, H. Ziereis, and M. Zöger. "ML-CIRRUS: The Airborne Experiment on Natural Cirrus and Contrail Cirrus with the High-Altitude Long-Range Research Aircraft HALO". In: *Bull. Amer. Meteor. Soc.* 98.2 (Feb. 2017), pp. 271–288. DOI: 10.1175/bams-d-15-00213.1. URL: https://doi.org/10.1175%2Fbams-d-15-00213.1.

[48] F. S. Binkowski and U. Shankar. "The Regional Particulate Matter Model: 1. Model description and preliminary results". In: *J. Geophys. Res. Atmos.* 100.D12 (1995), p. 26191. DOI: 10.1029/95jd02093. URL: https://doi.org/10.1029%2F95jd02093.

[49] B. Kärcher, M. M. Hirschberg, and P. Fabian. "Small-scale chemical evolution of aircraft exhaust species at cruising altitudes". In: *J. Geophys. Res. Atmos.* 101.D10 (June 1996), pp. 15169–15190. DOI: 10.1029/96jd01059.

[50] R. C. Brown, R. C. Miake-Lye, M. R. Anderson, C. E. Kolb, and T. J. Resch. "Aerosol dynamics in near-field aircraft plumes". In: *J. Geophys. Res. Atmos.* 101.D17 (Oct. 1996), pp. 22939–22953. DOI: 10.1029/96jd01918.

[51] A. G. Kraabøl and F. Stordal. "Modelling chemistry in aircraft plumes 2: the chemical conversion of NOx to reservoir species under different conditions". In: *Atmos. Environ.* 34.23 (2000), pp. 3951–3962. ISSN: 1352-2310. DOI: https://doi.org/10.1016/S1352-2310(00)00155-2. URL: https://www.sciencedirect.com/science/article/pii/S1352231000001552.

[52] S. Unterstrasser, R. Paoli, I. Sölch, C. Kühnlein, and T. Gerz. "Dimension of aircraft exhaust plumes at cruise conditions: effect of wake vortices". In: *Atmos. Chem. Phys.* 14.5 (2014), pp. 2713–2733. DOI: 10.5194/acp-14-2713-2014. URL: https://acp.copernicus.org/articles/14/2713/2014/.

[53] P. Jöckel, A. Kerkweg, A. Pozzer, R. Sander, H. Tost, H. Riede, A. Baumgaertner, S. Gromov, and B. Kern. "Development cycle 2 of the Modular Earth Submodel System (MESSy2)". In: *Geosci. Model Dev.* 3.2 (Dec. 2010), pp. 717–752. DOI: 10.5194/gmd-3-717-2010. URL: https://doi.org/10.5194%2Fgmd-3-717-2010.

[54] P. Jöckel, H. Tost, A. Pozzer, C. Brühl, J. Buchholz, L. Ganzeveld, P. Hoor, A. Kerkweg, M. G. Lawrence, R. Sander, B. Steil, G. Stiller, M. Tanarhte, D. Taraborrelli, J. van Aardenne, and J. Lelieveld. "The atmospheric chemistry general circulation model ECHAM5/MESSy1: consistent simulation of ozone from the surface to the mesosphere". In: *Atmos. Chem. Phys.* 6.12 (Nov. 2006), pp. 5067–5104. DOI: 10.5194/acp-6-5067-2006. URL: https://doi.org/10.5194%2Facp-6-5067-2006.

[55] P. Jöckel, H. Tost, A. Pozzer, M. Kunze, O. Kirner, C. A. M. Brenninkmeijer, S. Brinkop, D. S. Cai, C. Dyroff, J. Eckstein, F. Frank, H. Garny, K.-D. Gottschaldt, P. Graf, V. Grewe, A. Kerkweg, B. Kern, S. Matthes, M. Mertens, S. Meul, M. Neumaier, M. Nützel, S. Oberländer-Hayn, R. Ruhnke, T. Runde, R. Sander, D. Scharffe, and A. Zahn. "Earth System Chemistry integrated Modelling (ESCiMo) with the Modular Earth Submodel System (MESSy) version 2.51". In: *Geosci. Model Dev.* 9.3 (Mar. 2016), pp. 1153–1200. DOI: 10.5194/gmd-9-1153-2016. URL: https://doi.org/10.5194%2Fgmd-9-1153-2016.

[56] P. Jöckel, R. Sander, A. Kerkweg, H. Tost, and J. Lelieveld. "Technical Note: The Modular Earth Submodel System (MESSy) - a new approach towards Earth System Modeling". In: *Atmos. Chem. Phys.* 5.2 (Feb. 2005), pp. 433–444. DOI: 10.

5194/acp-5-433-2005. URL: https://doi.org/10.5194%2Facp-5-433-2005.

[57] J. C. Kaiser, J. Hendricks, M. Righi, P. Joeckel, H. Tost, K. Kandler, B. Weinzierl, D. Sauer, K. Heimerl, J. P. Schwarz, A. E. Perring, and T. Popp. "Global aerosol modeling with MADE3 (v3.0) in EMAC (based on v2.53): model description and evaluation". In: *Geosci. Model Dev.* 12.1 (Feb. 2019), pp. 541–579. DOI: 10.5194/gmd-12-541-2019. URL: https://doi.org/10.5194%2Fgmd-12-541-2019.

[58] M. Bickel, M. Ponater, U. Burkhardt, M. Righi, J. Hendricks, and P. Jöckel. "Contrail Cirrus Climate Impact: From Radiative Forcing to Surface Temperature Change". In: *Journal of Climate* 38.8 (Apr. 2025), pp. 1895–1912. ISSN: 1520-0442. DOI: 10.1175/jcli-d-24-0245.1.

[59] E. R. Whitby and P. H. McMurry. "Modal Aerosol Dynamics Modeling". In: *Aerosol Sci. Technol.* 27.6 (Jan. 1997), pp. 673–688. DOI: 10.1080/02786829708965504. URL: https://doi.org/10.1080%2F02786829708965504.

[60] E. R. Whitby, P. H. McMurry, U. Shankar, and F. S. Binkowski. *Modal aerosol dynamics modelling*. Tech. rep. Research Triangle Park, NC, US: Environmental Protection Agency, 1991, p. 280.

[61] V. Aquila, J. Hendricks, A. Lauer, N. Riemer, H. Vogel, D. Baumgardner, A. Minikin, A. Petzold, J. P. Schwarz, J. R. Spackman, B. Weinzierl, M. Righi, and M. Dall'Amico. "MADE-in: a new aerosol microphysics submodel for global simulation of insoluble particles and their mixing state". In: *Geosci. Model Dev.* 4.2 (Apr. 2011), pp. 325–355. DOI: 10.5194/gmd-4-325-2011. URL: https://doi.org/10.5194%2Fgmd-4-325-2011.

[62] H. Vehkamäki, M. Kulmala, I. Napari, K. E. J. Lehtinen, C. Timmreck, M. Noppel, and A. Laaksonen. "An improved parameterization for sulfuric acid–water nucleation rates for tropospheric and stratospheric conditions". In: *J. Geophys. Res. Atmos.* 107.D22 (2002). DOI: 10.1029/2002jd002184. URL: https://doi.org/10.1029%2F2002jd002184.

[63] M. Kulmala, A. Laaksonen, and L. Pirjola. "Parameterizations for sulfuric acid/water nucleation rates". In: *Journal of Geophysical Research: Atmospheres* 103.D7 (Apr. 1998), pp. 8301–8307. ISSN: 0148-0227. DOI: 10.1029/97jd03718.

[64] S. Metzger, F. Dentener, S. Pandis, and J. Lelieveld. "Gas/aerosol partitioning: 1. A computationally efficient model". In: *J. Geophys. Res. Atmos.* 107.D16 (2002). DOI: 10.1029/2001jd001102. URL: https://doi.org/10.1029%2F2001jd001102.

[65] S. Metzger, N. Mihalopoulos, and J. Lelieveld. "Importance of mineral cations and organics in gas-aerosol partitioning of reactive nitrogen compounds: case study based on MINOS results". In: *Atmospheric Chemistry and Physics* 6.9 (July 2006), pp. 2549–2567. DOI: 10.5194/acp-6-2549-2006.

[66] F. S. Binkowski and S. J. Roselle. "Models-3 Community Multiscale Air Quality (CMAQ) model aerosol component 1. Model description". In: *J. Geophys. Res. Atmos.* 108.D6 (Mar. 2003). DOI: 10.1029/2001jd001409. URL: https://doi.org/10.1029%2F2001jd001409.

[67] A. Lauer, J. Hendricks, I. Ackermann, B. Schell, H. Hass, and S. Metzger. "Simulating aerosol microphysics with the ECHAM/MADE GCM – Part I: Model description and comparison with observations". In: *Atmos. Chem. Phys.* 5.12 (Dec. 2005), pp. 3251–3276. DOI: 10.5194/acp-5-3251-2005. URL: https://doi.org/10.5194%2Facp-5-3251-2005.

[68] C. G. Beer, J. Hendricks, and M. Righi. "Impacts of ice-nucleating particles on cirrus clouds and radiation derived from global model simulations with MADE3 in EMAC". In: *EGUsphere* (Sept. 2023). DOI: 10.5194/egusphere-2023-1983.

[69] U. Schumann, P. Konopka, R. Baumann, R. Busen, T. Gerz, H. Schlager, P. Schulte, and H. Volkert. "Estimate of diffusion parameters of aircraft exhaust plumes near the tropopause from nitric oxide and turbulence measurements". In: *J. Geophys. Res. Atmos.* 100.D7 (1995), p. 14147. DOI: 10.1029/95jd01277.

[70] B. Kärcher. "A trajectory box model for aircraft exhaust plumes". In: *J. Geophys. Res. Atmos.* 100.D9 (1995), pp. 18835–18844. DOI: https://doi.org/10.1029/95JD01638. eprint: https://agupubs.onlinelibrary.wiley.com/doi/pdf/10.1029/95JD01638.

[71] X. T. Centrich, E. Shehab, P. Sydor, T. Mackley, P. John, and A. Harrison. "An Aerospace Requirements Setting Model to Improve System Design". In: *Procedia CIRP* 22 (2014). Proceedings of the 3rd International Conference in Through-life Engineering Services, pp. 287–292. ISSN: 2212-8271. DOI: https://doi.org/10.1016/j.procir.2014.07.127.

[72] J. Czarnigowski, K. Skiba, and K. Dubienski. "Investigations of the temperature distribution in the exhaust system of an aircraft piston engine". In: *Combustion Engines* 177.2 (May 2019), pp. 12–18. ISSN: 2658-1442. DOI: 10.19206/ce-2019-203.

[73] H. Appleman. "The Formation of Exhaust Condensation Trails by Jet Aircraft". In: *Bulletin of the American Meteorological Society* 34.1 (Jan. 1953), pp. 14–20. DOI: 10.1175/1520-0477-34.1.14.

[74] R. Paoli and K. Shariff. "Contrail Modeling and Simulation". In: *Annu. Rev. Fluid Mech.* 48.1 (Jan. 2016), pp. 393–427. DOI: 10.1146/annurev-fluid-010814-013619.

[75] K. Gierens, U. Schumann, M. Helten, H. Smit, and A. Marenco. "A distribution law for relative humidity in the upper troposphere and lower stratosphere derived from three years of MOZAIC measurements". In: *Annales Geophysicae* 17.9 (Sept. 1999), pp. 1218–1226. ISSN: 1432-0576. DOI: 10.1007/s00585-999-1218-7.

[76] R. Teoh, Z. Engberg, U. Schumann, C. Voigt, M. Shapiro, S. Rohs, and M. Stettler. "Global aviation contrail climate effects from 2019 to 2021". In: *EGU sphere* (Oct. 2023). DOI: 10.5194/egusphere-2023-1859.

[77] K. Wolf, N. Bellouin, and O. Boucher. "Sensitivity of cirrus and contrail radiative effect on cloud microphysical and environmental parameters". In: *Atmos. Chem. Phys.* 23.21 (Nov. 2023), pp. 14003–14037. ISSN: 1680-7324. DOI: 10.5194/acp-23-14003-2023.

[78] U. Schumann, H. Schlager, F. Arnold, R. Baumann, P. Haschberger, and O. Klemm. "Dilution of aircraft exhaust plumes at cruise altitudes". In: *Atmos. Environ.* 32.18 (Sept. 1998), pp. 3097–3103. DOI: 10.1016/s1352-2310(97)00455-x.

[79] M. Sharma, M. Righi, J. Hendricks, A. Schmidt, D. Sauer, and V. Grewe. "A double-box model for aircraft exhaust plumes based on the MADE3 aerosol microphysics (MADE3 v4.0)". In: *EGUsphere* 2025 (2025), pp. 1–38. DOI: 10.5194/egusphere-2025-1137. URL: https://egusphere.copernicus.org/preprints/2025/egusphere-2025-1137/.

[80] T. Jurkat, C. Voigt, F. Arnold, H. Schlager, J. Kleffmann, H. Aufmhoff, D. Schäuble, M. Schaefer, and U. Schumann. "Measurements of HONO, NO, NO_y and SO_2 in aircraft exhaust plumes at cruise". In: *Geophys. Res. Lett.* 38.10 (May 2011), n/a–n/a. DOI: 10.1029/2011gl046884. URL: https://doi.org/10.1029%2F2011gl046884.

[81] R. C. Miake-Lye, M. Martinez-Sanchez, R. C. Brown, and C. E. Kolb. "Plume and wake dynamics, mixing, and chemistry behind a high speed civil transport aircraft". In: *J. Aircr.* 30.4 (1993), pp. 467–479. DOI: 10.2514/3.46368.

[82] B. Kärcher, O. Möhler, P. J. DeMott, S. Pechtl, and F. Yu. "Insights into the role of soot aerosols in cirrus cloud formation". In: *Atmos. Chem. Phys.* 7.16 (Aug. 2007), pp. 4203–4227. DOI: 10.5194/acp-7-4203-2007. URL: https://doi.org/10.5194%2Facp-7-4203-2007.

[83] J.B. Burkholder, S.P. Sander, J.P.D. Abbatt, J.R. Barker, R.E. Huie, C.E. Kolb, M.J. Kurylo, V.L. Orkin, D.M. Wilmouth, and P.H. Wine. *Chemical Kinetics and Photochemical Data for Use in Atmospheric Studies, Evaluation Number 18*. 2015. DOI: 10.13140/RG.2.1.2504.2806.

[84] J. B. Burkholder, S. P. Sander, J. Abbatt, J. R. Barker, C. Cappa, J. D. Crounse, T. S. Dibble, R. E. Huie, C. E. Kolb, M. J. Kurylo, V. L. Orkin, C. J. Percival, D. M. Wilmouth, and P. H. Wine. *Chemical Kinetics and Photochemical Data for Use in Atmospheric Studies, Evaluation No. 19*. JPL Publication 19-5. Pasadena: Jet Propulsion Laboratory, 2019. URL: https://jpldataeval.jpl.nasa.gov.

[85] R. Atkinson. "Kinetics of the gas-phase reactions of OH radicals with alkanes and cycloalkanes". In: *Atmos. Chem. Phys.* 3.6 (Dec. 2003), pp. 2233–2307. DOI: 10.5194/acp-3-2233-2003. URL: https://doi.org/10.5194%2Facp-3-2233-2003.

[86] C. M. Spivakovsky, J. A. Logan, S. A. Montzka, Y. J. Balkanski, M. Foreman-Fowler, D. B. A. Jones, L. W. Horowitz, A. C. Fusco, C. A. M. Brenninkmeijer, M. J. Prather, S. C. Wofsy, and M. B. McElroy. "Three-dimensional climatological distribution of tropospheric OH: Update and evaluation". In: *Journal of Geophysical Research: Atmospheres* 105.D7 (Apr. 2000), pp. 8931–8980. ISSN: 0148-0227. DOI: 10.1029/1999jd901006.

[87] J. A. Logan, M. J. Prather, S. C. Wofsy, and M. B. McElroy. "Tropospheric chemistry: A global perspective". In: *Journal of Geophysical Research: Oceans* 86.C8 (Aug. 1981), pp. 7210–7254. ISSN: 0148-0227. DOI: 10.1029/jc086ic08p07210.

[88] B. Kärcher. “Physicochemistry of aircraft-generated liquid aerosols, soot, and ice particles: 1. Model description”. In: *J. Geophys. Res. Atmos.* 103.D14 (July 1998), pp. 17111–17128. DOI: 10.1029/98jd01044.

[89] S. Unterstrasser, K. Gierens, and P. Spichtinger. “The evolution of contrail microphysics in the vortex phase”. In: *Meteorol. Z.* 17.2 (Apr. 2008), pp. 145–156. DOI: 10.1127/0941-2948/2008/0273.

[90] A. Bier and U. Burkhardt. “Impact of Parametrizing Microphysical Processes in the Jet and Vortex Phase on Contrail Cirrus Properties and Radiative Forcing”. In: *J. Geophys. Res. Atmos.* 127.23 (Dec. 2022). DOI: 10.1029/2022jd036677.

[91] P. Spichtinger and K. M. Gierens. “Modelling of cirrus clouds – Part 1a: Model description and validation”. In: *Atmospheric Chemistry and Physics* 9.2 (Jan. 2009), pp. 685–706. ISSN: 1680-7324. DOI: 10.5194/acp-9-685-2009.

[92] P. Spichtinger and K. M. Gierens. “Modelling of cirrus clouds – Part 1a: Model description and validation”. In: *Atmos. Chem. Phys.* 9.2 (Jan. 2009), pp. 685–706. DOI: 10.5194/acp-9-685-2009. URL: https://doi.org/10.5194%2Facp-9-685-2009.

[93] S. Unterstrasser. “Large-eddy simulation study of contrail microphysics and geometry during the vortex phase and consequences on contrail-to-cirrus transition”. In: *J. Geophys. Res. Atmos.* 119.12 (2014), pp. 7537–7555. DOI: https://doi.org/10.1002/2013JD021418. eprint: https://agupubs.onlinelibrary.wiley.com/doi/pdf/10.1002/2013JD021418.

[94] C. Mahnke, R. Gomes, U. Bundke, M. Berg, H. Ziereis, M. Sharma, M. Righi, J. Hendricks, A. Zahn, A. Wahner, and A. Petzold. “Properties and Processing of Aviation Exhaust Aerosol at Cruise Altitude Observed from the IAGOS-CARIBIC Flying Laboratory”. In: *Environ. Sci. Technol.* (Apr. 2024). ISSN: 1520-5851. DOI: 10.1021/acs.est.3c09728.

[95] V. Grewe, T. Champougny, S. Matthes, C. Frömming, S. Brinkop, O. A. SØvde, E. A. Irvine, and L. Halscheidt. “Reduction of the air traffic’s contribution to climate change: A REACT4C case study”. In: *Atmos. Environ.* 94 (Sept. 2014), pp. 616–625. DOI: 10.1016/j.atmosenv.2014.05.059. URL: https://doi.org/10.1016%2Fj.atmosenv.2014.05.059.

[96] R. K. Dischl, D. Sauer, C. Voigt, T. Harlaß, F. Sakellariou, R. S. Märkl, U. Schumann, M. Scheibe, S. Kaufmann, A. Roiger, A. Dörnbrack, C. Renard, M. Gauthier, P. Swann, P. Madden, D. Luff, M. Johnson, D. Ahrens, R. Sallinen, T. Schripp, G. Eckel, U. Bauder, and P. Le Clercq. “Measurements of particle emissions of an A350-941 burning 100% sustainable aviation fuels in cruise”. In: *EGU sphere* (Apr. 2024). DOI: 10.5194/egusphere-2024-1224.

[97] J. T. Wilkerson, M. Z. Jacobson, A. Malwitz, S. Balasubramanian, R. Wayson, G. Fleming, A. D. Naiman, and S. K. Lele. “Analysis of emission data from global commercial aviation: 2004 and 2006”. In: *Atmos. Chem. Phys.* 10.13 (July 2010), pp. 6391–6408. DOI: 10.5194/acp-10-6391-2010.

[98] F. Berkes, N. Houben, U. Bundke, H. Franke, H.-W. Pätz, F. Rohrer, A. Wahner, and A. Petzold. "The IAGOS NOx instrument – design, operation and first results from deployment aboard passenger aircraft". In: *Atmospheric Measurement Techniques* 11.6 (June 2018), pp. 3737–3757. ISSN: 1867-8548. DOI: 10.5194/amt-11-3737-2018.

[99] T. Harlass, R. Dischl, S. Kaufmann, R. Märkl, D. Sauer, M. Scheibe, P. Stock, T. Bräuer, A. Dörnbrack, A. Roiger, H. Schlager, U. Schumann, M. Pühl, T. Schripp, T. Grein, L. Bondorf, C. Renard, M. Gauthier, M. Johnson, D. Luff, P. Madden, P. Swann, D. Ahrens, R. Sallinen, and C. Voigt. "Measurement report: In-flight and ground-based measurements of nitrogen oxide emissions from latest-generation jet engines and 100% sustainable aviation fuel". In: *Atmospheric Chemistry and Physics* 24.20 (Oct. 2024), pp. 11807–11822. ISSN: 1680-7324. DOI: 10.5194/acp-24-11807-2024.

[100] E. A. Ray, F. L. Moore, H. Garny, E. J. Hintsa, B. D. Hall, G. S. Dutton, D. Nance, J. W. Elkins, S. C. Wofsy, J. Pittman, B. Daube, B. C. Baier, J. Li, and C. Sweeney. "Age of air from in situ trace gas measurements: insights from a new technique". In: *Atmospheric Chemistry and Physics* 24.21 (Nov. 2024), pp. 12425–12445. ISSN: 1680-7324. DOI: 10.5194/acp-24-12425-2024.

[101] G. Kuhlmann, G. Broquet, J. Marshall, V. Clément, A. Löscher, Y. Meijer, and D. Brunner. "Detectability of CO2 emission plumes of cities and power plants with the Copernicus Anthropogenic CO2 Monitoring (CO2M) mission". In: *Atmospheric Measurement Techniques* 12.12 (Dec. 2019), pp. 6695–6719. ISSN: 1867-8548. DOI: 10.5194/amt-12-6695-2019.

[102] R. Sausen and U. Schumann. "Estimates of the climate response to aircraft CO_2 and NO_x emissions scenarios". In: *Clim. Change* 44.1/2 (2000), pp. 27–58. DOI: 10.1023/a:1005579306109. URL: https://doi.org/10.1023/A:1005579306109.

[103] S. Rodríguez, R. Van Dingenen, J.-P. Putaud, S. Martins-Dos Santos, and D. Roselli. "Nucleation and growth of new particles in the rural atmosphere of Northern Italy—relationship to air quality monitoring". In: *Atmospheric Environment* 39.36 (Nov. 2005), pp. 6734–6746. ISSN: 1352-2310. DOI: 10.1016/j.atmosenv.2005.07.036.

[104] R. H. Moore, K. L. Thornhill, B. Weinzierl, D. Sauer, E. D'Ascoli, J. Kim, M. Lichtenstern, M. Scheibe, B. Beaton, A. J. Beyersdorf, J. Barrick, D. Bulzan, C. A. Corr, E. Crosbie, T. Jurkat, R. Martin, D. Riddick, M. Shook, G. Slover, C. Voigt, R. White, E. Winstead, R. Yasky, L. D. Ziemba, A. Brown, H. Schlager, and B. E. Anderson. "Biofuel blending reduces particle emissions from aircraft engines at cruise conditions". In: *Nature* 543.7645 (Mar. 2017), pp. 411–415. DOI: 10.1038/nature21420.

[105] B. Kärcher, R. P. Turco, F. Yu, M. Y. Danilin, D. K. Weisenstein, R. C. Miake-Lye, and R. Busen. "A unified model for ultrafine aircraft particle emissions". In: *J. Geophys. Res. Atmos.* 105.D24 (Dec. 2000), pp. 29379–29386. DOI: 10.1029/2000jd900531. URL: https://doi.org/10.1029%2F2000jd900531.

[106] F. Tan, H. Zhang, K. Xia, B. Jing, X. Li, S. Tong, and M. Ge. "Hygroscopic behavior and aerosol chemistry of atmospheric particles containing organic acids and inorganic salts". In: *npj Climate and Atmospheric Science* 7.1 (Aug. 2024). ISSN: 2397-3722. DOI: 10.1038/s41612-024-00752-9.

[107] H. Zhu, S. Yang, H. Zhao, Y. Wang, and R. Li. "Complex interplay of sulfate aerosols and meteorology conditions on precipitation and latent heat vertical structure". In: *npj Climate and Atmospheric Science* 7.1 (Aug. 2024). ISSN: 2397-3722. DOI: 10.1038/s41612-024-00743-w.

[108] M. Tang, C. K. Chan, Y. J. Li, H. Su, Q. Ma, Z. Wu, G. Zhang, Z. Wang, M. Ge, M. Hu, H. He, and X. Wang. "A review of experimental techniques for aerosol hygroscopicity studies". In: *Atmospheric Chemistry and Physics* 19.19 (Oct. 2019), pp. 12631–12686. ISSN: 1680-7324. DOI: 10.5194/acp-19-12631-2019.

[109] M. Kanakidou, J. H. Seinfeld, S. N. Pandis, I. Barnes, F. J. Dentener, M. C. Facchini, R. Van Dingenen, B. Ervens, A. Nenes, C. J. Nielsen, E. Swietlicki, J. P. Putaud, Y. Balkanski, S. Fuzzi, J. Horth, G. K. Moortgat, R. Winterhalter, C. E. L. Myhre, K. Tsigaridis, E. Vignati, E. G. Stephanou, and J. Wilson. "Organic aerosol and global climate modelling: a review". In: *Atmospheric Chemistry and Physics* 5.4 (Mar. 2005), pp. 1053–1123. ISSN: 1680-7324. DOI: 10.5194/acp-5-1053-2005.

[110] E. Commission, S. A. Directorate-General for Employment, Inclusion, E. Young, FBK-Irvapp, O. Evidence, Valdani, and V. Associati. *Study supporting the impact assessment of an EU initiative introducing the European Disability Card – Final report – Executive summary*. Publications Office of the European Union, 2024. DOI: doi/10.2767/915075.

[111] International Civil Aviation Organization. *Carbon Offsetting and Reduction Scheme for International Aviation (CORSIA)*. 2024. URL: https://www.icao.int/environmental-protection/CORSIA/pages/default.aspx (visited on 05/13/2025).

[112] V. Grewe, A. Gangoli Rao, T. Grönstedt, C. Xisto, F. Linke, J. Melkert, J. Middel, B. Ohlenforst, S. Blakey, S. Christie, S. Matthes, and K. Dahlmann. "Evaluating the climate impact of aviation emission scenarios towards the Paris agreement including COVID-19 effects". In: *Nature Communications* 12.1 (June 2021). ISSN: 2041-1723. DOI: 10.1038/s41467-021-24091-y.

[113] H. Herrmann, D. Hoffmann, T. Schaefer, P. Bräuer, and A. Tilgner. "Tropospheric Aqueous-Phase Free-Radical Chemistry: Radical Sources, Spectra, Reaction Kinetics and Prediction Tools". In: *ChemPhysChem* 11.18 (Nov. 2010), pp. 3796–3822. ISSN: 1439-7641. DOI: 10.1002/cphc.201000533.

[114] J. Li, K. Li, H. Zhang, X. Zhang, Y. Ji, W. Chu, Y. Kong, Y. Chu, Y. Ren, Y. Zhang, H. Zhang, R. Gao, Z. Wu, F. Bi, X. Chen, X. Wang, W. Wang, H. Li, and M. Ge. "Effects of OH radical and SO2 concentrations on photochemical reactions of mixed anthropogenic organic gases". In: *Atmospheric Chemistry and Physics* 22.16 (Aug. 2022), pp. 10489–10504. ISSN: 1680-7324. DOI: 10.5194/acp-22-10489-2022.

[115] M. A. Pimlott, R. J. Pope, B. J. Kerridge, B. G. Latter, D. S. Knappett, D. E. Heard, L. J. Ventress, R. Siddans, W. Feng, and M. P. Chipperfield. “Investigating the global OH radical distribution using steady-state approximations and satellite data”. In: *Atmos. Chem. Phys.* 22.16 (Aug. 2022), pp. 10467–10488. DOI: 10.5194/acp-22-10467-2022.

[116] M. O. Andreae, C. D. Jones, and P. M. Cox. “Strong present-day aerosol cooling implies a hot future”. In: *Nature* 435.7046 (June 2005), pp. 1187–1190. DOI: 10.1038/nature03671. URL: https://doi.org/10.1038%2Fnature03671.

[117] R. S. Märkl, C. Voigt, D. Sauer, R. K. Dischl, S. Kaufmann, T. Harlaß, V. Hahn, A. Roiger, C. Weiß-Rehm, U. Burkhardt, U. Schumann, A. Marsing, M. Scheibe, A. Dörnbrack, C. Renard, M. Gauthier, P. Swann, P. Madden, D. Luff, R. Sallinen, T. Schripp, and P. Le Clercq. “Powering aircraft with 100% sustainable aviation fuel reduces ice crystals in contrails”. In: *Atmos. Chem. Phys.* 24.6 (Mar. 2024), pp. 3813–3837. ISSN: 1680-7324. DOI: 10.5194/acp-24-3813-2024.

ACKNOWLEDGEMENTS

I would like to extend my deepest gratitude to everyone who contributed to the successful completion of this thesis. Their unwavering support, encouragement, and guidance have been invaluable throughout this journey, especially given the unprecedented challenges I faced starting my PhD at the peak of the COVID pandemic, a time when pursuing such an endeavor seemed almost impossible.

First and foremost, I am profoundly grateful to my daily supervisor, Dr. Mattia Righi, whose patience, understanding, and encouragement were especially significant during the early stages of my research. Despite the challenging circumstances, Dr. Righi not only enlighten my path with his expert guidance but also fostered a supportive environment that encouraged critical thinking and independent working, which motivated me to persevere. I am incredibly fortunate to have worked under such a compassionate and knowledgeable mentor.

I also extend my heartfelt thanks to the members of my thesis committee, Prof. Volker Grewe (promotor) and Dr. Irene Dedoussi (copromotor) for their invaluable insights, thought-provoking discussions, constructive feedback which has immensely helped me throughout the dissertation. I would like bestow my humble gratitude to Dr. Johannes Hendricks (DLR) for his expert guidance and steadfast support to help me deepen my understanding of the topic micro to macro level. Their thoughtful input helped me refine my research and deepen my understanding of the subject which has greatly contributed in shaping the direction of my research. A special thanks to ECO2Fly, ACACIA and SENECA for the financial support without which this research would not have been possible. The resources and opportunities were only possible due to their support and were instrumental in the successful completion of this study.

Special thanks to Prof. Anja Schmidt, head of the ESM department at the Institute of Atmospheric Physics- DLR Oberpfaffenhofen, for her exceptional support and encouragement to the successful completion of my PhD. I am deeply grateful to my colleagues and dear friends from the aerosol group at the PA-ESM, Dr. Christof Beer, Dr. Jingmin Li, and Dr. Christopher Kaiser for their invaluable support and generous dedication of time throughout my research. I would also like to formally extend my gratitude to all my colleagues at the Institute of Atmospheric Physics, DLR Oberpfaffenhofen: Dr. Patrick Joeckel, Dr. Daniel Sauer, Dr. Simon Unterstrasser, Dr. Sigrun Matthes, Dr. Tina Jurkart, Dr. Bernd Kärcher and Dr. Ulrike Burkhardt, and to my external colleagues, Dr. Andrea Petzold and Dr. Christopher Mahnke at the Forschungzentrum Jülich for their unwavering support, and the invaluable expertise that they generously shared, all of which significantly contributed to this thesis. I am truly grateful to all my colleagues and friends at the DLR and TU Delft for their companionship and intellectual engagement as they have been an essential source of motivation.

In memoriam of my beloved colleague Anja Blum, whose unwavering support and kindness has left a lasting impact on my journey. I will always be grateful for her invalu-

able guidance and encouragement.

I am immensely grateful to my grandfather and my parents, your belief in my abilities and constant reassurance gave me the strength to persevere, even during the most challenging phases of this journey. To my partner, Patrick Peter, thank you for standing by my side and for being a constant source of inspiration for me. Your support has been a powerful reminder of the value of hard work and determination.

Finally, I am deeply appreciative of Shraddha and Joggy who are my supportive guardians in Germany, and my dear friends: Agatha, Sheena, Inge and Armin, who, through their words and actions, showed me that I was never alone on this path. Their encouragement, patience, and kindness have left an indelible mark on this journey. I am truly blessed to have such a supportive network of friends.

To all the individuals and organizations mentioned here, and to everyone who has contributed in any way to the completion of this thesis, I offer my heartfelt gratitude. This accomplishment would not have been possible without your unconditional support and encouragement. Above all, I want to express my gratitude to myself for persevering and remaining resilient throughout this journey.

CURRICULUM VITÆ

Monica SHARMA

25-02-1991 Born in Uttar Pradesh, India.

EDUCATION

2020–2025 PhD candidate at Delft University of Technology, Netherlands
Scientific Researcher at Deutsches Zentrum für Luft- und Raumfahrt, Germany
Thesis: Quantifying the effect of plume processes on aviation-induced aerosol: towards an improved estimate of the aviation-aerosol effect
Promotor: Prof. dr. V. Grewe

2016–2020 Master of Science (Environmental Geoscience)
Technische Universität Bergakademie Freiberg, Germany

2009–2013 Bachelor in Technology (Environmental Engineering)
Hindustan College of Science & Technology, Uttar Pradesh, India

2006–2009 K.D.B Public School, India (High school, 2006–2007)
K.D.B Public School, India (10+2, 2006–2007)

PROFESSIONAL / RESEARCH EXPERIENCE

2020–Present	Scientific Researcher Institute of Atmospheric Physics Deutsches Zentrum für Luft- und Raumfahrt, Oberpfaffenhofen, Germany
2019	Research Assistant Institut für Geologie, Technische Universität Bergakademie Freiberg, Germany
2018	Research Assistant EUS Research Unit Environmental Simulation, Helmholtz-Zentrum München
2017–2018	Research Assistant Institut für Geologie, Technische Universität Bergakademie Freiberg, Germany
2015–2016	Environmental Engineer J.M. Environet, India
2014–2015	Project Manager Gyanwave Technologies- IT Consultancy, India

RESEARCH INTERESTS

Climate modelling; atmospheric physics and chemistry; aerosol microphysics; aviation emissions and the impact of future aviation technologies on climate; data visualization using Python; and plant communication, including the effects of climate change and inevitable future extreme weather events on plant defense mechanisms and signaling processes.

LIST OF PUBLICATIONS

1. **M. Sharma**, M. Righi, J. Hendricks, A. Schmidt, D. Sauer, V. Grewe, *A double-box model for aircraft exhaust plumes based on the MADE3 aerosol microphysics (MADE3 v4.0)*, Geoscientific Model Development, https://doi.org/10.5194/gmd-18-8485-2025

2. J. Maruhashi, M. Righi, **M. Sharma**, J. Hendricks, P. Jöckel, V. Grewe, and I. C. Dedoussi: *AIRTRAC v2.0: a Lagrangian aerosol tagging submodel for the analysis of aviation SO4 transport patterns*, EGUsphere [preprint], https://doi.org/10.5194/egusphere-2025-4204, 2025

3. C. Mahnke, R. Gomes, U. Bundke, M. Berg, H. Ziereis, **M. Sharma**, M. Righi, J. Hendricks, A. Zahn, A. Wahner, and A. Petzold, *Properties and Processing of Aviation Exhaust Aerosol at Cruise Altitude Observed from the IAGOS-CARIBIC Flying Laboratory*, Environmental Science & Technology, Vol. 58, No. 16, 6945-6953, https://doi.org/10.1021/acs.est.3c09728 (2024)

4. R. Grote, **M. Sharma**, A. Ghirardo and J-P. Schnitzler, *A New Modeling Approach for Estimating Abiotic and Biotic Stress-Induced de novo Emissions of Biogenic Volatile Organic Compounds From Plants*, Front. For. Glob. Change 2:26, https://doi.org/10.3389/ffgc.2019.00026 (2019)

”The plume corrections quantified in this work directly impact the aviation-induced particle number concentration and, when considered in global models, may impact the climate effect from aerosol-cloud interactions (ERFaci) in low-level clouds.”

Sharma et al., 2025

Cover photo: Jonas Hendricks, Aircraft landing at Corfu Airport.